Spring 1-1-2013

The Development of Chemoattractant Plumes in Complex Flows and the Role of the Chemotactic Strategies Employed by Sperm to Navigate the Plumes to Fertilize an Egg

Allison Bell
University of Colorado at Boulder, allisonbell4@gmail.com

The development of chemoattractant plumes in complex flows and the role of the chemotactic strategies employed by sperm to navigate the plumes to fertilize an egg

by

Allison F. Bell

B.A., Connecticut College, 2009

A thesis submitted to the

Faculty of the Graduate School of the

University of Colorado in partial fulfillment

of the requirements for the degree of

Masters of Civil Engineering

Department of Civil, Environmental and Architectural Engineering

2013

This thesis entitled:
The development of chemoattractant plumes in complex flows and the role of the chemotactic strategies employed by sperm to navigate the plumes to fertilize an egg
written by Allison F. Bell
has been approved for the Department of Civil, Environmental and Architectural Engineering

John P. Crimaldi

Prof. Roseanna Neupauer

Prof. Harihar Rajaram

Date

The final copy of this thesis has been examined by the signatories, and we find that both the content and the form meet acceptable presentation standards of scholarly work in the above mentioned discipline.

Bell, Allison F. (MS, Civil Engineering)

The development of chemoattractant plumes in complex flows and the role of the chemotactic strategies employed by sperm to navigate the plumes to fertilize an egg

Thesis directed by Prof. John P. Crimaldi

The ability of benthic invertebrate sperm to utilize chemotaxis and chemokinesis to locate an egg during broadcast spawning is examined under a variety of flow conditions. During the fertilization process, males release a cloud of sperm and females release a cloud of eggs into the ambient flow. The two plumes are brought together due to turbulent stirring. Individual eggs release a mass of chemoattractant into the flow upon being spawned. The motile sperm are tasked with swimming to an egg for fertilization to occur. The sperm are able to sense the concentration of chemoattractant released by a conspecific egg and change their swimming behavior. Chemotaxis, the orientation due to a chemoattractant, and chemokinesis, the increase in speed due to a chemoattractant, aid the sperm in finding and reaching the egg in a flow. The mechanics of this process are not well understood. The flow around an egg in a linear shear flow is modeled for both a constant linear shear rate and for an unsteady turbulent flow where the linear shear changes direction and magnitude. Sperm are placed in a mass at an initial location and advect due to their swimming behavior and the flow. The rate at which the sperm reach the egg is quantified. The efficacy of several possible response behaviors are tested within 5 flows: quiescent flow, two constant linear shear flows with different shear rates and two levels of complexity for the unsteady linear shear flows, and from different initial locations.

Dedication

I dedicate this thesis to Jackson Cone.

Acknowledgements

Professor John Crimaldi: I can not thank you enough for all that you have done for throughout this process. You have an unbelievable way of motivating and pushing your students without causing undue stress. The respect your research group has for you speaks for itself. From my first class with you in an undergraduate fluids course to a Master's Thesis has been an educational, inspiring journey. Thank you for providing me with the opportunity to pursue research in such an interesting field, that also happened to be filled with endless comedy.

My Thesis Committee: You provided me with all the tools I needed to complete this study. Coming from limited engineering experience, your patience, guidance and teaching skills have allowed me to have a more purposeful, enlightening experience in Graduate School.

The Crimaldi Research Group: Your knowledge, advice and support were imperative to the completion of my research.

Tanaya Kawakami: Thank you for always 'talking it out' and being supportive.

Angie Borgert: Your endless support and understanding as well as home cooked meals and comedy have gotten me through everything.

My Family: Thank you for all the encouragement.

Contents

Chapter

Tables

Table

Figures

Figure

Chapter 1

Introduction and Background

1.1 Introduction

Broadcast spawning is a fertilization technique utilized by a variety of aquatic benthic invertebrates. The adult females release a cloud of eggs and the adult males release a cloud of sperm during the same period. Females release about 3 million eggs and males release 10 billion sperm into the ambient flow in each cycle [22, 68]. The males and females are separated by a distance on the order of tens of centimeters to meters, so these clouds are distinct from each other and are encompassed by a third fluid, sea water. The two masses of sperm and eggs rely on the stirring and mixing characteristics of the local flow to bring the clouds close together. There is abundant information regarding the impact of stirring on the reaction rates of two scalars initially in contact with each other and the general dynamics of mixing of two scalars [50]. It has been shown extensively that stirring accelerates reaction due to the increase in the scalar interface between the two scalars [4]. For two initially distinct diffusive scalars, it has been shown that the stirring and mixing properties of turbulent fluids enhances reaction [7–9]. The two scalars coalesce and then diffuse together to accomplish a reaction. In the case of sperm and eggs, this reaction is fertilization, but the individual sperm and egg are too large to undergo any significant diffusion. Instead, sperm motility can provide the effective mixing step, bridging the gap between the sperm and the egg.

Sperm motility can be guided by a chemoattractant released from a conspecific egg. This movement towards a chemical attractant is chemotaxis. Additionally, the speed of the sperm can be enhanced by the chemoattractant, a process known as chemokinesis. Chemotaxis has been

observed in organisms ranging from white blood cells detecting an infection [31] and bacteria finding nutrients [49, 57], to sperm locating an egg. For benthic invertebrate sperm, there is a distinct and specific 'scent' or chemical cue associated with the egg of each individual species. Resact, speract, asterosap, peptides, misact, and tryptophan have been shown to be the sole chemoattractant for sea urchins (*Arbacia punctulata* and *Strongylocentrous purpuratus*), star fish (*Asterias amurenis*), mollusks, sand dollar (*Clypeaster japonicus*) and red abalone (*Haliotis rufescens*), respectively [3, 22, 28, 29, 54, 55, 61, 64]. These chemicals are released from the egg, providing a path for the sperm to potentially follow to successfully reach an egg.

In benthic invertebrates, while chemotaxis has been observed [11, 32], has been proven to enhance fertilization rates, [54], and has been recognized as imperative to successful, sustained fertilization, the micro scale dynamics of fertilization and the strategies to accomplish fertilization are not well understood [3, 61]. This study will explore possible strategies used to accomplish chemotaxis, determine their efficacy, and understand what abilities within chemotaxis the sperm actually need to possess in order to maintain a substantial fertilization rate. The physics of the flow and its impact on the plume will be replicated in a few possible scenarios: quiescent flow, simple shear flow, representative of the instantaneous structure within the normal environment of most benthic invertebrates, and several more complex flows, representing the unsteady, turbulent flows that exist at the scale of fertilization, with an additional consideration of initial distance from the egg. In terms of fluid dynamics, benthic invertebrate gametes are relatively small, smaller than the Kolmogorov scale, but operate in a large, oceanic environment. This dichotomy causes them to thrive and reproduce in a physical world that exists at the interface between a laminar and a turbulent. Their location within the scales they operate within are depicted below in Fig. 1.1.

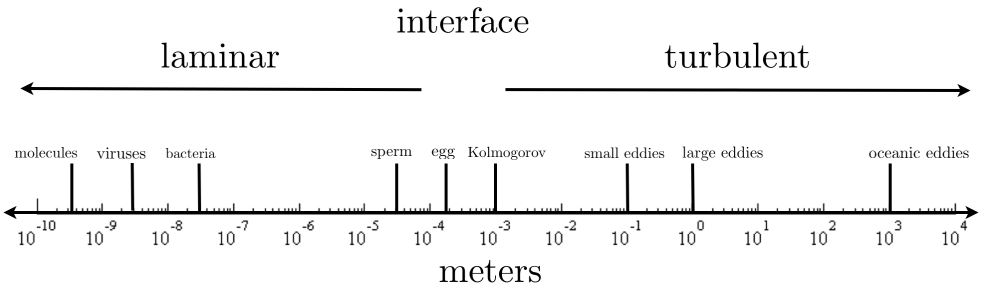

Figure 1.1: Log-based scale to illustrate where the gametes exist in turbulent modeling.

1.2 Background

1.2.1 Physical

In order to better understand the impact of sperm motility on fertilization, a sense of the physics that come into play is introduced. Upon spawning, each individual egg releases its own chemoattractant plume into the flow. The oceanic habitats of many benthic invertebrates are similar, consisting of crevices and rocky shelves or large coral reefs. Since they are usually somewhat sheltered, the velocity of the water is relatively retarded, but because of the rocky ledges, the roughness and irregularities of coral, benthic invertebrates exist within turbulent environments [44, 56, 68]. The existing stirring abilities of the flow brings the clouds close together, but sperm motility is ultimately required to lead to fertilization. Due to their small size and environment, both sperm and eggs operate at a very low Reynolds regime. The attractant plume released by the egg is stretched and stirred at this low scale, and the sperm must swim, sensing this plume, to locate the egg. The flow around an egg needs to be understood in order to know how the attractant plume is released and how it will then develop within the flow to eventually investigate the sperm's ability to locate the egg.

Benthic invertebrate eggs are smaller than the smallest eddies present in turbulence; they are smaller than the Kolmogorov scale. The average diameter of a benthic invertebrate egg is $100 - 400$ μm and the sperm range from $30 - 50$ μm. The Kolmogorov length scale is on the order

of millimeters and is determined by the properties of the flow:

$$\eta = \left(\frac{\nu^3}{\epsilon}\right)^{1/4}$$

where ν is the kinematic viscosity of the fluid and ϵ is the dissipation rate of turbulent kinetic energy. This small size is associated with a low Stokes Number, indicating that neither the sperm nor the eggs impact the flow. The following process was used to approximate the non-dimenstional Stokes number:

$$St = 2/9 \left(\frac{a}{L}\right)^2 Re$$

$$St_{\text{egg}} = 10 \text{ E} - 6$$

$$St_{\text{sperm}} = 3 \text{ E} - 6$$

where a is the characteristic radius of the particle (50 μm for a sperm, 100 μm for an egg), L is the characteristic length scale of the fluid the particle is operating within (the maximum vortex modeled is 15E2 μm) and Re is the Reynold's number ($Re \ll 1$ for benthic invertebrates).

The flow around a fixed cylinder or sphere has known analytical solutions in the Stokes limit. In this case, the cylinder is an egg, which is not fixed, but is instead free. The eggs are also very small, causing any variations in the flow around them to result in a simple linear shear. When examined at small scales, any flow appears to be linear. The linear shear flow causes the free egg to rotate due to an imbalance in the shear stress, resulting in a net torque. Eventually, this torque will disappear, and the egg will continue to rotate. Mikulencak and Morris (2004) provide non-dimensional analytical solutions that prescribe this flow for low Reynolds numbers [45]:

$$\boldsymbol{U}_x{}^* = \frac{1}{2}\boldsymbol{y}^* \left(1 - \boldsymbol{r}^{*-4}\right) + \frac{1}{2}\boldsymbol{y}^* \left(1 - \boldsymbol{r}^{*-2}\right) - 2\boldsymbol{x}^{*2}\boldsymbol{y}^* \left(\boldsymbol{r}^{*-4} - \boldsymbol{r}^{*-6}\right) - \frac{\Omega \boldsymbol{y}^*}{\boldsymbol{r}^{*2}} \tag{1.1}$$

$$\boldsymbol{U}_y{}^* = \frac{1}{2}\boldsymbol{x}^* \left(1 - \boldsymbol{r}^{*-4}\right) + \frac{1}{2}\boldsymbol{x}^* \left(1 - \boldsymbol{r}^{*-2}\right) - 2\boldsymbol{x}^*\boldsymbol{y}^{*2} \left(\boldsymbol{r}^{*-4} - \boldsymbol{r}^{*-6}\right) - \frac{\Omega \boldsymbol{x}^*}{\boldsymbol{r}^{*2}} \tag{1.2}$$

where $\Omega = -\frac{1}{2}$ to allow the cylinder to rotate. In this solution, there is assumed to be no net force on the cylinder and the torque required to initiate the rotation is ignored. The flow around the egg needs to be considered in the context of turbulence to accurately portray how the attractant plume is altered.

Turbulence consists of different scales of eddies interacting with each other. Each eddy has its own lifetime and energy. The larger eddies pass energy to smaller eddies which pass energy on to even smaller eddies until viscosity dominates and the energy is dissipated into heat. In general, the smaller the eddy, the shorter its lifetime. Since eggs are so small, the flow that can impact the attractant plume at any one time is confined to a single, small eddy. Within an evolving turbulent field, the direction and magnitude of the velocities are constantly changing. The small scale eddies dissipate into heat and the egg is then picked up by a new eddy. The flow within a single eddy, or vortex, is not uniform. In general, the velocity decreases from the center, where there is only solid body rotation. There are several solutions to the Navier-Stokes equations that are used to model a vortex flow: Taylor-Green, Lamb-Oseen and Rankine. In this study, we focus on the Lamb-Oseen solution, which models an ideal vortex with a distinct core size, r_{core}. For points where $r \gg r_{\text{core}}$, there is a $1/r$ velocity decay due to viscosity. This relates to a strain rate decay of $1/r^2$:

$$V_\theta(r,t) = \frac{\Gamma}{2\pi r}\left(1 - \exp\left[\frac{-r^2}{r_{\text{core}}^2(t)}\right]\right) \tag{1.3}$$

for radius r, viscosity ν, and circulation Γ.

While in the ambient fluid, the attractant plume diffuses out of the surface of the egg at a constant rate [22, 34, 55, 56, 68]. The diffusion occurs via the diffusive-flux relationship:

$$F = -D\left(\frac{\partial C}{\partial r}\right)$$

where F is the flux, D is the diffusivity of the attractant, C is the concentration and r is the radial distance from the center of the egg. This plume then diffuses and advects with the flow.

The shear serves to stretch the plume of chemoattractant, increasing its size beyond what it would become due just to diffusion. The short lifespan of the small eddies causes the shear direction and magnitude for the egg to constantly evolve, stretching and increasing its size [36]. This produces a similar stretching, stirring and folding present for a the large clouds of eggs and sperm.

The small-scale turbulence causes the attractant plumes to stretch and fold, resulting in an increased scalar interface, but this also relates to a potentially more complex gradient field. It is not immediately clear if these processes serve to aid or hinder fertilization. The majority of the studies regarding chemotaxis have involved only a pure diffusion setting. Very few have included the effects of an unsteady, natural flow [25,49]. Benthic invertebrate gametes must operate and fertilize within the physical world below the Kolmogorov scale. The large plumes of eggs and sperm are stirred and mixed within the flow. Once they are close enough, the sperm must swim and navigate the attractant plume to find the egg. This plume is distorted, stretched and folded within the smallest eddies of a turbulent flow. The tools the gametes utilize and the specifics of their biology permit them to successfully thrive in this environment.

1.2.2 Biological

An understanding of broadcast spawning also depends on the biological details of the sperm, the egg and the processes by which the two produce a fertilized gamete. The egg releases a chemoattractant, and the resulting plume serves as a stimulus to motile sperm. The structure of the egg, the release of the chemoattractant and knowledge of the motility and chemotactic response of the sperm need to be understood. These processes have been studied in the laboratory and in field experiments as well as modeled using numerical techniques. In this section, we review the various aspects of these biological processes and provide a summary of the existing studies of fertilization rates. First, a general understanding of taxis is presented. This is followed by a description of observed swimming behaviors of sperm and the basics behind chemotaxis. A summary of the studies involving fertilization rates and the factors that can hinder fertilization is also included.

Taxis is the guided directional response of an organism to an external stimuli or the gradient

of a stimuli. Stimuli for taxis include: light (phototaxis), gravity (gravitaxis), temperature (thermotaxis) or chemicals (chemotaxis). A wide variety of species exhibit taxis, ranging from bacteria, gametes and individual human cells to fish and insects such as cockroaches. Taxis is employed for various purposes including: reproduction, sustenance, optimization of metabolic activity and avoidance of predators. The process of taxis and its implications have been studied for a range of reasons: from understanding how taxis aids micro-organisms in finding nutrient [49] to contributing to space experiments to observe organisms' reaction to gravity [21]. In the context of reproduction, chemotaxis and thermotaxis have been shown to help direct sperm to the egg. For example, human sperm use thermotaxis to follow temperature gradients surrounding an egg [2]. Benthic invertebrates, however, have only been observed to guide their directional response using chemotaxis. They have also been observed to alter their speed in a gradient of chemoattractant realized by an egg, a similar process known as chemokinesis.

Each egg that is released by a female has a reservoir of the chemoattractant. Upon being released by an adult female into the ambient flow, a chemoattractant begins diffusing out of the egg. This chemical diffuses and advects within the flow, creating an attractant plume concentration field according to the fluid dynamics described above. In the present study, we will focus on the eggs and chemoattractant plumes associated with the red abalone. We make this choice due to the high volume of research on the identity of the chemoattractant L-tryptophan, the molecular understanding of tryptophan in water, and the abalone habitat and the intricacies associated with their fertilization [56, 68]. L-tryptophan has been identified as the sole attractant released by red abalone eggs that elicits a response from conspecific sperm [22, 54, 55, 61]. This was verified by comparing the response of red abalone sperm to other isolated chemicals known to be released by the eggs [34] and comparing the response of red abalone sperm to attractants of other species, such as brine shrimp [55, 56] and green abalone [54]. Tryptophan in other organisms and other parts of the organism provides additional important services. The amino acid is required for protein formation, part of the system to create other signals (eg., brain neuromodulators), and its metabolite, serotonin, is necessary for nervous system development [34]. L-tryptophan is assimilated

in the diet of the red abalone and becomes integrated in the eggs upon their creation.

The eggs from many species of benthic invertebrates are encased in a jelly coat. For some species, like the *A. puntulata*, sperm show a chemotactic response to a peptide that exists only in the jelly coat [65]. For red abalone eggs, the jelly coat does not source any attractant, but the attractant does need to diffuse through the coat to exit the egg [34].The coat of the red abalone is a glycoproteinaceous vitelline envelope and is actually rigid [62]. It ranges in thickness from 5 μm to 50 μm [14]. It is a vital aspect of the reproductive process, as sperm must breach this barrier to enter the egg and begin the fertilization process.

In laboratory experiments, the rate at which the eggs release the tryptophan has been measured between $0.18 - 0.3$ mol egg^{-1} min^{-1} [22, 34]. The release is even throughout the surface of the egg and remains constant for about 40-45 minutes. The concentrations of tryptophan were seen to increase linearly around the eggs for the first 45 minutes. Following this time, the concentration in the surrounding solution saw a fast decline. Eggs eventually stop releasing tryptophan and then were found to be infertile [34]. This length of time is considered well outside the appropriate window in which fertilization occurs, suggesting that the limited duration of the chemoattractant release does not impact fertility rates. The diffusivity of tryptophan in water in a typical temperature in the benthos has been estimated around $6\text{E} - 9$ m^{2}sec^{-1} [43, 51, 68].

The chemoattractant released from the egg has been known to elicit a chemotactic response from the sperm. In this study, we draw on studies detailing the behavior of sperm from a range of species. Sperm of a multitude of species have exhibited similar swimming patterns, chemotactic responses, and operate under analogous flow dynamics. Even mammalian sperm and benthic invertebrate sperm actually experience similar shear forces within the flows where reproduction occurs [68]. Additionally, the swimming behaviors of both the sperm of a star fish and the sperm of several sea urchin species have been described as 'similar' with the same description applying to each in one study [3]. While the focus on the concentration model is based solely on the red abalone, the information used to model the sperm swimming is a synthesis of information.

Sperm of any species are very simplistic cells. The body consists of a head and a flagellum

with an average length of 50 μm [28]. The sperm of benthic invertebrates rely on chemical reactions within their relatively minute bodies to determine how they swim, how they enter the egg and how to accomplish fertilization. Because their swimming motion corresponds to low Reynolds numbers, with a very high experienced viscosity of water, the propulsion of the flagellum is the main source of movement for sperm [17]. The flagellum is controlled by calcium ion, Ca^{2+}, chemical reactions within the sperm that can be stimulated by exterior chemoattractants. The flagella of the sperm are covered in chemoattractant receptors that are used by the sperm to sense the chemoattractant. Receptor densities between 14E3 and 1E6 receptors per sperm have been reported [28]. Motor proteins from reactions in the flagellum create the bending waves that produce the swimming patterns of the sperm.

In the absence of any chemoattractant stimulus, sperm exhibit a loitering behavior which is typically described as a helical path (in 3D) [16, 17, 56] or as drifting circles (2D) [1, 3, 15, 28]. For example, the sperm of the sea urchin, *A. punctulata*, swim in tight circles with low drifting speed [29]. The path of a loitering sperm has been described as random, with no bias towards the egg before a threshold concentration of the chemoattractant is sensed [47, 54–56, 63]. The paths of several species of loitering sperm have been captured using video imaging. These paths show variations in the size of the circles created, the direction of the path of the circles and the speed of the net drift [3, 6, 11, 15, 28, 29, 66]. It has been suggested that due to the actual, unsteady nature of plumes in a real environment, repetitive loops are a navigational strategy for discontinuous concentration fields [28]. The actual average parameters of each aspect of the swimming pattern have been quantified for a variety of species. The average values of parameters for the various aspects of the swimming patterns are summarized in the table below. The second column, Circle Parameters describes the curvature, κ, the time to complete one circle, T or the rotational speed, ω. The average radius of the circle created in a loitering path is included in the third column, Circle Radius. Additionally, the speed at which the sperm swim to complete the drifting circle path is shown in the third column, Swim Speed.

Table 1.1: Loitering Swimming Parameters

Species	**Circle Parameters**	**Radius**	**Swim Speed**	**Cite**
Sea urchin (*A. punctulata*)	$\kappa = 39 \pm 6$ mm^{-1} $T = 1.4 \pm 0.2$ sec	26 ± 4 μm	120 ± 13 μm sec^{-1}	[1]
Sea urchin (*S. purpuratus* and *L. pictus*)	$\omega = 1.67$ rev sec^{-1}	24.9 ± 1.0 μm		[19]
Red abalone			$25 - 37\mu$m sec^{-1}	[55]
Red abalone			30 μm sec^{-1}	[68]
Red abalone			$63.2, 65.5, 48.3$ and 33.9 μm sec^{-1}	[56]
Sea urchin	$\kappa = 0.025 - 0.05$ μm^{-1}		$100 - 200$ μm sec^{-1}	[17]
Sea Urchin (*A.punctulata*)		56 ± 13 μm	218 ± 30 μm sec^{-1}	[29]
Sea Urchin			197 ± 59 μm sec	[3]
Sea urchin	1.5 rev sec^{-1}	$13.2 \pm 2.8\mu m$	$125 \pm 21\mu$m sec^{-1}	[53]
Human	$\omega = 3 - 20$ rev sec^{-1}		$20 - 100$ μmsec^{-1}	[59]
Sea Urchin (*A.punctulata*)		$50 - 60$ μm		[65]
Sea Urchin(*A.punctulata*)		41 ± 6 μm	205 ± 5 μm sec^{-1}	[66]
Asterias			334 ± 86 μm sec^{-1}	[3]

Loitering sperm that encounter a concentration above a threshold will alter their swimming behavior and exhibit a response behavior. A chemotactic or chemokinetic response has only been observed above a threshold concentration, identified in several experiments to range between 3E $-$ 10 mol L^{-1} and 4E $-$ 9 mol L^{-1} for the red abalone [54, 68]. Other studies have noted that within a certain proximity to a purely diffusive source, the sperm show a change in behavior. This would also suggest that a certain strength of concentration is necessary to elicit a response. Some species of sperm have exhibited a detectable reaction to just one molecule of an attractant [29] or just a femtomolar concentration [27]. For example, the sperm of the sea urchin (*A. punctulata*) are able to sense and show a detectable response when just one molecule of its attractant, resact, binds to the flagellum. While some response is detected, this is not considered a true chemo-response as the response does not last long enough to result in a notable change in the swimming pattern. A response to the threshold includes a change in the orientation of the swimming path, chemotaxis, and an increase in swimming speed, chemokinesis.

There is considerable evidence that the swimming characteristics of benthic invertebrate sperm is controlled by the flagellum's flicking frequency and the ability of the sperm to suppress

the response of the flagellum to chemoattractant. A series of turns, arcs and runs, a suppression of curvature, a change between asymmetric and symmetric beating and a change in the size of the circles before and after stimulation are all behaviors that have been observed and modeled numerically and analytically [1,3,19,20,28,29]. It is still not well understood why many observations indicate that when the sperm are stimulated, they still execute turns. These turns are followed by a run, or depressed curvature, but then another turn is completed. It is argued that it is possible that the sperm are not constantly sensing the gradient [27] or that these actions are a consequence of delays in the chain reaction of chemical reactions that occur once the sperm is stimulated [61]. It is also believed that the sperm are in fact constantly monitoring the concentrations around them. The importance of modeling this helical attribute has been argued and modeled from a mathematical standpoint [13], a biological and behavioral view [3, 20] and a stochastic stance [15–17]. While there is no one clear explanation of what processes motivate chemotaxis, how the body of the sperm respond to a chemoattractant and what that equates to in their swimming behavior, there exists a plethora of studies, observations and models that provide significant insight.

The most agreed upon theory of how the sperm respond to a chemoattractant relates to the decrease in curvature, resulting in an increased drifting speed [54, 65, 68]. One well-studied chemotactic response has been referred to as a combination and superposition of chemotactic drift and effective diffusion [15]. Once a sufficient gradient is sensed, the sperm alter the path from drifting circles to a path more akin to a trochoid or prolate trochoid [3, 20, 27, 28]. The variation on the direction the sperm travel in the gradient and the acceleration they experience has been seen to be relative to the strength of the concentration or gradient [17]: the drift velocity and the noise on the paths are based on the concentration that the sperm are sensing [15]. The circles completed by excited sperm are tighter as they make turns away from the gradient and then much larger, relating to a lower curvature. Combined with an increase in drift speed, this also relates to longer runs with shorter and faster turn phases. These factors have been observed to be directly related to the response to the stimulus [1].

It has also been observed in several laboratory experiments [3, 22, 34, 54, 56, 68] that once

a threshold concentration is sensed, sperm will exit the circling pattern, reorient toward the egg with an increased speed. The paths have been descried as straight, with no remaining turns [22, 47, 54–56, 68]. *L. pictus* sea urchin sperm have exhibited stimulated behavior in which turns can no longer be recognized, but instead there is a 'gradual increase in the size of the circular spermatozoa swimming trajectory' [19]. The ability of sperm to suppress Ca^{2+} fluctuations and control the flagellum while in a positive gradient has also been recognized. It has been observed to be relative to the gradient. In a stronger gradient, greater suppression can occur, resulting in a longer, straighter run [19, 54]. It has been seen in laboratory experiments [19, 54, 55, 65] and analytical models [15, 17] that the increase in speed once a sperm is stimulated is not necessarily constant. Instead, as the gradient or concentration of the attractant increases and the distance to the egg decreases (as for pure diffusion), the sperm increasingly speeds up. This has never been modeled numerically, but analytically, a noise coefficient, considered an effective diffusivity, has been used to recreate this method. This behavior has only been observed and described as a relative increase, but has not yet been quantified. As soon as the maximum concentration is reached (10^{-6} mol L^{-1}), the maximum speed in red abalone sperm has been maintained [55].

While an increase in speed has been noted in a majority of the literature, some works has observed that sperm only reorient and decrease the variation on their paths in response to the appropriate gradient. The same drifting speed is maintained [28], but the size of the circles becomes more constant and the direction of the path becomes more direct with an increasing gradient. In three dimensions, sperm have been exhibited a change in direction, but no quantifiable change in speed was observed [15, 35]. Other findings of chemokinesis in some sperm have noted that not all sperm display the addition of an increase in speed. This swimming behavior that lacks a speed component tests the theory of the necessity of chemokinesis in addition to chemotaxis. Another observed response similar to these is that as the concentration increases, the sperm have been observed to show highly asymmetric flagellar waveforms which result in tight, orientated circles [67]. There has been no clear study to determine the difference in these possible chemotactic strategies and what abilities are necessary for fertilization, especially in response to a complex

plume in turbulence.

The majority of the literature has noted the same over-arching chemotactic and chemokinetic response, but there is one study that deterred from the average. At high densities, 6E3 cells/mm^2 the sperm of two sea urchin species, *Strongylocentrous droebachinsis* and *S. purpuratus*, arranged themselves into an array of vortices with about 10 ± 2 sperm per vortex. Groups of sperm completed circles around the same center. At times, sperm moved to new vortices or vortices would merge. The vortex centers had a diffusion coefficient of 6.2 ± 0.9 μm^{2}sec^{-1}. The array was found to have a hexagonal order. The average spacing between vortices was 49 ± 9 μm and the lifespan of the structure is short. The sperm within the same vortex did not exhibit the same swimming speed or beat frequency of the flagellum [53].

Table 1.2 below is a synthesis of some observed parameters of stimulated sperm, including again the rotational speed, ω, the radius of the circles completed and the swimming speed.

Table 1.2: Stimulated Swimming Parameters

Species	**Circle Parameters**	**Radius**	**Swim Speed**	**Cite**
Sea urchin (*S. purpuratus* and *L. pictus*)	1.45 rev sec^{-1}	62.5 ± 7.7 μm		[19]
Sea Urchin (*A.punctulata*)	$\omega = 1$ rev sec^{-1}	$50 - 60$ μm	200 μm sec^{-1}, drift: $25 - 50$ μm sec^{-1}	[28]
Red abalone			$75 - 79$ μm sec^{-1}	[55]
Red abalone			70 μm sec^{-1}	[22]
Red abalone			$30 - 70$ μm sec^{-1} (in shear)	[68]
Red abalone			$60 - 65$ μm sec^{-1} (in shear)	[54]
Sea Urchin			284 ± 105 μm sec^{-1}	[3]
Asterias			446 ± 88 μm sec^{-1}	[3]

The actual mechanics that precipitate these observed chemotactic responses are complicated and still unresolved for all species. A simplified explanation helps understand the workings of the chemotactic behaviors. For chemotaxis to occur, the molecules from the appropriate chemoattractant bind to the corresponding surface receptors on the sperm's flagellum. As the sperm swim in a gradient of chemoattractant, the sperm ascertain how many molecules have been able to bind

to the receptors and been activated. After about 300 ms, these molecule become deactivated, and a new set of molecules, representing the change in concentration, binds to the receptors. Herein lies the change in concentration they are able to detect [28]. This then leads to the creation of the Ca^{2+} signals within the flagellum. The selective timing of the Ca^{2+} fluctuations in a descending gradient is a characteristic of chemotaxis and separates other responses to Ca^{2+} from being considered chemotaxis [20]. This leads to a chain reaction of chemical processes within the body of the sperm. It has been argued that the rate at which the concentration of these Ca ions change in the flagellum is what determines the manner in which the flagellum moves [1]. The angle of the path is also related to the Ca^{2+} rate. This same relationship was found amongst sperm of two other species of sea urchin [1]. The specific mechanics that follow are outside the scope of this study, but the resulting swimming behavior has been described as the result of these chemical reactions on the perceived control of the flick of the flagellum. There is no one clear understanding of the exact nature of the sperm's response.In addition to the chemical reactions, there are numerous other factors that must be considered before chemotaxis or chemokinesis can be completed.

A gradient of chemoattractant is necessary to produce a change in behavior. A uniform gradient inhibits the ability of sperm to control the orientation with the gradient. A uniform concentration field higher than the threshold only increased the swimming speed of the sperm, but provided no directional aid [54, 55, 65]. Sperm of the sea urchin (*A. punctulata*) were shown to have the ability to deduce a relative change in the concentration, or a gradient, or resact, but do not ascertain transient, absolute concentration levels. In red abalone gametes, there exists a cap on the concentration of tryptophan. Above values of $1\text{E}-6$ mol L^{-1}, there was no net change in swimming speed [55]. This is related to an no occurrence of change in the fertilization rate, making the argument that both chemotaxis and chemokinesis are required to improve fertilization rates. Saturation of the receptors is not an issue during this process in any studied species, especially over short periods of time. The receptors have a high density and are able to maintain a large range of concentrations [3, 29]. The receptors respond when there is both a detectable change in the concentration from one monitoring period to the next and when the appropriate chemoattractant

binds to them.

Sperm can generally only react to the attractant from an egg of their own species. A green abalone sperm showed an extremely decreased chance of fertilizing an egg of a red abalone [12, 54, 56]. Additionally, tryptophan initiated no response from sperm of *Haliotis sorenseni, Haliotis corrugata* or *Haliotis fulgens*, all species of abalone that inhabit the same environment with similar reproductive timing [68]. An observation of several species of coral sperm showed that any response was species-specific [47]. Only the *L. pictus* sea urchin exhibited a chemotactic response to speract, whereas the *S. purpuratus* sea urchin did not [19]. Red abalone sperm were observed to reorient towards a red abalone egg and increase their speed, but displayed completely random behavior and no change in swimming speed in the presence of brine shrimp eggs [55, 56]. The sea urchin *A. punctulata* did not show a response to speract, but the *S. purpuratus* did [65]. One study recognized that the extracellular Ca^{2+}, caused by SAPs (spermatozoa-activating peptides), specifically speract, for the sea urchin (*S. purpuratus*), and the resulting turning episodes were necessities for any chemotaxis of any species, but this was proven incorrect in the *L. pictus*, a painted sea urchin. This sea urchin accomplished the same types of turn and run patterns due to these Ca^{2+} fluctuations as a response to speract, but the orientation was random, not directed toward the egg or any one target [19]. In addition to understanding the mechanics of chemotaxis and reproduction, the rate of fertilization and factors that either contribute or hinder this rate are considered.

The effect of chemotaxis has been recognized and calculated using: the linear equation chemotaxis index (LECI) [19], interpreting the orientation of sperm's path with respect to the egg [22,54,68], timing of a chemotactic response [20,29,66], measure of the relative changes in speed and direction, numerical assessments [13] and analytical studies [15, 17, 63]. A popular method for quantifying fertilization is a model from Vogel *et al.,* 1982:

$$\beta_0 = v \times \sigma_0$$

for v, the mean sperm velocity and σ_0, the cross-sectional area of the egg [63]. It has been modeled

analytically based on the theories of Brownian motion and the modeling of the estimated flux of both the attractant and the guided movement of the sperm [30]. The effect of the diffusivity of the attractant has been modeled using a biased random-walk to model the sperm's response [25].

Various techniques have been implemented in order to quantify the impact of chemotaxis. Sperm paths have been observed and recorded under a microscope [10,22,24,34,41,44,54–56,68], egg mimics equipped with pharmaceutical drug delivery methods have been used to elicit a response [22], responses to chemoattractants of non-corresponding species [34, 54–56], use of a uniform gradient [54], analysis of the impact of egg size [26] levitan, computational studies modeling the sperm reaction as a biased-random walk [25] and swimming behavior has been varied [35]. In addition to testing the effect of chemotaxis on fertilization, the effect of outside factors on both chemotaxis and fertilization rates have been studied.

The impact of stress produced by flow akin to that in their natural habitats on the fertilization rates of red abalone sperm has been examined using a Taylor-Couette Flow [56, 68]. These studies found that shear enhanced the fertilization rates for lower shear rates, less than $\alpha = 1$ sec^{-1}, compared to no flow, but decreased rates beyond this value. Red abalone inhabit kelp forests, generally located amongst crevices and underneath ledges in the ocean. From field measurements, it was determined that these habitats are most likely where the abalone live and carry out broadcast spawning. The range of shear strengths, the only experienced fluid dynamics at the scale of an egg, observed in these habitats was 0.3 to 2.4 sec^{-1} [56]. Once shear rate exceeded 4 sec^{-1}, the sperm began to rotate without control in the flow. The higher the shear, the faster the egg rotates. Starting at shear strengths of 2 sec^{-1}, the sperm began having increased difficulty attaching to the egg and would slip off. However, shear has not been proven to cause any adverse damage to any aspect of either gamete [56]. Fertilization studies in laboratory experiments revealed that the abalone's natural habitat provides the most suitable and successful environment for spawning. Replicating the same shear strengths, Pe number associated with the environment and flow velocities produced the highest fertilization rates [56]. Additionally, the effect of energy dissipation rates on the success of reproduction has been examined. The gametes of the purple sea urchin, *S. purpuratus*, were

found to withstand energy dissipation rates around 2200 W m^{-3} before fertilization success fell below 80%. In the range of 40 - 600 W m^{-3} fertilization success rates increased [10]. Fertilization success of the mussels (*Dreissena polymorphs* and *D. bugensis*) was measured with respect to bed roughness. It was determined that the success of fertilization is similar to that of shear stress; the turbulence created enhanced fertilization compared to no flow, but only for moderate levels of roughness [52].

Other hurdles to chemotaxis and successful fertilization are fluctuations due to preciseness of the measurement of the concentration, the chemotactic signaling system, noise within the motor ensemble-results in fluctuations in the swimming speed and unstable and disconnected concentration gradients [15]. The timing, population levels, density levels, fluid dynamics and the ability to self-fertilize proved to be important factors in fertilization success for several coral species. In one study, the species of coral whose gametes spawned in sync with each other with high populations of males and females, high densities of gamete, small volumes of water, such as at low tide and could self-fertilize had the highest fertilization rates [46]. Spawning activities are actually limited to only a portion of the abalone, and some abalone only release a portion of their gametes if they even spawn [18]. Food source and abundance affects gamete production, health and ability to spawn in benthic invertebrates. For example, kelp is the main source of food for red abalone. Periods of high gamete production and spawning occur during the seasons when kelp is plentiful [18]. The spawning timing, both individually and in groups, can contribute to another issue: sperm limitation and sperm density.

Sperm limitation and density as well as sperm dilution are major considerations in past fertilization studies amongst benthic invertebrates. The ratio of sperm to eggs was found to be a determining factor in fertilization rates of red abalone. For an extreme ratio in favor of sperm, the sperm were seen to become limiting or they saturated the egg, preventing any further impact from chemotaxis. At intermediate ranges, around $10 - 1,000$ sperm: 1 egg, the fertilization rate was found to increase as a function of the chemoattractant strength [54]. In a case of the *Paracentrotus lividus*, a high ratio of sperm to egg was necessary to achieve a high fertilization rate [63]. The

purple sea urchin, *S. purpuratus*, inhabits very energetic, rocky shores, with lots of turbulent mixing. The possibility of gamete dilution, damage to the eggs or sperm, a possibility separating the gametes and preventing fertilization, or the inability of the sperm to remain attached the egg long enough to successfully fertilize all exists under these conditions and have hindered the urchin's fertilization rates [44]. Scleractinian coral (*Goniastrea fabulous*) more commonly brain coral, release their gametes asynchronously. The eggs are released first, and they remain on the surface of the coral colony during the rest of the spawning period within a mucous. The sperm gametes are then released, about 20- 30 minutes later, in several phases. Once the sperm reach the egg mucous, they become stuck. Fertilization was found to be 94.7% after 8 hours, noted as the highest recorded percentage in coral. This value closely matched that found in lab experiments, 88%, suggesting that in the location of the study, sperm limitation does not negatively impact fertilization [46] The egg mucous served as a method to avoid the risks involved with sperm limitation.

Egg size has been a long considered factor in fertilization and chemotactic studies [39]. This has been considered both from the perspective of the effective target size of the egg, due to the chemoattractant, and the actual size of the egg due to its jelly coat and natural diameter. Some studies have found that the amount of sperm and the size of the egg required to achieve a certain percent of fertilization have an inverse relationship. For example, a test was performed with the goal of achieving a 50% fertilization of egg. Within the study, the *S.pupuratus* had the smallest eggs and needed the highest amount of sperm. The *S. droebachiensis*, having the largest eggs, needed the smallest concentration of sperm to achieve the desired fertilization [42]. The size of the egg has been found to be a more determining factor in success rates [40]. The cross-sectional area of the egg has been observed to be proportional to the fertilization rate for a study on sea urchins [63]. It has been shown to directly determine fertility rate in the sea squirt [26], the rate has been shown to be proportional to the cross-sectional area of the egg. The size of the egg has also been seen to impact the success rates of the sand dollar (*Dendraster excentricus*) [38] and the sea urchin [37], most likely due to a larger chance of collision between the gametes as the size of the target increased. Additionally, the size of the egg has proven to be a significant factor in determining the impact

of chemotaxis. However, in a study of the red abalone in shear, it was determined that if the egg were to actually increase in size, this would increase the shear stress that it creates, which would negatively impact the fertilization rate, decreasing the ability of the sperm to attach to the egg [68]. The velocity of the sperm, as seen in the sea urchin (*Lytechninus variegatus*), can predict the fertilization rates of the species, as faster sperm showed a higher rate than slower sperm. This also correlated with the longevity of the sperm. The fitter, faster sperm were more successful in fertilizing the egg. This result was duplicated for the *Galeolaria caespitosa* [35].

Once the sperm reaches the egg, fertilization is not a guarantee. Several steps still need to be taken to complete fertilization. There are a few factors that can inhibit fertilization once the sperm reaches the egg, such as viability of both the egg and sperm and the ability to fuse with the cell. First, the sperm must stick to the outer envelope. This may be difficult for instance of high shear, where the egg rotates too quickly for the sperm to stick [68]. The egg's envelope then initiates a reaction in the sperm, opening its acrosome granule. The sperm is then able to create a hole in the envelope with the release of proteins and enter the egg. This is where sperm from a different species encounter another barrier, where the sperm cannot penetrate the egg or the sperm does not even recognize it has located an egg [62]. Biologically, it is clear that without extenuating circumstances, the sperm of red abalone cannot fertilize an egg of a pink abalone [61]. Necrosis is also prevalent in the ovaries of a few species of broadcast spawners, such as red abalone, clams and sea urchin [18]. This would prevent the gametes ability to successful reproduce. If the sperm does enter the egg and if both the egg and the sperm are vital, fertilization is a safe assumption.

An exterior potential threat to fertilization is an increase in the acidity of the ocean, where spawning take place. An increase in CO_2 concentrations has resulted in increasing ocean acidification. In an experiment with gravid coral colonies (*Acropora digitizer*) and sea cucumber (*Holothuria*), when pH was less than less than or equal to 7.7, less than 20% of the sperm of the coral remained motile, and less than 30% of the sea cucumber sperm were still motile [48]. There is also the possibility of more than one sperm fertilizing one egg, resulting in polyspermy. Polyspermy can lead to death of the gamete or abnormal larval development [58]. Even before the

egg is reached, it is possible that a sperm will terminate the path towards a viable egg of the same species due to some preference for another egg of the same species. An experiment showed that sperm exhibited a preference for eggs in the mussel, *Myitlus galloprovincialis*. Some sperm showed a preference towards unfertilized eggs and a different preference of eggs within the same species. This could potentially be due to the perceived viability of the egg and its age, or some other unknown reason [12]. So, even if a sperm has the ability to reach an egg, it may chose not to due to its own preferences. It is unclear whether this limits fertilization rates, or enhances successful fertilization by avoiding potentially unsuccessful partnerships.

Chemotaxis, chemokinesis and the swimming behavior of sperm have been explained in a variety of ways testing many different species. Some of the major responses and notable behaviors will be modeled to determine their efficacy in fertilization. Aspects of others and theorized behaviors will also be tested to understand what abilities the sperm could potentially possess or what is necessary for a successful fertilization strategy. This will be accomplished in varying flows and starting locations to ascertain both the impact on the fertilization rates in difference flows, and the efficacy of different responses within different flows.

Chapter 2

Model Description

This chapter explains each of the models used in this study. (Sec. 2.1) models the flux of the chemoattractant across the egg, using a particle-tracking method. The mass flux is then used in the Flow Model (Sec. 2.2) to dictate the motion of the particles representing the chemoattractant mass. Then, sperm are introduced into the flow in the Fertilization Model (Sec. 2.3), where the efficacy of various sperm chemotactic strategies are quantified in 4 different flows using a monte-carlo approach. The resulting data is processed in the Processing Model (Sec. 2.4) and finally a sensitivity analysis is detailed in (Sec. 2.5).

2.1 Chemoattractant Flux Model

When female red abalone release eggs into the surrounding fluid, each egg produces a plume of chemoattractant. We use a particle tracking method to model the release and transport of the chemoattractant. The model for chemoattractant release assumed a constant flux of tryptophan across the egg surface for a given egg size and chemoattractant diffusivity. The parameters used in the chemoattractant flux model are summarized in Table 2.1.

Table 2.1: Flux Input Parameters

Parameter	**Name**
Chemoattractant diffusivity	D
Egg radius	R_{egg}
Flux of Chemoattractant	F
Mass release rate	$\dot{M}$
Jelly coat width	j_coat
Position of particles	x, y
Mass of a particle	M_{particle}
Particles released at each time-step	Np
Time-step	dt
End time	$tfinal$

We convert the 3D tryptophan flux from the literature into a 2D flux to be used in our model. Based on the literature [22, 34, 55, 56, 68] and the suggestion of Dick Zimmer (personal communication), we chose a flux of $F_{\text{lit}} = 0.18\frac{\text{fmol/egg}}{\text{min}}$. This flux will be transformed into a mass release rate, $\dot{M}$, that is released from an even distribution around the egg surface in the model.

Flux in units of $\frac{\text{mol}/\mu\text{m}^2}{\text{sec}}$:

$$F = \left(0.18\frac{\text{fmol/egg}}{\text{min}}\right)\left(\frac{1\text{E}-15\text{ mol}}{\text{fmol}}\right)\left(\frac{1\text{ min}}{60\text{ sec}}\right)\left(\frac{1\text{ egg}}{S_{\text{sphere}}}\right) = 2.39\text{E}-23\frac{\text{mol}/\mu\text{m}^2}{\text{sec}}$$

for $S_{\text{sphere}} = 4\pi R_{\text{egg}}^2$ and $R_{\text{egg}} = 100$ μm. In order to create an equivalent flux in a 2D realm, we considered a circumferential band of width δ surrounding the egg (Fig. 2.1), where δ is small relative to the radius of the egg, such that the area of the band is $S_{\text{band}} = 2\pi R_{\text{egg}}\delta$, giving $S_{\text{band}} = 628\delta$ μm^2. As this band becomes thinner, normalizing the resulting concentration byδ will produce a value that is equivalent to the 3D concentrations.

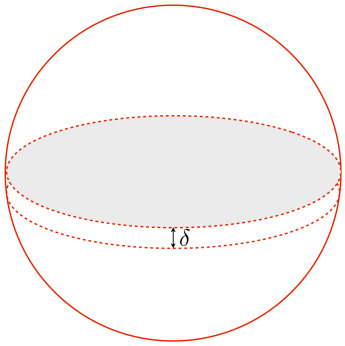

Figure 2.1: A spherical egg with a circumferential band of width δ.

The rate of chemoattractant mass that is released through the band, the mass rate, that will be used in this simulation is calculated as:

$$\dot{M}_{\text{band}} = (F)\,(S_{\text{band}}) \tag{2.1}$$

where $\dot{M}_{\text{band}}$ will be in units of $[\frac{\text{mol}}{\text{sec}}]$. Subsequent radial concentration profiles calculated by the model are insensitive to δ so long as δ is small (Fig. 2.2).

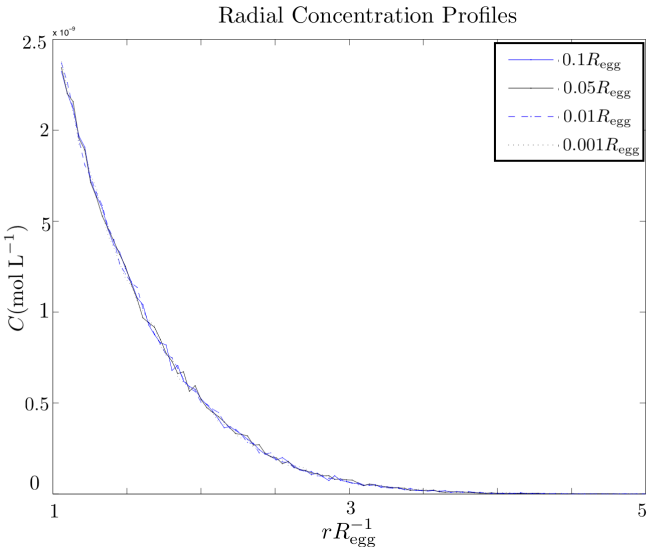

Figure 2.2: Radial concentration plots to show the concentration remains constant for increasingly smaller values of δ. The x axis is the radial distance from the egg normalized by the egg radius. The y axis represents the chemoattractant concentration in units of $[\frac{\text{mol}}{\text{L}}]$.

Tryptophan is released from the egg and subsequently has to diffuse through a jelly coat, (Fig. 2.3). A uniform jelly coat thickness of 25 μm was chosen for this study.

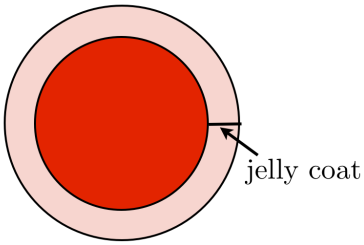

Figure 2.3: Schematic of the egg (red) and jelly coat (pink).

To produce the chemoattractant mass flux from the egg within this jelly coat, particles are randomly distributed around the surface of the egg at the interface between the egg and the jelly coat. The particles are assigned a mass according to the mass release rate, $\dot{M}$, calculated from the flux, F:

$$M_{\text{particle}} = \dot{M} dt / Np$$

where Np is the number of particles and dt is the time step. This provides a particle mass in units of moles that will be used in the calculation of the concentrations in Sec. 2.2.7.

We impose a boundary condition at the surface of the egg to ensure that the modeled flux points radially outward. Any particles that diffuse into the interior of the egg are reflected outside by the same distance.

The released particles move using a particle-tracking method that implements a random-walk diffusion. The particle-tracking method models a scalar using individual points, or particles. The x and y location of each particle is tracked and updated at each time-step. Each particle is subjected to the following calculation at each time-step:

$$\boldsymbol{x}_n = \boldsymbol{x}_{n-1} + \boldsymbol{Z}\sqrt{2Ddt} \tag{2.2}$$

$$\boldsymbol{y}_n = \boldsymbol{y}_{n-1} + \boldsymbol{Z}\sqrt{2Ddt} \tag{2.3}$$

where $\boldsymbol{x}_{n-1}$ and $\boldsymbol{y}_{n-1}$ are the x and y coordinate positions at the previous time step, D is the diffusivity, dt is the time-step and $\boldsymbol{Z}$ is a normally distributed random vector that has a mean of zero and a variance of one. The random-walk approach has the advantage that is has no numerical dispersion. Representative radial distribution plots and concentration images for 3 times are shown in Figs 2.39 and 2.5.

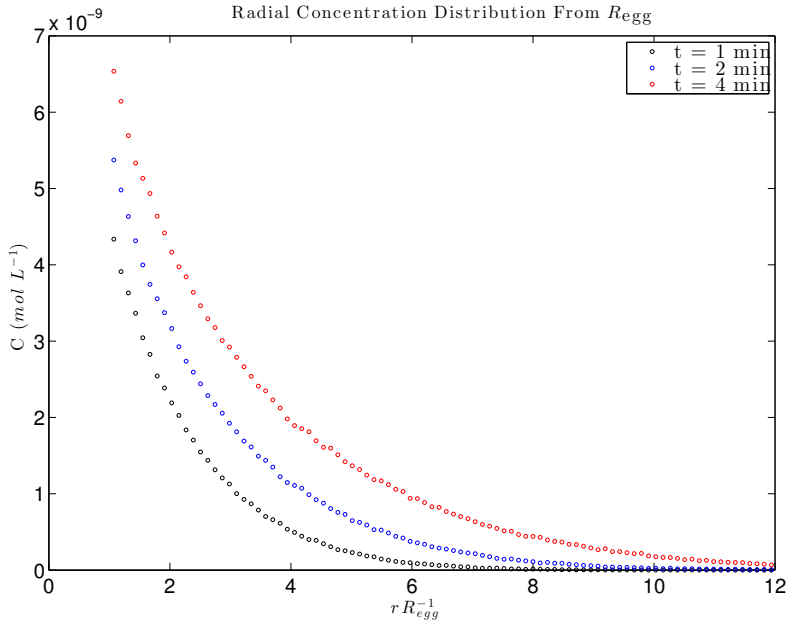

Figure 2.4: Radial concentration plots resulting from diffusion taken after $t = 1, 2,$ and 4 min of mass release.

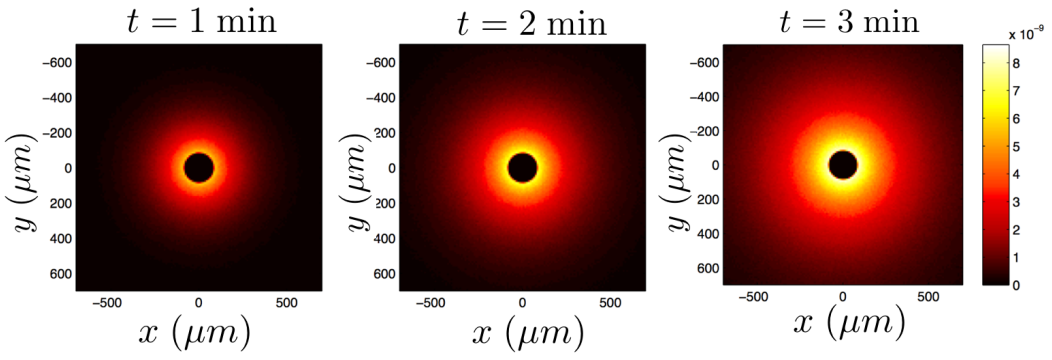

Figure 2.5: Concentration (in units of mol μm^{-3}) images representing the mass around the egg following $t = 1, 2,$ and 4 min of mass release in pure diffusion.

2.1.1 Verification of the Chemoattractant Flux Model

The total chemoattractant mass outside of the egg should equal the integral of the surface flux over time. The total mass of the chemoattractant released by the egg at time t is given by:

$$M = \dot{M}t \tag{2.4}$$

For example, after $t = 240$ sec, the total mass from Eq. 2.4 should be:

$$M = \left(1.5\text{E}-20\frac{\text{mol}}{\text{sec}}\right)(240\text{ sec}) = 3.6\text{E}-18\text{ mol}$$

Integrating the total concentrations around the egg from the model using:

$$M = \int_0^{2\pi}\int_{R_{\text{egg}}}^{\infty} C(r)\, r\, \text{d}r\, \text{d}\theta\, \delta = 2\pi\delta \int_{R_{\text{egg}}}^{\infty} r\, C(r)\, \text{d}r \tag{2.5}$$

We find that

$$\int_0^{2\pi}\int_{R_{\text{egg}}}^{\infty} r\, C(r)\, \text{d}r = 5.73\text{E}-19\ \frac{\text{mol}}{\mu\text{m}^2}$$

$$M = 2\pi\delta\left(5.73\text{E}-19\ \frac{\text{mol}}{\mu\text{m}^2}\right) = 3.6\text{E}-18\text{ mol}$$

Therefore, the mass calculated from the numerical simulation matches the analytical value.

The second check is to ensure that the flux at the surface of the egg, F, calculated earlier, is in agreement with with gradient flux relationship defined as:

$$F = -\text{D}\frac{\partial C}{\partial r}\bigg|_{r=R_{egg}}$$

The values used in the simulation are

$$D = 660\frac{\mu\text{m}^2}{\text{sec}},\ F = 2.38\text{E}-23\frac{\text{mol}/\mu\text{m}^2}{\text{sec}}\delta$$

Therefore, $\left.\frac{\partial C}{\partial r}\right|_{r=R_{egg}}$ should be $3.6\text{E}-11\frac{\text{mol}}{\mu\text{m}^4}$ for δ=1 μm. The concentration gradient immediately outside of the egg surface matches the prescribed slope given the flux, as shown in Fig. 2.6.

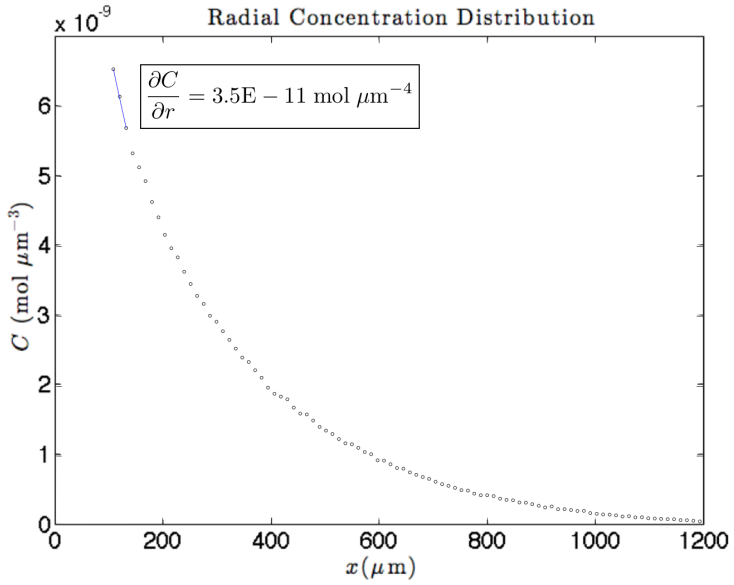

Figure 2.6: A radial concentration plot after 4 minutes to show that gradient near the surface of the egg matches the expected value.

Finally, the flux from a 2D point can be modeled using the Theis solution for long periods of time at far distances [5]. At a far distance, the egg resembles a point and most of the conditions in the chemoattractant flux model agree with the Theis assumptions: the aquifer, or surrounding fluid, is homogeneous and isotropic, there is a constant pumping (or flux) rate, and an infinite domain.

$$s = \frac{Q}{4\pi T}W(u)$$

$$u = \frac{r^2 S}{4Tt}$$

where Q is the pumping rate, T is the transmissivity, W is the exponential integral, S is the storativity of the aquifer, r is the radial distance from the well and t is the total pumping time. For our purposes, the T is equivalent to the diffusivity of the chemoattractant, D and S is equal to one. After 10 minutes, the radial concentration profile from the simulation closely matches the

Theis solution at far distances (Fig. 2.7)

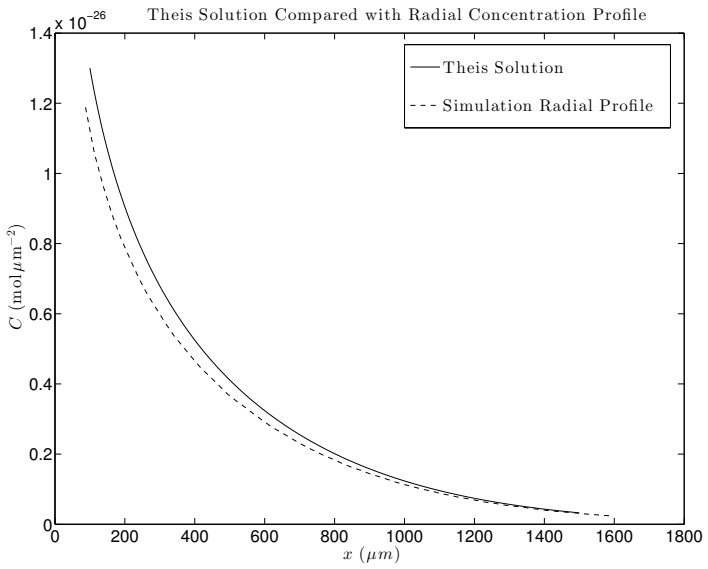

Figure 2.7: The Theis solution plotted with the radial concentration profiles for t= 10 minutes.

The actual values of the parameters used for every simulation follow in Table 2.2.

Table 2.2: Flux Input Parameters: Actual and Calculated Values

Parameter	**Name**	**Value**
Chemoattractant diffusivity	D	660 μm^2 sec^{-1}
Egg radius	R_{egg}	100 μm
Flux of chemoattractant	F	2.38E $-$ 23 mol (μm^2 sec)$^{-1}$
Mass release rate	$\dot{M}$	1.5E - 20 mol sec^{-1}
Jelly coat width	j_coat	25 μm

2.2 Flow Model

In this section we describe the analytical solutions to the Navier-Stokes equations that are used to govern the flow field around the egg. In this study, the flow fields will consist of:

(1) Quiesant Flow (Pure Diffusion)

(2) Two Simple Shear Flows (high and low shear rate)

(3) Two Complex Flows (high and low shear rate)

2.2.1 Simple Shear

The two simple shear flows model a steady linear shear flow modified by the presence of a freely rotating egg using the solutions in Eqs 1.1 and 1.2. The solutions are dimensionalized using the length scale, R_{egg}, and the velocity scale, αR_{egg}:

$$\boldsymbol{u}_x^* = \frac{\boldsymbol{u}_x}{\alpha R_{\text{egg}}}, \quad \boldsymbol{u}_y^* = \frac{\boldsymbol{u}_y}{\alpha R_{\text{egg}}}, \quad \boldsymbol{x}^* = \frac{\boldsymbol{x}}{R_{\text{egg}}}, \quad \boldsymbol{y}^* = \frac{\boldsymbol{y}}{R_{\text{egg}}}, \quad \boldsymbol{r}^* = \frac{\boldsymbol{r}}{R_{\text{egg}}}$$

Dimensionally, these equations are:

$$\begin{aligned}\boldsymbol{U}_x = \frac{1}{2}\alpha \boldsymbol{y}\left[1-\left(\frac{\boldsymbol{r}}{R_{\text{egg}}}\right)^{-4}\right] + \frac{1}{2}\alpha \boldsymbol{y}\left[1-\left(\frac{\boldsymbol{r}}{R_{\text{egg}}}\right)^{-2}\right] \ldots \\ - 2\alpha\left(\frac{\boldsymbol{x}}{R_{\text{egg}}}\right)^2 \boldsymbol{y}\left[\left(\frac{\boldsymbol{r}}{R_{\text{egg}}}\right)^{-4} - \left(\frac{\boldsymbol{r}}{R_{\text{egg}}}\right)^{-6}\right] - \frac{\alpha\Omega \boldsymbol{y}}{\left(\frac{\boldsymbol{r}}{R_{\text{egg}}}\right)^2}\end{aligned} \tag{2.6}$$

$$\begin{aligned}\boldsymbol{U}_y = \frac{1}{2}\alpha \boldsymbol{x}\left[1-\left(\frac{\boldsymbol{r}}{R_{\text{egg}}}\right)^{-4}\right] + \frac{1}{2}\alpha \boldsymbol{x}\left[1-\left(\frac{\boldsymbol{r}}{R_{\text{egg}}}\right)^{-2}\right] \ldots \\ - 2\alpha\left(\frac{\boldsymbol{y}}{R_{\text{egg}}}\right)^2 \boldsymbol{x}\left[\left(\frac{\boldsymbol{r}}{R_{\text{egg}}}\right)^{-4} - \left(\frac{\boldsymbol{r}}{R_{\text{egg}}}\right)^{-6}\right] - \frac{\alpha\Omega \boldsymbol{x}}{\left(\frac{\boldsymbol{r}}{R_{\text{egg}}}\right)^2}\end{aligned} \tag{2.7}$$

These equations represent the effect of a linear shear flow in the presence of a freely rotating egg. This flow can be decomposed into the sum of the pure linear shear plus a perturbation flow, where the perturbation flow is calculated by subtracting a linear shear from the total solution (Fig. 2.8).

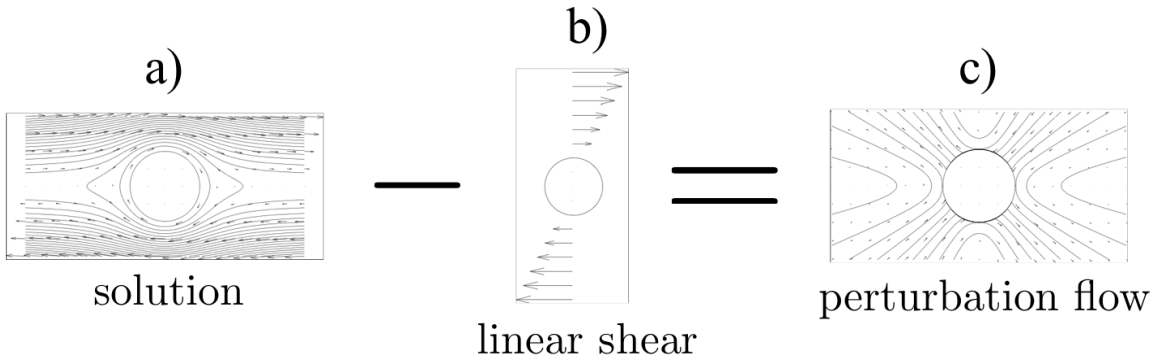

Figure 2.8: Decomposition of velocity field: a) Total Flow (Eqs. 2.6 and 2.7) b) Linear Shear c) Perturbation Flow. When the perturbation flow is added to a linear shear flow, the resulting flow corresponds to a free cylinder in a linear shear flow.

Additionally, the stream functions are presented non-dimensionally by Kossack and Acrivos (1973) in Eq 15. [33]:

$$\boldsymbol{\psi}^*_{\text{total}} = \frac{1}{2}\boldsymbol{r}^{*2}\sin^2\theta - \frac{1}{4}\left[1 + \left(\boldsymbol{r}^{*-2} - 2\right)\cos 2\theta\right] \tag{2.8}$$

where $\boldsymbol{r}^*$ and $\boldsymbol{\psi}^*_{\text{total}}$ are dimensionalized as

$$\boldsymbol{r}^* = \frac{\boldsymbol{r}}{R_{\text{egg}}} \quad \text{and} \quad \boldsymbol{\psi}^*_{\text{total}} = \frac{\boldsymbol{\psi}}{\alpha R^2_{\text{egg}}}$$

using a length scale of R_{egg} and velocity scale of αR_{egg}. For the linear shear flow, $\boldsymbol{U}_x$, the associate stream function is $\frac{\partial \boldsymbol{\psi}}{\partial y}$. Dimensionally, this equation becomes

$$\boldsymbol{\psi}_{\text{total}} = \alpha R^2_{\text{egg}}\left[\frac{1}{2}\left(\frac{\boldsymbol{r}}{R_{\text{egg}}}\right)^2 \sin^2\theta - \frac{1}{4}\left[1 + \left(\left(\frac{\boldsymbol{r}}{R_{\text{egg}}}\right)^{-2} - 2\right)\cos 2\theta\right]\right] \tag{2.9}$$

$\boldsymbol{U}_x = \alpha \boldsymbol{y}$ defines the linear shear flow and $\boldsymbol{U}_x = \frac{\partial \psi}{\partial \boldsymbol{y}}$. Solving for $\boldsymbol{\psi}_{\text{shear}}$ yields $\boldsymbol{\psi}_{\text{shear}} = \frac{1}{2}\alpha \boldsymbol{y}^2$. The stream function for the perturbation flow is given by:

$$\boldsymbol{\psi}_{\text{perturbation}} = \boldsymbol{\psi}_{\text{total}} - \frac{1}{2}\alpha \boldsymbol{y}^2 \tag{2.10}$$

The following plots demonstrate the effect of the α and R_{egg} parameters on the velocity profiles near

the egg. Figures 2.9 and 2.10 show the vertical profile of the horizontal velocities for 3 different shear rates and three different egg sizes, respectfully. Figure 2.11 shows a non-dimensionalized vertical velocity profile of the horizontal velocities. The distance in the x axis is non-dimensionalized by the shear rate, α and the horizontal velocity, U_x and the distance in the y axis is non-dimensionalized by the radius of the egg, R_{egg}

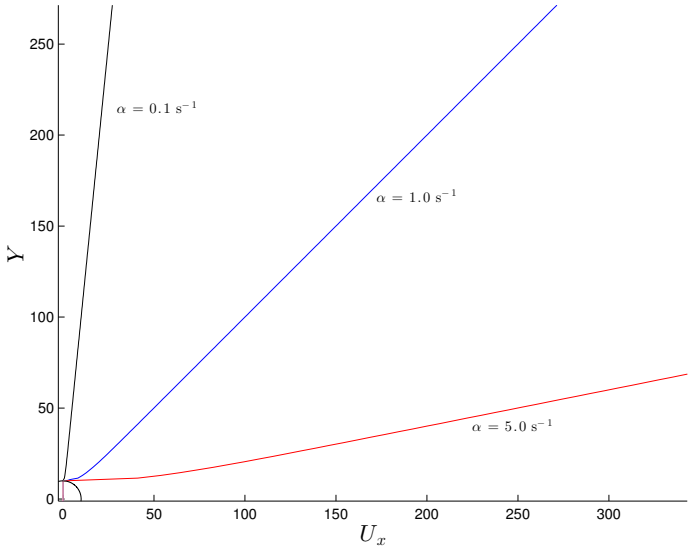

Figure 2.9: The effect of α on the velocity $\boldsymbol{U}_x$ for a given egg radius taken from a slice at $x = 0$. As the shear increases, the velocities increase for a given y value, following the equation $\boldsymbol{U}_x = \alpha \boldsymbol{y}$.

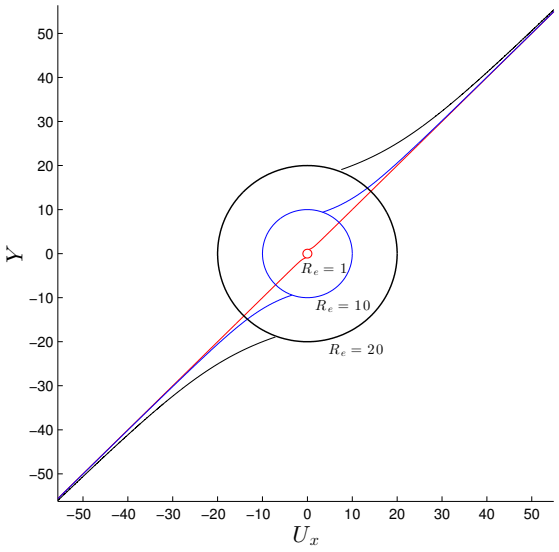

Figure 2.10: The impact of the size of the egg on the velocity field. As R_{egg} increases, the behavior remains the same, but is scaled according to the size of the egg.

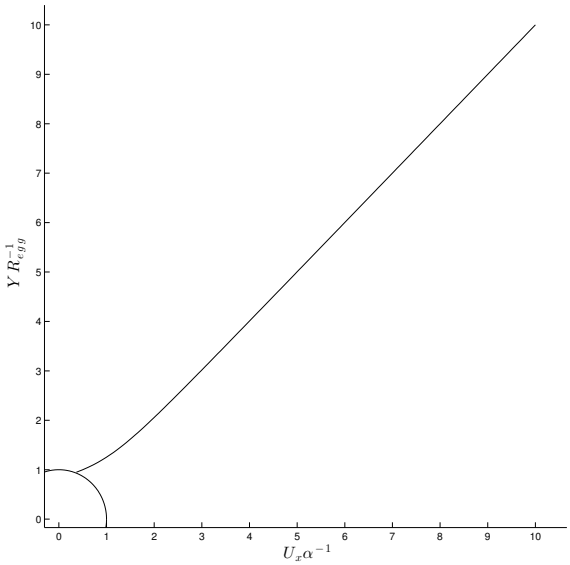

Figure 2.11: Non-dimensionalized plot of the impact of α and R_{egg} on the flow. This reiterates that when the y position is scaled by R_{egg}, the behavior is the same.

In the model, two shear rates are tested: $\alpha = 0.5$ and 1.25 sec^{-1}. Both the shear rate and the orientation of the shear are held constant. The domain is considered infinite.

2.2.2 Complex Flows

We also consider a more complex flow that is intended to mimic the behavior of an egg in turbulence. Within such a flow, the smallest vortices, where the egg lies, are constantly evolving. They have a short lifespan, on the order of seconds, and as they dissipate, another vortex picks up the egg [23]. An egg in an unsteady turbulent flow field experiences a linear shear whose direction and magnitude evolve with time. In this model, the size of the vortices will be held constant.

2.2.3 $\phi(t)$, Angle of Shear

The orientation of the shear varies with time. For the complex flows, the angle of the shear is modeled using a random-walk approach give by:

$$\phi_{\text{new}} = \phi_{\text{old}} + \Delta\phi \cdot dt \tag{2.11}$$

$$\Delta\phi = \boldsymbol{Z}\sigma_{\phi} \tag{2.12}$$

where $\boldsymbol{Z}$ is a normally distributed random number with mean 0 and standard deviation σ_{ϕ}. Each angle is taken as the modulus of 2π, keeping the angles in the range $[0, 2\pi]$. The standard deviation (σ_{ϕ}) was chosen to be $\pi/10$ for the simulations. The rate of change of ϕ at one standard deviation is π rad/sec. A representative set of values for ϕ is shown in Fig. 2.12. The function is created for the range of times needed to create the complex flow. The same $\boldsymbol{\phi}(t)$ is used for both of the complex flows.

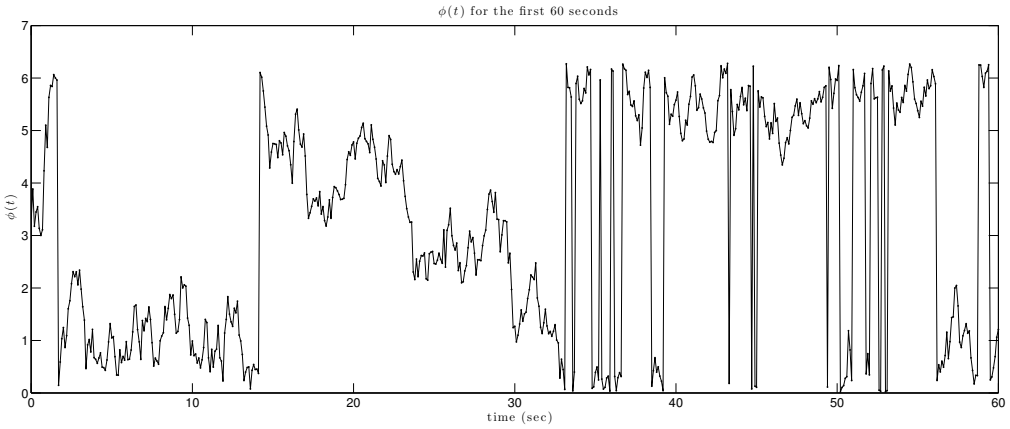

Figure 2.12: A sample of the function describing how the angle of the shear changes with time. At each discrete point in time, an angle is chosen to describe the orientation of the shear.

2.2.4 $g(t)$, Evolution of α

The magnitude of the shear is also varied as a function of time.This expression determines the complexity of the flow. It is a simple sinusoidal function with a set amplitude, α_{amp}, to define the maximum absolute shear rates and a period, α_{period}, to determine the frequency of the sinusoid. The period was chosen to be 60 sec and the amplitudes, α_{amp}, were: $\alpha_{\text{amp}} = 1.25$ sec^{-1} for the morecomplex case and $\alpha_{\text{amp}} = 0.5$ sec^{-1} for the less complex case. These amplitudes correspond to the constant shear rates used in the simple shear cases. The higher amplitude creates a more complex plume due to enhanced stretching and stirring. Note that the maximum α value is held well below 2 sec^{-1}, the shear strength at which it has been shown that the sperm have increased difficulty attaching to the egg because the egg is rotating too fast [56]. The function for the magnitude of the shear over time is:

$$\boldsymbol{g}(t) = \alpha_{\text{amp}} \sin\left(\alpha_{\text{period}}\, \boldsymbol{t}\right) \tag{2.13}$$

for the duration of the flow, $\boldsymbol{t}$. A portion of the function, $\boldsymbol{g}(t)$ is shown in Fig. 2.13.

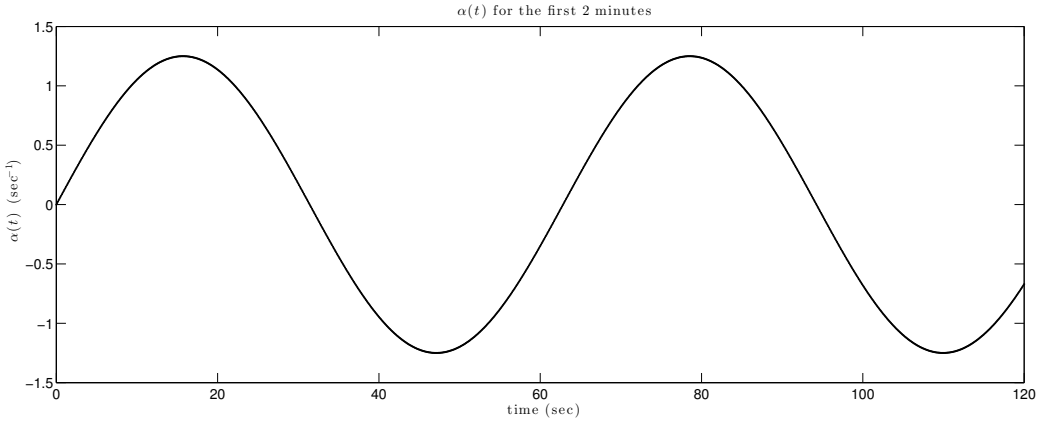

Figure 2.13: A sample of the function varying α with time. At each specified time, a corresponding α is defined. Here, $\alpha_{\text{amp}} = 1.25$ sec^{-1}

2.2.5 $\boldsymbol{h}(r)$, Vortex Decay Function

In order to mimic the shear behavior within a single vortex, a spatial decay is imposed on the shear rate. The decay rate used, Eq. 2.14, corresponds to the decay associated with an Oseen vortex:

$$\boldsymbol{h}(r) = \frac{1}{(\boldsymbol{r}/r_{\text{core}})^2}\left[1 - \exp\left[-\left(\frac{\boldsymbol{r}}{r_{\text{core}}}\right)^2\right]\right] \tag{2.14}$$

where r_{core} is the size of the eddy and r is radial distance.

The parameters and the values or the functions used in the complex flow model are summarized in Table 2.3.

Table 2.3: Flow Input Parameters & Values

Parameter	**Name**	**Value**
Standard deviation for $\boldsymbol{\phi}(t)$	σ_ϕ	$\pi/10$ rad
Orientation of shear	ϕ	$\boldsymbol{\phi}(t)$
Shear rate	α	$\boldsymbol{g}(t)$
Shear strength amplitude	α_{amp}	1.25 and 0.5 sec^{-1}
Period of sinusoid	α_{period}	0.1 sec^{-1}
Radius of vortex core	r_{core}	1.5E 3

2.2.6 Transformation

A transformation matrix is used to rotate the shear for the complex flow cases. The position vectors, $\boldsymbol{x}$ and $\boldsymbol{y}$, that represent the location of each particle of the chemoattractant at time t, are rotated counter-clockwise by the desired angle, ϕ, from the function $\boldsymbol{\phi}(t)$ using a transformation matrix:

$$\begin{bmatrix} \boldsymbol{x}' \\ \boldsymbol{y}' \end{bmatrix} = \begin{bmatrix} \cos(\phi) & \sin(\phi) \\ -\sin(\phi) & \cos(\phi) \end{bmatrix} \begin{bmatrix} \boldsymbol{x} \\ \boldsymbol{y} \end{bmatrix} \tag{2.15}$$

The velocity vectors are calculated from Eqs. 2.6 and 2.7 using the transformed position vectors:

$$\begin{aligned} \boldsymbol{U}_x' = \frac{1}{2}\alpha \boldsymbol{y}' \left[1 - \left(\frac{\boldsymbol{r}}{R_{\text{egg}}}\right)^{-4}\right] + \frac{1}{2}\alpha \boldsymbol{y}' \left[1 - \left(\frac{\boldsymbol{r}}{R_{\text{egg}}}\right)^{-2}\right] ... \\ - 2\alpha \left(\frac{\boldsymbol{x}'}{R_{\text{egg}}}\right)^2 \boldsymbol{y} \left[\left(\frac{\boldsymbol{r}}{R_{\text{egg}}}\right)^{-4} - \left(\frac{\boldsymbol{r}}{R_{\text{egg}}}\right)^{-6}\right] - \frac{\Omega \boldsymbol{y}'}{\left(\frac{\boldsymbol{r}}{R_{\text{egg}}}\right)^2} \end{aligned} \tag{2.16}$$

$$\begin{aligned} \boldsymbol{U}_y' = \frac{1}{2}\alpha \boldsymbol{x}' \left[1 - \left(\frac{\boldsymbol{r}}{R_{\text{egg}}}\right)^{-4}\right] + \frac{1}{2}\alpha \boldsymbol{x}' \left[1 - \left(\frac{\boldsymbol{r}}{R_{\text{egg}}}\right)^{-2}\right] ... \\ - 2\alpha \left(\frac{\boldsymbol{y}'}{R_{\text{egg}}}\right)^2 \boldsymbol{x}' \left[\left(\frac{\boldsymbol{r}}{R_{\text{egg}}}\right)^{-4} - \left(\frac{\boldsymbol{r}}{R_{\text{egg}}}\right)^{-6}\right] - \frac{\Omega \boldsymbol{x}'}{\left(\frac{\boldsymbol{r}}{R_{\text{egg}}}\right)^2} \end{aligned} \tag{2.17}$$

The vectors are then rotated clockwise by the same angle, ϕ

$$\begin{bmatrix} \boldsymbol{U}_x \\ \boldsymbol{U}_y \end{bmatrix} = \begin{bmatrix} \cos(\phi) & -\sin(\phi) \\ \sin(\phi) & \cos(\phi) \end{bmatrix} \begin{bmatrix} \boldsymbol{U}_x{}' \\ \boldsymbol{U}_y{}' \end{bmatrix} \tag{2.18}$$

The velocity vectors are then multiplied by the decay function, $\boldsymbol{h}(t)$, resulting in the velocity field used to describe the flow for the complex flows.

$$\boldsymbol{U}_x = \boldsymbol{U}_x \cdot \boldsymbol{h}(t) \tag{2.19}$$

$$\boldsymbol{U}_y = \boldsymbol{U}_y \cdot \boldsymbol{h}(t) \tag{2.20}$$

In summary, to model the complex flows, at each time step for time t:

(1) An angle, ϕ corresponding to the orientation of the shear is determined from $\boldsymbol{f}(t)$

(2) A magnitude of the shear is chosen according to $\boldsymbol{g}(t)$

(3) The position vectors, $\boldsymbol{x}$ and $\boldsymbol{y}$, of the particles are rotated according to angle ϕ

(4) Equations 2.6 and 2.6 are solved to find $\boldsymbol{u}'_x$ and $\boldsymbol{u}'_y$ using the prescribed α value and the transformed position vectors, $\boldsymbol{x}'$ and $\boldsymbol{y}'$

(5) The velocity vectors are rotated in the opposite direction and returned to the axes before the transformation as $\boldsymbol{U}_x$ and $\boldsymbol{U}_y$.

Equations for the velocity ($\boldsymbol{U}_x$ and $\boldsymbol{U}_y$), calculated for the simple shear cases or the complex cases, are added to the calculations used to diffuse the particles from Eqs. 2.2 and 2.3 to describe the movement of the particles that represent the mass of chemoattractant in a flow:

$$\boldsymbol{x}_n = \boldsymbol{x}_{n-1} + \boldsymbol{U}_x(\boldsymbol{x}_{n-1})dt + \boldsymbol{Z}\sqrt{2Ddt} \tag{2.21}$$

$$\boldsymbol{y}_n = \boldsymbol{y}_{n-1} + \boldsymbol{U}_y(\boldsymbol{y}_{n-1})dt + \boldsymbol{Z}\sqrt{2Ddt} \tag{2.22}$$

2.2.7 Binning Process

A binning process is used to calculate the spatial distribution of concentration from the simulations. A uniform grid is constructed in the region of interest where concentrates are calculated. The grid is made up of uniform bins and the number of particles within each bin is counted. Using the geometry and dimensions of the individual bins, as well as the mass represented by each particle, a concentration in units of $[\frac{\text{mol}}{\text{area}}]$ is determined. The domain is measured from $-scale$ to $scale$. The length of each side of the bins, wid_bin, is equal and is calculated based on the variable num_bin, the number of bins that span one egg diameter.

$$wid\_bin = 2/((1/R_{\text{egg}}) \times num\_bin)$$

The binning code produces a matrix of values, representing the number of particles in each bin (Fig. 2.14).

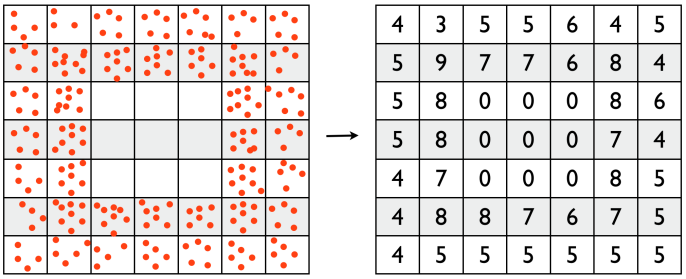

Figure 2.14: On the left, the particles are captured within bins. The right shows the resulting matrix where each number represents the number of particles in that location.

This matrix is then multiplied by the mass of each particle, divided by the area of the bin (wid_bin^2), normalized by δ, and converted into units of : $[\frac{\text{mol}}{\text{L}}]$:

$$C = \begin{bmatrix} 4 & 3 & 5 & 5 & 6 & 4 & 5 \\ 5 & 9 & 7 & 7 & 6 & 8 & 4 \\ 5 & 8 & 0 & 0 & 0 & 8 & 6 \\ 5 & 8 & 0 & 0 & 0 & 7 & 4 \\ 4 & 7 & 0 & 0 & 0 & 8 & 5 \\ 4 & 8 & 8 & 7 & 6 & 7 & 5 \\ 4 & 5 & 5 & 5 & 5 & 5 & 5 \end{bmatrix} \cdot \text{M}_{\text{particles}}(\text{mol}) \left(\frac{1}{wid\_bin^2(\mu\text{m})^2}\right) \left(\frac{1}{\delta(\mu\text{m})}\right) \left(\frac{1\mu\text{m}^3}{1\text{E}-15\text{L}}\right) \quad (2.23)$$

Recall that $\text{M}_{\text{particles}} = \dot{M}/(Np/dt)$ and δ is the aforementioned band used in Eq. 2.1. From this concentration matrix, concentration images can be created in Matlab. Additionally, gradient vectors can be calculated from these matrices. Each value in the matrix is the average concentration within its corresponding bin. This value is considered to be located at the center of each bin. An x-direction and a y-direction change in concentration over the distance between the center of the bins surrounding it can be calculated. The hypotenuse of these two components represents the

gradient within each bin. The parameters used in the binning process are provided in Table 2.4.

Table 2.4: Concentration Input Parameters

Parameter	**Name**
Domain length, from center	*scale*
Bins across an egg diameter	*num_bin*
Width of a bin	*widbin*

2.2.7.1 Concentration and Gradient Field Images

Concentration images and gradients for the quiescent flow (Figs 2.15 and 2.16) and simple shear flow (Figs 2.17 and 2.18) created using the binning procedure above are shown. Figures 2.19 and 2.20 show snapshots of the concentration fields for the 2 complex flows at different times.

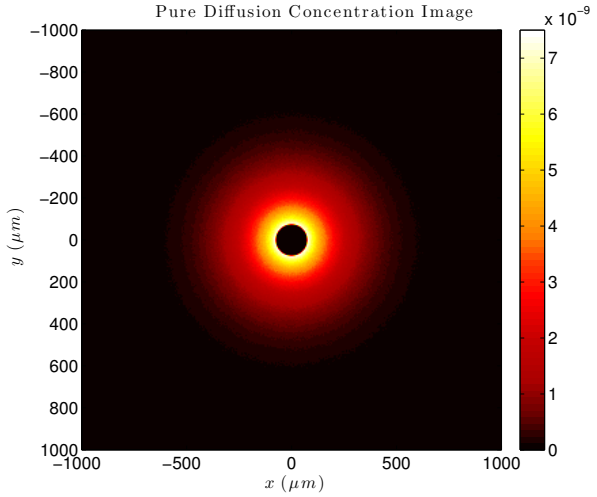

Figure 2.15: Image representing the attractant plume (in units of mol μm^{-3}) after 1 minute of flux in a quiescent flow.

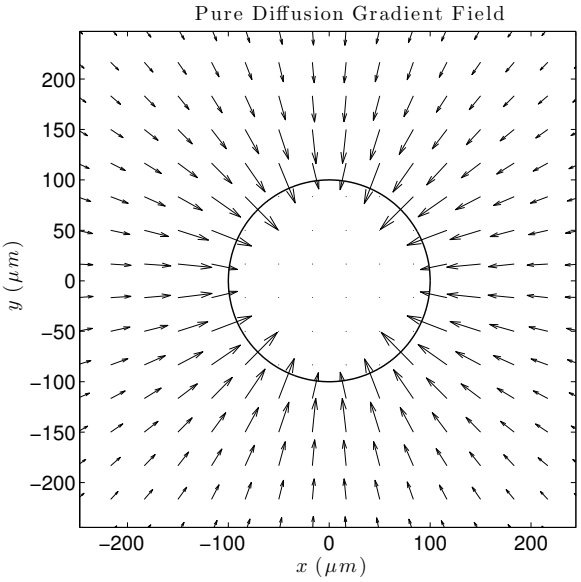

Figure 2.16: The resulting gradient from the concentration field created from the image above (Fig. 2.15).

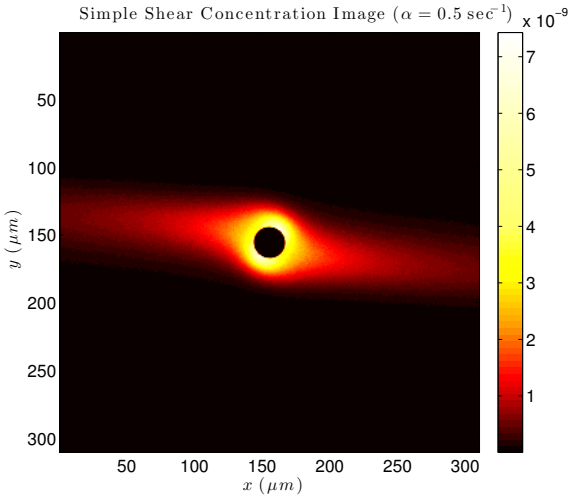

Figure 2.17: Image representing the attractant plume (in units of mol $\mu\mathrm{m}^{-3}$) in a simple shear flow, ($\alpha = 0.5\ \mathrm{sec}^{-1}$) after 1 minute of chemoattractant flux.

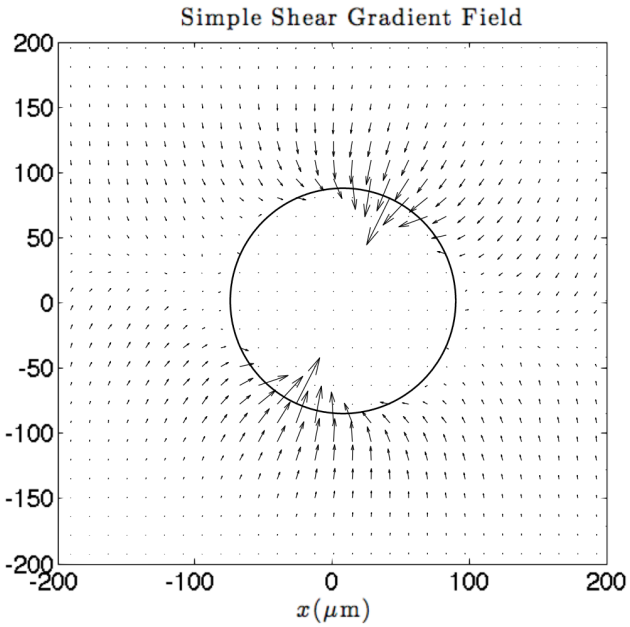

Figure 2.18: Resulting gradient from the concentration image field created by a simple shear flow (Fig. 2.17). The image is magnified to show the gradient near the egg.

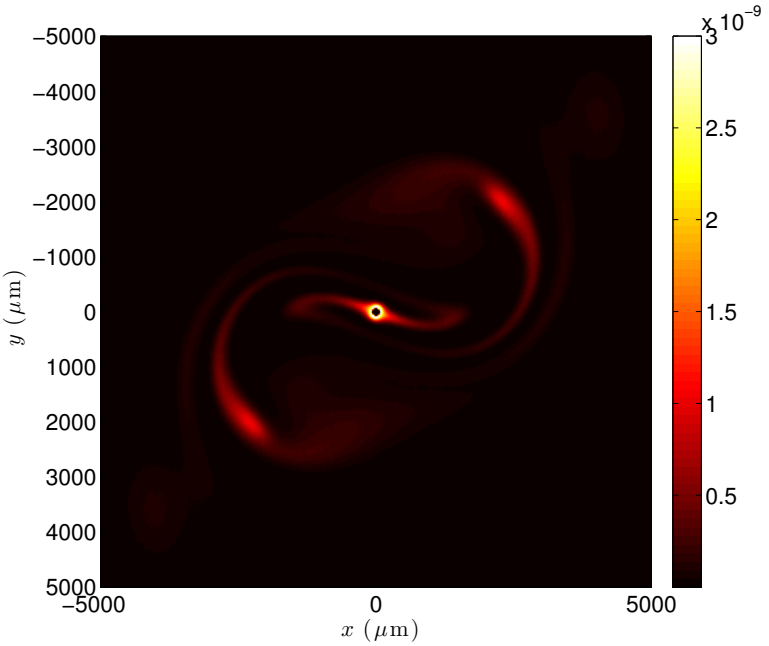

Figure 2.19: Snapshot concentration (in units of mol $\mu\mathrm{m}^{-3}$) image of the attractant plume in high complex flow.

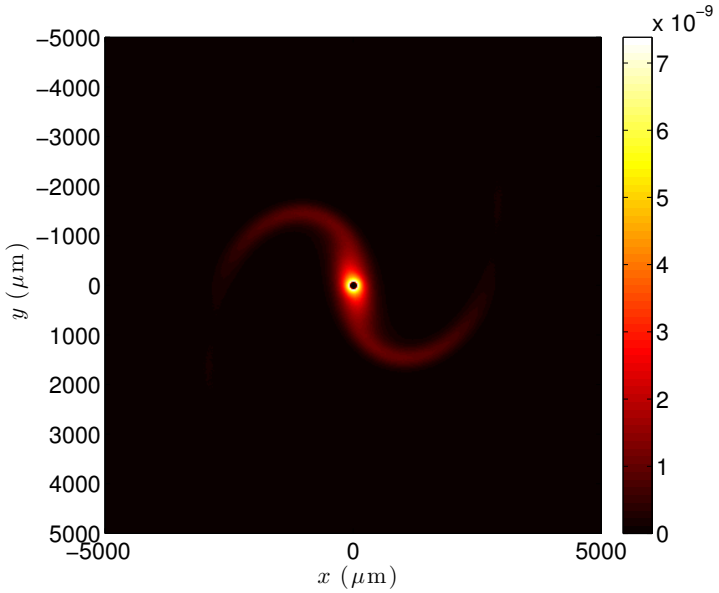

Figure 2.20: Snapshot concentration image (in units of mol μm^{-3}) of the attractant plume in a low complex flow.

2.3 Fertilization Model

For each flow case, the concentration and flow model produces concentration and gradient fields (Figures 2.16 - 2.20) that represent the plume concentrations. A mass of sperm are placed at an initial location and then advect with the flow and swim according to their prescribed behavior, sensing the local concentrations and gradients. The location of each sperm at each time-step corresponds to a concentration and gradient value: the sperm are binned using the same grid used to bin the concentration of the chemoattractant (Fig 2.21).

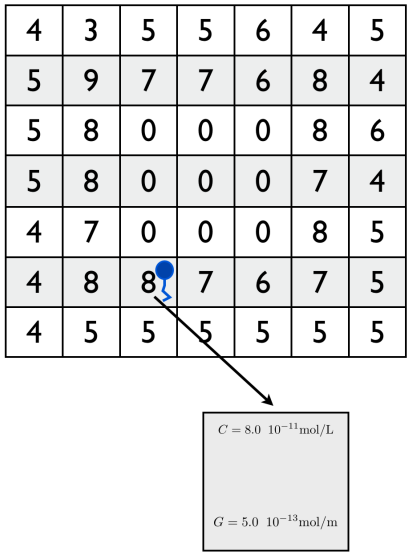

Figure 2.21: An example of a binned sperm. The sperm is then associated with a concentration value and a gradient value.

If the sperm's location corresponds to a level below the threshold ($1E-9$ mol L^{-1}), the sperm swim according to their loitering behavior. If the location belongs to a concentration equal to or above the threshold level, the sperm transition into a response behavior. The sperm then swim according to the chosen response. If the sperm moves to a location of lower concentration, the sperm will exit the response strategy and return to the loitering behavior. Each sperm is also noted as being either inside or outside of the egg boundary. This produces a matrix that identifies when and if each sperm has reached the egg. That matrix is then processed (Section 2.4) to analyze the results and determine the success rate and total fertilization rate.

In general, the loitering swimming behavior resembles drifting circles. The modifications to this swimming pattern are in Section 2.3.1. Three different response behaviors are examined in this study: 1. Drifting Circle, the sperm are only chemotactic and can control their direction, 2. Turn and Run, the sperm can control both direction and speed, and 3. Run, the sperm are able to exit a circling pattern and perform a run, controlling both speed and direction. They are explained further in Sec. 2.3.2.

The sperm are modeled as individual particles using the particle-tracking method. They

move according to the flow,$\boldsymbol{U}_x$ and $\boldsymbol{U}_y$ and their swimming velocity, $\boldsymbol{u}_{\text{sperm}}$ and $\boldsymbol{v}_{\text{sperm}}$:

$$\boldsymbol{x}_{\boldsymbol{s}_n} = \boldsymbol{x}_{\boldsymbol{s}_{n-1}} + \boldsymbol{U}_x(\boldsymbol{x}_{\boldsymbol{s}_{n-1}})dt + (\boldsymbol{u}_{\text{sperm}})(\boldsymbol{x}_{\boldsymbol{s}_{n-1}})dt \tag{2.24}$$

$$\boldsymbol{y}_{\boldsymbol{s}_n} = \boldsymbol{y}_{\boldsymbol{s}_{n-1}} + \boldsymbol{U}_y(\boldsymbol{y}_{\boldsymbol{s}_{n-1}})dt + (\boldsymbol{v}_{\text{sperm}})(\boldsymbol{y}_{\boldsymbol{s}_{n-1}})dt \tag{2.25}$$

where $\boldsymbol{x}_{\boldsymbol{s}}$ and $\boldsymbol{y}_{\boldsymbol{s}}$ are now the position vectors for the sperm, $\boldsymbol{U}_x$ and $\boldsymbol{U}_y$ are still the velocity vectors calculated for the flow and $\boldsymbol{u}_{\text{sperm}}$ and $\boldsymbol{v}_{\text{sperm}}$ are determined by a combination of the swimming velocity superimposed with the drifting parameters:

Swimming:

$$\theta_{\text{new}} = \theta_{\text{old}} + \dot{\theta} \cdot dt$$

$$\text{swim}_x = \boldsymbol{u}_{\text{swim}} \cdot \cos(\theta) \cdot dt$$

$$\text{swim}_y = \boldsymbol{u}_{\text{swim}} \cdot \sin(\theta) \cdot dt$$

Drifting:

$$\text{drift}_x = \boldsymbol{u}_{\text{drift}} \cdot \cos(\theta_{\text{drift}}) \cdot dt$$

$$\text{drift}_y = \boldsymbol{u}_{\text{drift}} \cdot \sin(\theta_{\text{drift}}) \cdot dt$$

Total sperm swimming:

$$\boldsymbol{u}_{\text{sperm}} = \text{swim}_x + \text{drift}_x$$

$$\boldsymbol{v}_{\text{sperm}} = \text{swim}_y + \text{drift}_y$$

Hence,

$$\boldsymbol{x}_{\text{new}} = \boldsymbol{x}_{\text{old}} + \boldsymbol{u}_{\text{sperm}} \tag{2.26}$$

$$\boldsymbol{y}_{\text{new}} = \boldsymbol{y}_{\text{old}} + \boldsymbol{v}_{\text{sperm}} \tag{2.27}$$

When flow is added, the final equation to describe the movement of the sperm is the same as Eqs. (2.24 and 2.25):

$$\boldsymbol{x}_{\text{new}} = \boldsymbol{x}_{\text{old}} + \boldsymbol{u}_{\text{sperm}} dt + \boldsymbol{U}_x \cdot dt \tag{2.28}$$

$$\boldsymbol{y}_{\text{new}} = \boldsymbol{y}_{\text{old}} + \boldsymbol{v}_{\text{sperm}} dt + \boldsymbol{U}_y \cdot dt \tag{2.29}$$

We chose 8 initial locations in each flow to analyze the sensitivity to location. Two radial distances, one considered close and one considered far are chosen. These locations are sufficient for the symmetric pure diffusion case, but for the remained flows, 3 equally spaced locations are tested around the egg for each distance. The initial locations are listed below in Table 2.5.

Table 2.5: Initial Locations

Flow	**Close**	**Far**
Pure Diffusion	$(0, 4R_{\text{egg}})$	$(0, 12R_{\text{egg}})$
Sheared Flows (4)	$(0, 4R_{\text{egg}})$	$(0, 12R_{\text{egg}})$
	$(0, -4R_{\text{egg}})$	$(0, -12R_{\text{egg}})$
	$(-4R_{\text{egg}}, 0)$	$(-12R_{\text{egg}}, 0)$
	$(0, 4R_{\text{egg}})$	$(0, 12R_{\text{egg}})$

The sperm are introduced into each flow after the flows have reached a quasi-steady state. The condition of the flow when the sperm are added and the development of the flow throughout the simulation are depicted in Table 2.6:

Table 2.6: Conditions of flow for sperm's entry

Flow	**Time**	**State**	**Simulation**
Pure Diffusion	10 min	Quasi- Steady	Constant
Simple Shear ($\alpha = 0.5$ sec^{-1})	5 min	Quasi- Steady	Constant
Simple Shear ($\alpha = 1.25$ sec^{-1})	5 min	Quasi- Steady	Constant
Less Complex ($\alpha_{\text{amp}} = 0.5$ sec^{-1})	3 min	Quasi-Steady	Evolving
More Complex ($\alpha_{\text{amp}} = 1.25$ sec^{-1})	3 min	Quasi-Steady	Evolving

The quiescent and simple shear flow cases all have a constant concentration field for the duration of the fertilization simulations. For each case, after enough time has passed, the concentration profile does not change significantly enough to warrant a developing concentration field.

For the quiescent case, after 10 minutes, this steady behavior is maintained as is shown in a radial concentration profile for a range of times (Fig. 2.22) and two concentration images following 10 and 12 minutes of chemoattractant release (Fig. 2.23). For the two shear cases, the concentration surrounding the egg is relatively unchanged following 2 minutes of flux and flow as shown in radial concentration profiles taken along both the x and y axes for both shear rates (Figs 2.24 and 2.25) and comparing concentration images taken after 2 minutes of flux with images after 4 minutes of flux (Fig. 2.26).

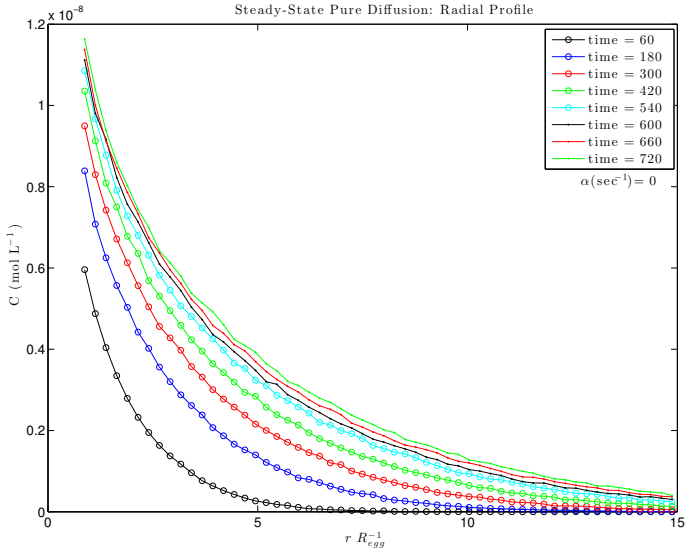

Figure 2.22: Steady-state radial plots averaged along both axes show that the radial distribution of the concentrations do not change significantly over time for the quiescent flow (pure diffusion) case.

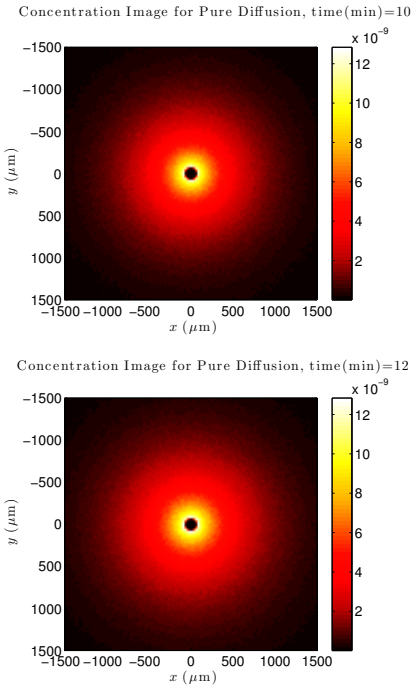

Figure 2.23: Concentration (in units of mol μm^{-3}) images at two late points in time highlight the limited change over time.

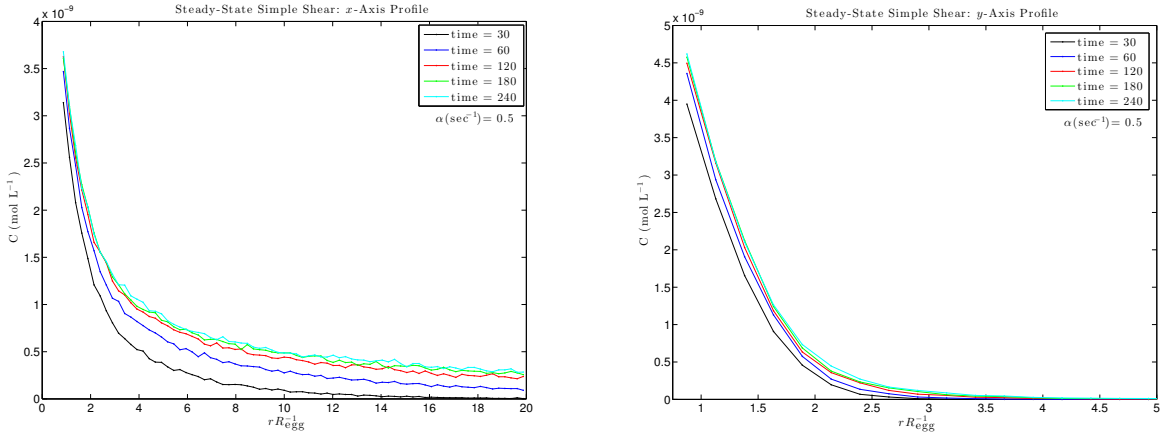

Figure 2.24: Steady-state radial plots along both axes show that the radial distribution of the concentrations do not change significantly over time for the low shear rate after 2 minutes have passed for the low shear rate.

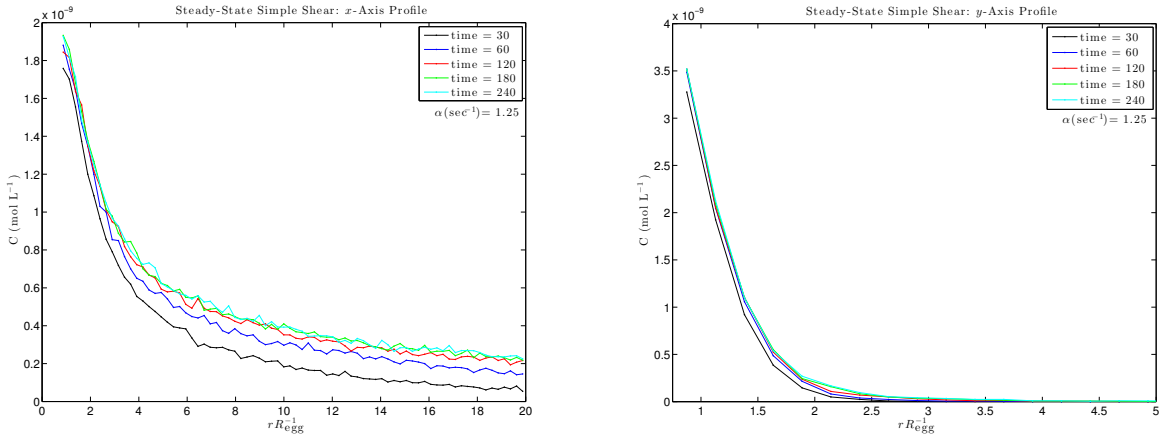

Figure 2.25: Steady-state radial plots along both axes show that the radial distribution of the concentrations do not change significantly over time for the high shear rate following 2 minutes of release in a linear shear flow with the high shear rate.

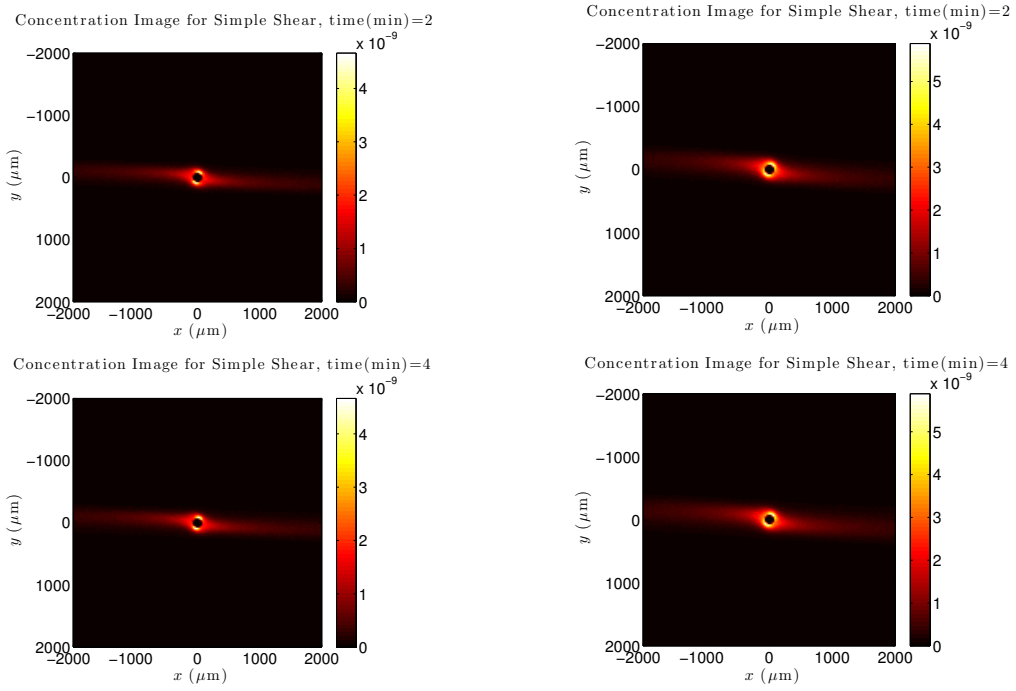

Figure 2.26: Concentration images (in units of mol μm^{-3}) at two late times also indicate limited change in the concentration field for either shear case.

The starting times of the two complex cases were chosen after the simulations appeared to reach a quasi-steady-state. Although the exact concentration images will not be duplicated at later

points in time, the general state and development of the plume is considered steady.

2.3.1 Loitering Behavior

The flick of the flagellum is the only method sperm use to swim. The flicking causes the sperm to complete circles. As the rate at which these circles are completed is not held constant, this change in rate produces a net movement. This is perceived as a drifting circle. In this model, the resulting drifting circle and the rate the turns are completed are considered separate parameters. These parameters can be altered in both the loitering and the response behaviors. The path of the drift is random. There is variation on the drifting speed, the direction of the drift and the rate of turn to complete the circles. The sperm are given initial conditions and then, at each time-step, these parameters are altered according to the given variation parameters. The parameters are presented in Table 2.7. The actual values used in the simulation are shown later in Table2.8.

Table 2.7: Loitering Sperm Input Parameters

Parameter	**Name**
Swimming velocity	u_{swim}
Swimming direction	θ
Turning rate	$\dot{\theta}$
Drift direction	θ_{drift}
Drift velocity	u_{drift}
Standard deviation for drifting direction variation	$\sigma_{\theta_{\text{drift}}}$
Standard deviation for drifting speed variation	$\sigma_{u_{\text{drift}}}$
Standard deviation for turning rate	$\sigma_{\dot{\theta}}$

2.3.1.1 Initial Conditions

When the mass of sperm are placed at one point, each sperm is given an initial swimming speed, u_{swim}, swimming direction, θ, drifting speed, u_{drift}, drifting direction, θ_{drift} and turning rate, $\dot{\theta}$. Each directional parameter is randomly chosen from a uniform distribution within the range $[0, 2\pi]$. Both speeds are prescribed and represent an average speed from previous studies where the speed was quantified. The swimming speed dictates the speed the sperm swim to complete the circles. The drifting speed dictates the speed at which the sperm move along the given drifting

path. Finally, the turning rate, in conjunction with the swimming speed, determines the size and duration of the circles. The turning rate is in units of $[\frac{\text{Rad}}{T}]$ and represents the angle added to the previous angle at each time step. For a real sperm, this rate is periodic, resulting in the drifting circle. For this simulation, this rate will be a constant, with a possible variation. The initial parameters are depicted in Figs. 2.27- 2.29.

θ (Swimming Direction):

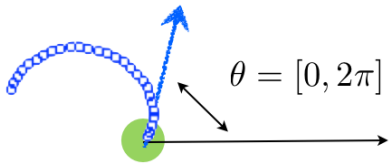

Figure 2.27: The starting direction each sperm swims in once the simulations is initiated. Each sperm is provided an initial θ from a random distributions ranging from 0 to π. From there, the sperm will continue to swim to complete a circle while drifting.

θ_{drift}, (Drift Direction):

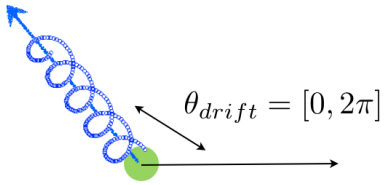

Figure 2.28: The direction of the drift. Each sperm is provided an initial θ_{drift} from a random distributions ranging from 0 to π. From there, the sperm will continue to swim on this path, though the directional parameter has the potential to vary at each time-step.

$\dot{\theta}$ (Turning Rate) and u_{swim} (Swimming Speed):

Each sperm is given a $\dot{\theta}$ and u_{swim} value . This value is the same for each sperm initially. The u_{swim} will remain constant for the loitering sperm, but $\dot{\theta}$ is varied at each time step.

(1) Radius of Circle: $\frac{u_{\text{swim}}}{\dot{\theta}} = R_{\text{drift circle}}$

(2) Time To Complete: $\frac{6sec}{\dot{\theta}} = T_{\text{circle}}$

(3) Ratio of $u_{swim} : \dot{\theta}$ maintains the radius of the circles

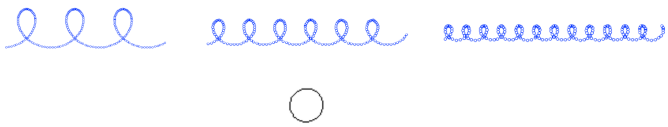

Figure 2.29: The path of a 3 sperm that all have the same swimming speed and drifting speed (u_{swim} and u_{drift}), but the $\dot{\theta}$ value is increased across the figure: 0.5, 1, 1.5 rad/sec. The size of the egg (100 μm) is shown below for comparison.

2.3.1.2 Alterations

It is possible to allow variations on any of these parameters throughout the simulation. Without doing so, the same swimming speed, drifting direction, drifting speed and turning rate are all maintained at every time-step. Figure 2.30 depicts the drifting circles without any alterations. The green dot indicates the starting point and the red dot shows the end point. The blue circles capture the sperm location every tenth of a second. Following are schematics of the alterations on the drift direction (Fig. 2.31), the drift speed (Fig. 2.32) and the turning rate (Fig. 2.33).

Base:

Figure 2.30: The path of a sperm without permitting any variations on the parameters. The green dot and the red dot indicate the start and end of the path.

Drift Direction, θ_{drift} ($\sigma_{\theta_{\text{drift}}}$) :

Figure 2.31: Examples of a sperm path with variation only on the drifting direction. The sperm in each path had all the same initial and swimming parameters and variation only on the drifting direction.

$\sigma_{\theta_{\text{drift}}}$ is a predetermined value that can control the variation on θ_{drift} at every time-step by the equations:

$$\Delta\theta_{\text{drift}} = \pi\Lambda \cdot \sigma_{\theta_{\text{drift}}} \tag{2.30}$$

$$\theta_{\text{drift}_{\text{new}}} = \theta_{\text{drift}_{\text{old}}} + \Delta\theta_{\text{drift}} \cdot dt \tag{2.31}$$

where Λ is a number chosen from the triangle distribution with a maximum of 1, a minimum of -1 and a mean of 0. Equation 2.32 produces a $\Delta\theta$ that ranges from $-\pi$ to π multiplied by the standard deviation value. The possible standard deviations range from 0, where $\Delta\theta$ would be held at 0 resulting in no change, to 1, where the largest absolute $\Delta\theta$ possible is π. This maintains a reasonable ability of the sperm to change directions. The largest possible change in 1 second is π radians.

Drift Speed, u_{drift} ($\sigma_{u_{\text{drift}}}$) :

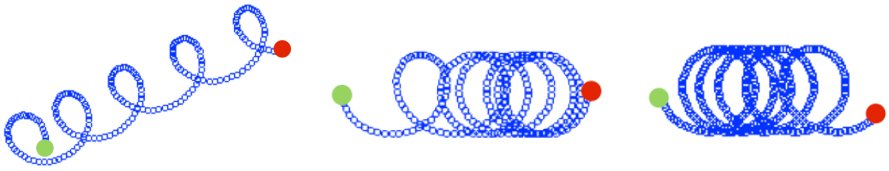

Figure 2.32: Examples of sperm paths with variation only on the drifting speed. The sperm in each path had all the same initial and swimming parameters and variation only on the drifting speed.

$\sigma_{u_{\text{drift}}}$ is a predetermined value that controls how the u_{drift} parameter can be altered at each

time-step. This is accomplished by the following equations:

$$\Delta u_{\text{drift}} = u_{\text{drift}} \Lambda \cdot \sigma_{u_{\text{drift}}} \tag{2.32}$$

$$u_{\text{drift}_{\text{new}}} = u_{\text{drift}_{\text{old}}} + \Delta u_{\text{drift}} \cdot dt \tag{2.33}$$

where, again, Λ is a number chosen from the triangle distribution with a maximum of 1, a minimum of -1 and a mean of 0. Equation 2.32 maintains the range of possible changes in the drifting speed with the u_{drift}, Λ and $\sigma_{u_{\text{drift}}}$ values. The possible $\sigma_{u_{\text{drift}}}$ values range between 0, where Δu_{drift} would always be 0, and 1, where the maximum change in the drifting speed within 1 second can be exactly the drifting speed. The $\sigma_{u_{\text{drift}}}$ value used was chosen to permit a reasonable, previously observed approximate change in speed.

Turning Rate, $\dot{\theta}$ ($\sigma_{\dot{\theta}}$):

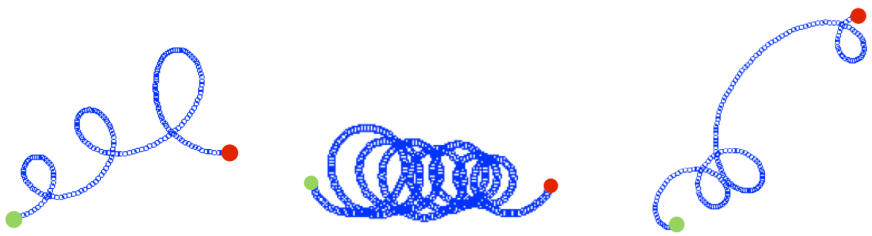

Figure 2.33: Examples of sperm paths with variation only on the turning rate. The sperm in each path had all the same initial and swimming parameters and variation only on the turning rate.

$\sigma_{\dot{\theta}}$ is a predetermined value that has the ability to change the $\dot{\theta}$ value at every time-step by the following calculations:

$$\Delta \dot{\theta} = \dot{\theta} \Lambda \cdot \sigma_{\dot{\theta}} \tag{2.34}$$

$$\dot{\theta}_{\text{new}} = \dot{\theta}_{\text{old}} + \Delta \dot{\theta} \cdot dt, \tag{2.35}$$

where, again, Λ is a number chosen from the triangle distribution with a maximum of 1, a minimum of -1 and a mean of 0. For a range of $\sigma_{\dot{\theta}}$ between 0 and 1, this allows the largest change in the turning rate to be $\dot{\theta} \cdot \sigma_{\dot{\theta}}$ in one second.

The loitering paths of the sperm are described by Eqs 2.26 and 2.27, where at every time-step, each parameter that makes up u_{sperm} and v_{sperm} can be altered as described above. The actual values used, unless otherwise specified are shown below in Table 2.8.

Table 2.8: Loitering Sperm Input Parameters: Values

Parameter	**Value**
u_{swim}	150 μm sec^{-1}
$\dot{\theta}$	3.5 rad sec^{-1}
u_{drift}	25 μm sec^{-1}
$\sigma_{\theta_{\text{drift}}}$	$2\pi/10$
$\sigma_{u_{\text{drift}}}$	$\pi/10$
$\sigma_{\dot{\theta}}$	$\pi/10$

2.3.2 Stimulated Behaviors

The possible responses the sperm can when they are stimulated are based on observed reactions. The response to the chemoattractant can impact both speed and directional behaviors. Chemotaxis is a directional response, allowing sperm to control their direction in line with a gradient. Chemokinesis is a speed response, allowing sperm to increase their speed in a gradient. It has never been clearly defined which of these aspects the sperm posses, how this impacts their swimming behavior or what abilities are necessary for successful fertilization in different flows. The three possible stimulated behaviors tested in this study (1. Drifting Circles, 2. Turn and Run and 3. Run) attempt to provide a better understanding of the mechanics. A Base behavior, or no response, is also tested for comparison. The changed parameters due to the change in swimming behavior are summarized below each behavior under the 'Parameters' heading. Within each behavior, there are a variety of parameters that can be altered. Within each behavior, the sensitivity to these behaviors will be examined. The results are shown in Sec. 3.5. These 'Test Parameters' are listed beneath each description of the individual response behaviors. Additionally, the efficacy of each

response in each flow is analyzed. The results are presented Table 2.9. Following the discussion, the values used are shown in Table 2.10

Table 2.9: Response Sperm Input Parameters

Parameter	Name
Drift speed range	$[u_{\text{drift}_{\text{low}}}, u_{\text{drift}_{\text{high}}}]$
Swim range	$[u_{\text{swim}_{\text{low}}}, u_{\text{swim}_{\text{high}}}]$
Turning rate range	$[\dot{\theta}_{\text{low}}, \dot{\theta}_{\text{high}}]$
Reduction on the variation on θ_{drift}	γ

Base Response: The sperm have no response to the threshold concentration, and their initial behaviors are preserved throughout the simulation.

1. Drifting Circles Response: This response models the observed sperm that do not alter their speed when stimulated, analyzing the effect on the ability of the sperm to reach the egg if they do not possess chemokinetic abilities. In actuality, this would indicate that the rate the sperm flick their flagellum is controlled in a manner to control direction, but does not result in a change in speed. This results from the perceived ability of a sperm to suppress the reaction causing a change in the flicking pattern, allowing a symmetric beating and a controlled path. As the sperm turns away from the gradient, the turning rate increases and then decreases as the sperm goes down gradient. The ratio between these changes results in the appearance of drifting circles, with no change in the distance gained. In terms of this model, once a sperm encounters a sufficient gradient, it maintains the same drifting circle pattern, but the variation on the θ_{drift} parameter, now referred to as $\sigma_{\theta_{\text{stim}}}$, is immediately reduced and aligns with the gradient. This reduction value γ_1, controls the range of the new $\sigma_{\theta_{\text{stim}}}$ value. It reduces the maximum variation on the path of the sperm once it is stimulated. The drift alignment is relative, so it becomes more accurate as the gradient increases. The path becomes more in line with the gradient with less variation on the direction. The variation on the drifting direction, $\sigma_{u_{\text{drift}}}$ is set to 0 to avoid any undue increase in drifting speed due to variation. The variation on the turning rate, $\sigma_{\dot{\theta}}$, is also immediately reduced to 0 to ensure reasonable turning rates do not change during stimulation. At the highest gradient,

this response would relate to a perfectly aligned circle with a path pointing down gradient and no variation on the drifting speed. This simulates the sperm's control of its turning rate and directional sense once it is stimulated. This behavior is depicted in Fig. 2.34.

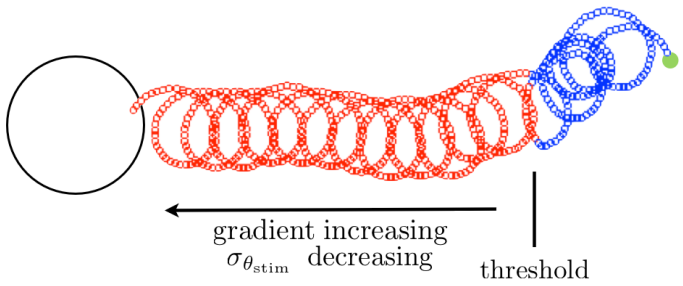

Figure 2.34: An example of a sperm path with the circle response. The loitering behavior is in blue, and the stimulated response path is shown in red. This color code is duplicated in the remained two response images.

Parameters:

(1) u_{swim}, θ : Unchanged

(2) $\sigma_{u_{\text{drift}}} = 0$: The drifting speed is maintained

(3) $\sigma_{\dot{\theta}} = 0$: The turning rate is maintained

(4) $\sigma_{\theta_{drift}} = \sigma_{\theta_{\text{stim}}}$: Factor on the standard deviation controlling the variation on the path of the sperm that navigate down gradient. This value is initially reduced:

$$\sigma_{\theta_{\text{stim}}} = \gamma_1 \cdot \sigma_{\theta_{\text{drift}}}$$

(5) θ_{drift}: chosen at each time-step by the calculations:

$$\Delta_{\theta_{\text{drift}}} = \sigma_{\theta_{\text{stim}}} \cdot \pi \mathbf{\Lambda}$$

$$\theta_{\text{drift}_{\text{new}}} = \theta_{\text{drift}_{\text{old}}} + \Delta_{\theta_{\text{drift}}} \cdot dt$$

where $\mathbf{\Lambda}$ is a number chosen from a triangle distribution with minimum of -1, a maximum of 1 and a center of 0. This allows the variation on the drifting direction to decrease as the gradient increases. Whereas the loitering range for the change in the direction was controlled by $\pi\sigma_{\theta_{\text{drift}}}$ and could range from $-\pi\sigma_{\theta_{\text{drift}}}$ to $\pi\sigma_{\theta_{\text{drift}}}$, it is now controlled by a decreased range. This range is decreased immediately by γ and continues to decrease as the gradient increases.

(6) θ: Calculated as in the loitering behavior:

$$\theta_{\text{new}} = \theta_{\text{old}} + \dot{\theta} \cdot dt$$

Once each parameter is set, the sperm in this response swim according the the equation:

$$\boldsymbol{u}_{\text{sperm}} = \boldsymbol{u}_{\text{swim}}\cos(\theta) \cdot dt + \boldsymbol{u}_{\text{drift}}\cos(\theta_{\text{drift}}) \cdot dt \tag{2.36}$$

$$\boldsymbol{v}_{\text{sperm}} = \boldsymbol{u}_{\text{swim}}\sin(\theta) \cdot dt + \boldsymbol{u}_{\text{drift}}\sin(\theta_{\text{drift}}) \cdot dt \tag{2.37}$$

Test Parameters:

(1) Immediate reduction factor: γ

2. Turn & Run: This response depicts a sperm with both chemotactic and chemokinetic abilities. The sperm still maintains the drifting circle behavior, but both the orientation and the speed are changed due to the stimulus. As the gradient increases, the variation on the path decreases and the drifting speed increases and the curvature is decreased by decreasing the turning rate. As in the Drifting Circle Response, once the gradient is sensed, the sperm maintains the same drifting circle pattern, but the $\sigma_{\theta_{\text{drift}}}$, now referred to as $\sigma_{\theta_{\text{stim}}}$, is immediately reduced by a factor of γ_2. It is then further decreased with an increasing gradient. The drifting speed is now confined within a specified range, $[u_{\text{drift}_{\text{low}}}, u_{\text{drift}_{\text{high}}}]$. The variation on the turning rate, $\sigma_{\dot{\theta}}$, is now held within a range, $[\dot{\theta}_{\text{low}}, \dot{\theta}_{\text{high}}]$, and decreases with increasing gradient. As the sperm completes

a turn, part of its path is away from the gradient. This section would then have a higher turning rate. Conversely, as the sperm turns towards the gradient, the turning rate decreases, resulting in a pattern of quick turns away from the gradient and longer runs towards the gradient. This, combined with an increase in the drifting speed, results in longer periods of straighter swimmer with quicker, smaller turns. In reality, this is accomplished by just a periodic change in the turning rate, where the rate as the sperm turns away from the gradient is faster and slower as the sperm faces the gradient. At the highest gradient, this results in a fast drifting speed aimed directly with the gradient. As the sperm turns away from the source, the turning rate is increased, causing a faster turn. Then as the sperm turns back down gradient, the turning rate is effectively decreased, resulting in a period of straighter swimming. This behavior is depicted in Fig. 2.35.

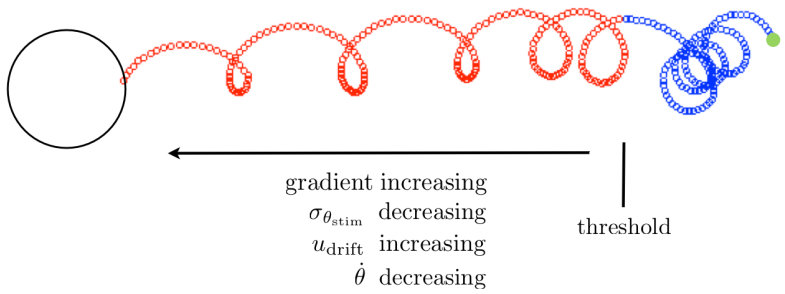

Figure 2.35: An example of a sperm path with a chemotactic and a chemokinetic response. The drifting speed, turning rate and drifting direction are all altered.

Parameters:

(1) u_{swim}, θ : Unchanged

(2) u_{drift}: The drift speed increases relative to the gradient. There is a specified range, $[u_{\text{drift}_{\text{low}}}, u_{\text{drift}_{\text{high}}}]$, within which the speed is kept. The calculation for the drift speed at each time-step is:

$$u_{\text{drift}_{\text{new}}} = u_{\text{drift}_{\text{low}}} + (u_{\text{drift}_{\text{high}}} - u_{\text{drift}_{\text{low}}}) \cdot (\text{percent over threshold})$$

(3) $\sigma_{\theta_{drift}} = \sigma_{\theta_{\text{stim}}}$: Factor on the standard deviation controlling the variation on the path of the sperm that navigate down gradient. The value is initially reduced:

$$\sigma_{\theta_{\text{stim}}} = \gamma_2 \cdot \sigma_{\theta_{\text{drift}}}$$

(4) θ_{drift} is then calculated as:

$$\Delta_{\theta_{\text{drift}}} = \sigma_{\theta_{\text{stim}}} \cdot (1 - \text{percent gradient}) \cdot \pi\mathbf{\Lambda}$$

$$\theta_{\text{drift}_{\text{new}}} = \theta_{\text{drift}_{\text{old}}} + \Delta_{\theta_{\text{drift}}} \cdot dt$$

where $\mathbf{\Lambda}$ is a number chosen from a triangle distribution with minimum of -1, a maximum of 1 and a center of 0. This allows the variation on the drifting direction to decrease as the gradient increases. Whereas the loitering range for the change in the direction was controlled by $\pi\sigma_{\theta_{\text{drift}}}$ and could range from $-\pi\sigma_{\theta_{\text{drift}}}$ to $\pi\sigma_{\theta_{\text{drift}}}$, it is now controlled by a decreased range. This range is decreased immediately by γ and continues to decrease as the gradient increases.

(5) $\sigma_{\dot{\theta}} = 0$: The variation on the turning rate is now dependent on the gradient.

(6) $\dot{\theta}$: Decrease in $\dot{\theta}$ as the gradient increases within the set range $[\dot{\theta}_{\text{low}}, \dot{\theta}_{\text{high}}]$. The expression to determine the turning rate is:

$$\dot{\theta_{\text{new}}} = \dot{\theta_{\text{low}}} + (\dot{\theta_{\text{high}}} - \dot{\theta_{\text{low}}}) \cdot (\text{percent over threshold})$$

(7) θ: Calculated as in the loitering behavior:

$$\theta_{\text{new}} = \theta_{\text{old}} + \dot{\theta} \cdot dt$$

Once each parameter is set, the sperm in this response swim according the the equation:

$$\boldsymbol{u}_{\text{sperm}} = \boldsymbol{u}_{\text{swim}}\cos(\theta) \cdot dt + \boldsymbol{u}_{\text{drift}}\cos(\theta_{\text{drift}}) \cdot dt \tag{2.38}$$

$$\boldsymbol{v}_{\text{sperm}} = \boldsymbol{u}_{\text{swim}}\sin(\theta) \cdot dt + \boldsymbol{u}_{\text{drift}}\sin(\theta_{\text{drift}}) \cdot dt \tag{2.39}$$

Test Parameters:

(1) Turning rate range: $[\dot{\theta}_{\text{low}}, \dot{\theta}_{\text{high}}]$

(2) Drifting speed range: $[u_{\text{drift}_{\text{low}}}, u_{\text{drift}_{\text{high}}}]$

(3) Immediate reduction factor: γ

3. **Run**: The Run Response models the ability of a sperm to exit the circling behavior and perform a straight run upon stimulation. Sperm from numerous species have been observed to decrease curvature so much that the circling behavior is lost. Other studies have observed an immediate straightening of the path at a certain level of concentration. It is not clear whether the circling pattern increases the fertilization rates, especially in chaotic flow. In this response, the sperm perform a straight run as long as they are within the elevated concentration. The path they swim decreases in variation, aligning with the gradient with greater accuracy as the gradient increases. The direction is now controlled by θ_{stim} which is, just as in the other responses, $\sigma_{\theta_{\text{drift}}}$ immediately reduced by γ_3 and then decreases with an increasing gradient. The sperm no longer as a drifting speed, and the swimming speed has been observed to at least double from the loitering swimming speed. This increase has mostly been described as a relative process. So, this increase will also be relative to the gradient. In a high enough gradient, the run performed is fast and directed in perfect alignment with the gradient. In terms of the abilities of an actual sperm, this replicates a sperm that is able to suppress curvature enough to eliminate any turning. This response is depicted in Fig. 2.36.

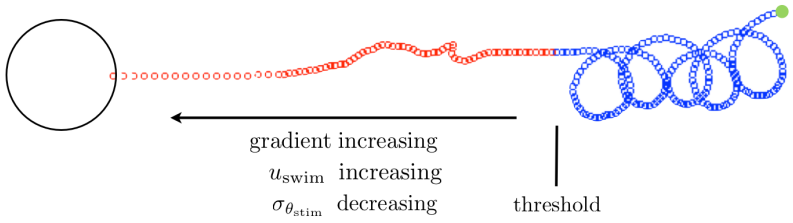

Figure 2.36: An example of a sperm path with the run response. The sperm no longer executes circles, but instead swims straight down gradient with increasing accuracy and speed.

Parameters:

(1) $\dot{\theta}, u_{\text{drift}}$ and $\theta_{\text{drift}} = 0$: No turning, drifting speed or direction

(2) $\sigma_{\theta_{\text{stim}}}$: The variation on the path the sperm swim on is now determined by $\sigma_{\theta_{\text{stim}}}$. This value is reduced from the original variation on the drifting direction:

$$\sigma_{\theta_{\text{stim}}} = \gamma_3 \cdot \sigma_{\theta_{\text{drift}}}$$

(3) θ_{stim}: Now calculated at each time-step by:

$$\Delta_{\theta_{\text{stim}}} = \sigma_{\theta_{\text{stim}}} \cdot (1 - \text{percent gradient}) \cdot \pi \mathbf{\Lambda}$$

$$\theta_{\text{stim}_{\text{new}}} = \theta_{\text{stim}_{\text{old}}} + \Delta_{\theta_{\text{stim}}} \cdot dt$$

where $\mathbf{\Lambda}$ is a number chosen from a triangle distribution with minimum of -1, a maximum of 1 and a median of 0. This allows the new direction to change in a range with a maximum absolute change of π reduced by $\sigma_{\theta_{\text{stim}}}$ and the strength of the gradient. Again, $\sigma_{\theta_{\text{drift}}}$ ranges from 0 to 1, where the maximum change in the direction is held between 0 and π in the loitering behavior. $\sigma_{\theta_{\text{stim}}}$ reduces the variation on the swimming direction once the sperm is stimulated.

(4) u_{swim}: Increase in swimming speed relative to the gradient within the range $[u_{\text{swim}_{\text{low}}}, u_{\text{swim}_{\text{high}}}]$.

The new swimming speed at each time-step is calculated as:

$$u_{\text{swim}_{\text{new}}} = u_{\text{swim}_{\text{low}}} + (u_{\text{swim}_{\text{high}}} - u_{\text{swim}_{\text{low}}}) \cdot (\text{percent over threshold})$$

Once each parameter is set, the sperm in this response swim according the the equation:

$$\boldsymbol{u}_{\text{sperm}} = \boldsymbol{u}_{\text{swim}} \cos(\theta_{\text{stim}}) \cdot dt \tag{2.40}$$

$$\boldsymbol{v}_{\text{sperm}} = \boldsymbol{u}_{\text{swim}} \sin(\theta_{\text{stim}}) \cdot dt \tag{2.41}$$

Test Parameters:

(1) Swimming speed range: $[u_{\text{swim}_{\text{low}}}, u_{\text{swim}_{\text{high}}}]$

(2) Immediate reduction factor: γ

Unless otherwise specified, the values for the stimulated parameters used are represented below in Table 2.10:

Table 2.10: Response Sperm Input Parameters: Values

Parameter	**Value**
$[u_{\text{drift}_{\text{low}}}, u_{\text{drift}_{\text{high}}}]$	$[2u_{\text{drift}}, 3u_{\text{drift}}]$
$[u_{\text{swim}_{\text{low}}}, u_{\text{swim}_{\text{high}}}]$	$[1u_{\text{swim}}, 2u_{\text{swim}}]$
$[\dot{\theta}_{\text{low}}, \dot{\theta}_{\text{high}}]$	$[0.5\dot{\theta}, 1\dot{\theta}]$
γ	$1/2$

2.3.3 Effective Diffusivity of Sperm Loitering & Stimulated Behaviors

When the sperm are released from the same initial location at the same time in a high enough quantity, the exhibited loitering behavior represents a diffusive system. The concentration of sperm spreads over time (Fig. 2.37) and a slice taken through at one time (Fig. 2.38) produces a distribution with Gaussian characteristics (Fig. 2.39).

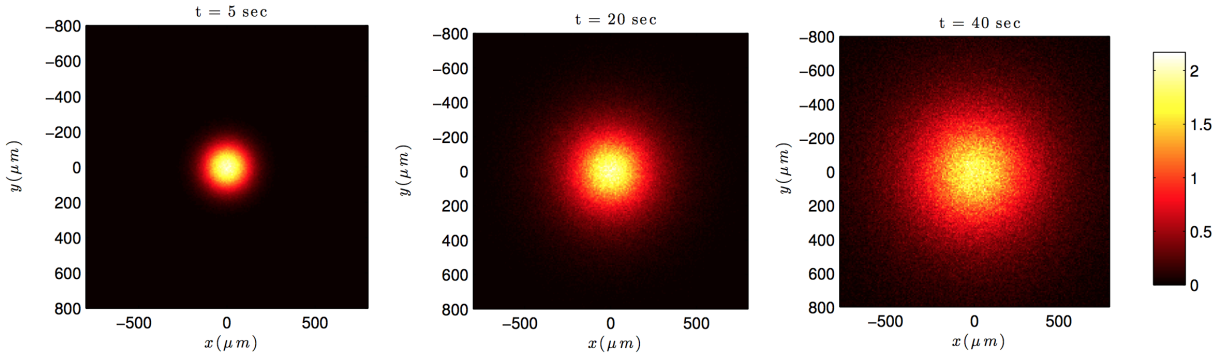

Figure 2.37: Development of sperm plume over time (in units of sperm/μm^3).

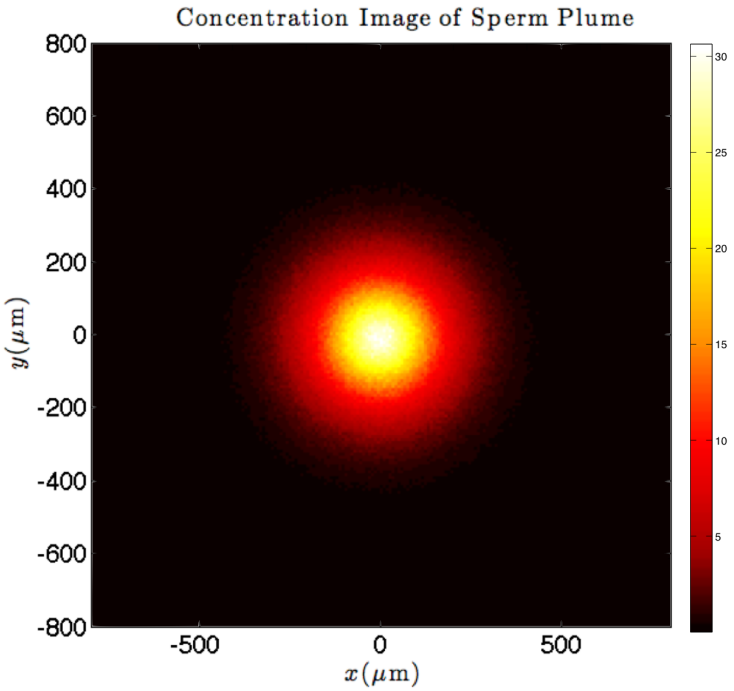

Figure 2.38: Concentration image of sperm (in units of sperm/μm^3) in a loitering plume.

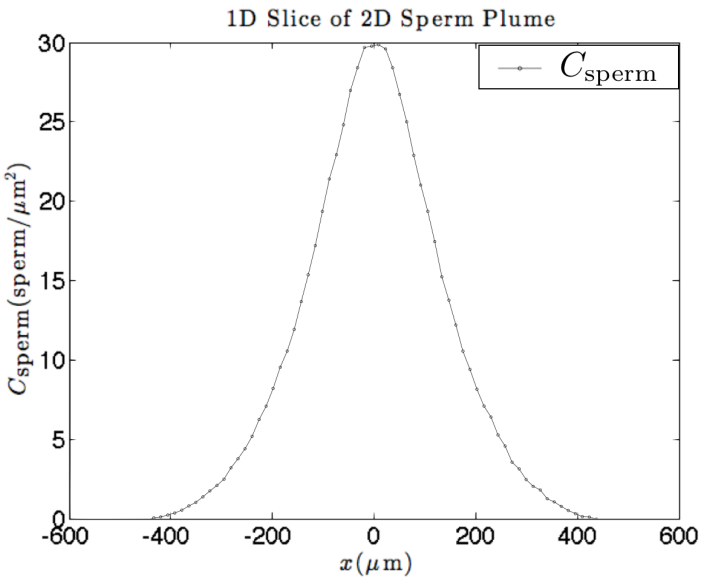

Figure 2.39: Plot of the 1-D slice through the 2-D plume. This plume represent the loitering behavior of the sperm used in the simulations.

An effective diffusivity can be estimated for the spreading of the loitering sperm. As a result, the impact of altering parameters within the loitering behavior can be better understood. In order to capture this condition, simulations were run without the presence of an egg. Taking into account the solution to the diffusion equation,

$$C(x,y) = \frac{M/L}{4Dt\pi}\left(\exp\left[-\frac{x^2}{4Dt} - \frac{y^2}{4Dt}\right]\right)$$

the variance in the x-direction can be calculated for a set of times. For just the x-direction,

$$C(x,y=0) = \frac{M/L}{4Dt\pi}\left(\exp\left[-\frac{x^2}{4Dt} - \frac{0^2}{4Dt}\right]\right)$$

$$C(x,y=0) = \frac{M}{4Dt\pi}\exp\left[-\frac{x^2}{4Dt}\right]$$

This highlights the relationship between the variance, diffusivity and time:

$$\sigma \sim \sqrt{4Dt}$$

$$\sigma^2 \sim 4Dt$$

When $\sigma^2/4$ is plotted against time, the slope of the resulting line reveals the effective diffusivity of the behavior. Figure 2.40 shows the variance plotted against time for a few variations on the loitering swimming parameters. The base loitering behavior refers to the behavior used for the simulations and random swim refers to a swimming pattern without any turning parameters, but a random swimming path. Figure 2.41 also includes the calculated diffusivities for each behavior.

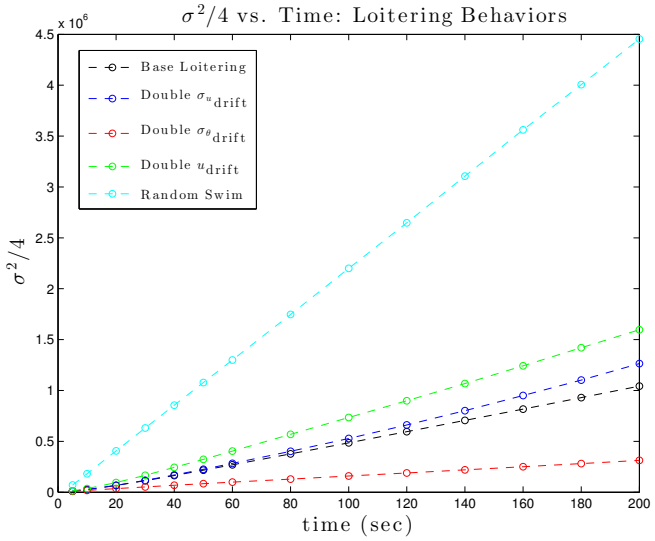

Figure 2.40: Loitering Behaviors: Variance calculated from simulations with varying parameters on the loitering behavior.

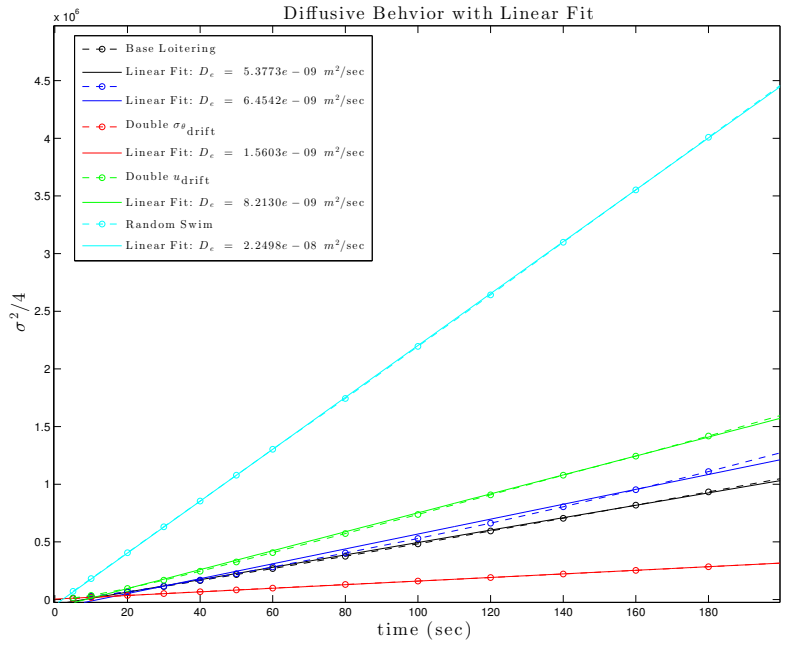

Figure 2.41: Loitering Behaviors: The linear fits of the variance plots with the calculated effective diffusivities associated with each behavior.

This analysis provides an effective diffusivity for several variations in the loitering behavior parameters. The base loitering behavior possesses one of the lowest diffusivities. When the variation on the drift direction is increased, the diffusivity is lowered. This is due to the reduction in the ability to maintain a single direction. The sperm are unable to make the same progress as with the smaller variation in the direction. The increase in the both the variation on and the magnitude of the drift speed caused an increase in diffusivity. These alterations resulted in an increased ability to gain distance without impacting direction. Lastly, the random swim loitering behavior exhibited the highest diffusivity. The sperm are not inhibited by creating circles and the diffusivity is a direct result of the speed and variation on the direction of swimming. While some studies have mentioned this as a possible loitering behavior, almost all of the literature suggests that the sperm do in fact swim in a circular pattern.

The diffusivities of the response behaviors were quantified using the same method (Fig. 2.42). The diffusivities were relatively similar to each other, with the Run Response proving to be the

most diffusive, followed by Turn and Run and finally the Drifting Circle Response was the least diffusive.

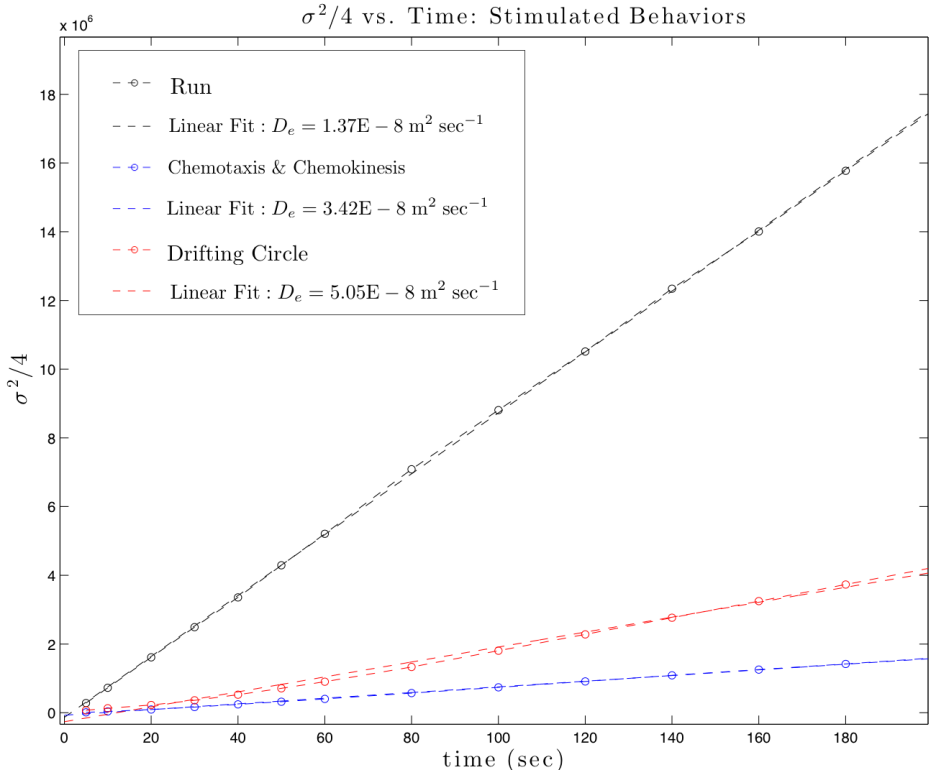

Figure 2.42: Stimulated Behaviors: Variance calculated from simulations on the stimulated behaviors along with the variance plots and their linear fits.

The effective diffusivity values calculated for both the loitering and the stimulated behaviors are similar to those calculated from observations of actual sperm swimming within the literature. The diffusivity of purple sea urchin sperm was found to fall in the range $3.24\text{E}-11-2.11\text{E}-8$ m^{2}sec^{-1} [24]. It is interesting to note that the diffusivity of the sperm is in the same range of magnitude as the quantified diffusivities of the attractants of benthic invertebrates. Ranges of the quantified diffusivity for sperm and chemoattractants from previous studies are collected in Table 2.11.

Table 2.11: Diffusivity of Sperm and Chemoattractants of Benthic Invertebrates. Both the chemoattractants and the sperm have diffusivity values of the same order of magnitude.

Species	**Parameter**	**D** (m^2sec^{-1})	**Source**
Sea Squirt *Ciona intestinalis*	attractant	$9.33 - 1.24 \times 10^{-10}$	[26]
Red Abalone	tryptophan	$2.5 - 5.9 \times 10^{-9}$	[43]
Purple Sea Urchin	sperm	$3.24 \times 10^{-11}, 2.11 \times 10^{-8}$	[24]
Average Benthic Invertebrate	attractant	5×10^{-8}	[57]
Sea Urchin *A. punctulata*	resact	3×10^{-9}	[3]

2.4 Fertilization Model

To understand the effect of initial location, flow and behavior on the ability of sperm to reach an egg, in each simulation, if and when a sperm reaches the egg, this time is recorded. We assume 2nd order fertilization kinetics. This rate is then integrated over the simulation time and the results are presented as the cumulative percent of the total amount of sperm to have reached the egg by each time. For these simulations, the this rate is recored for every 0.1 second. The simulations are run long enough for this cumulative plot to effectively asymptote. The change in the rate of sperm to reach the egg does not change significantly. A representative sample of the results are shown in Sec. 3.

2.5 Verification and Sensitivity Analysis

A sensitivity analysis was performed on the chemoattractant flux model, the flow model and the fertility model to determine the effects of altering the parameters. In the flux and flow models, the number of particles, Np (Sec. 2.5.1.1), the nature of the binning analysis (size of the bins, *widbin*, size of the domain, *scale*, and number of bins across the diameter of the egg, *bin_spread*) (Sec. 2.5.1.2) and time-step, dt (Sec. 2.5.1.3), could all potentially impact the resulting concentration and gradient fields. The success rate in the fertility model needs to be maintained regardless of the number of sperm, Nps (Sec. 2.5.2), used for each simulation.

2.5.1 Chemoattractant Flux and Flow Model

2.5.1.1 Number of Particles, Np

The value and location of the concentration of chemoattractant needs to be unaffected by the number of particles used in the simulations. In order to understand the necessary number of particles, all other parameters are held constant while an increasing number of particles were tested. The concentration and gradient in a small area about $2R_{\text{egg}}$ away from the center of the egg were measured after 1 minute of chemoattractant release for a range of particles. This was done until the results converged. It should be noted that this must be an iterative process, as the insensitivity of the results are dependent on the relationship between the size and amount of bins and the number of particles. The same methods were used to determine the sensitivity for each of the other flow conditions. An example of the analysis done for the quiescent flow is presented in this section. Both the concentration and the gradient sensitivities to number of particles are shown in Fig. 2.43 and 2.44. While the concentration remains constant after about 2E 5 particles per time-step, the gradient does not become consistent until about 3E 5 particles per time-step. The goal for the sensitivity of the gradient was to prevent the gradient from changing more than 2%. This was accomplished once the number of particles, in the chosen bin size, reached the aforementioned 3E 5 for each time-step.

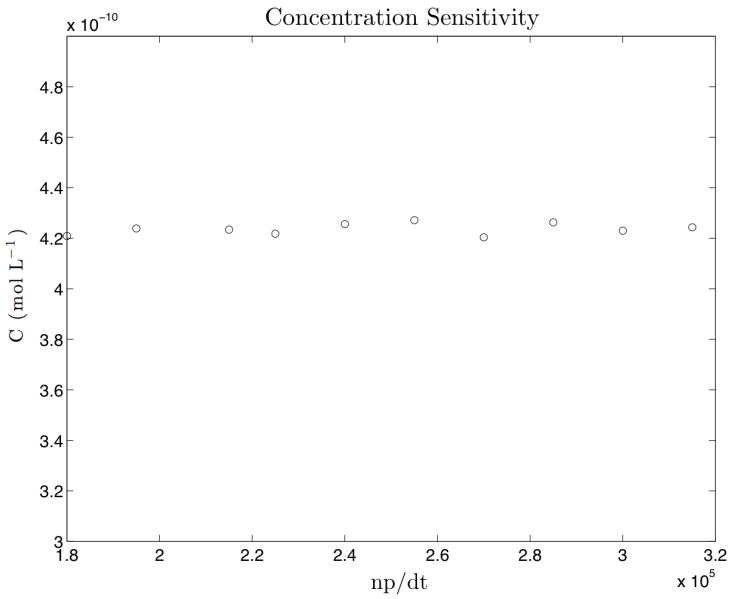

Figure 2.43: Concentration at an area measured after 1 minute of release with a range of particle amounts.

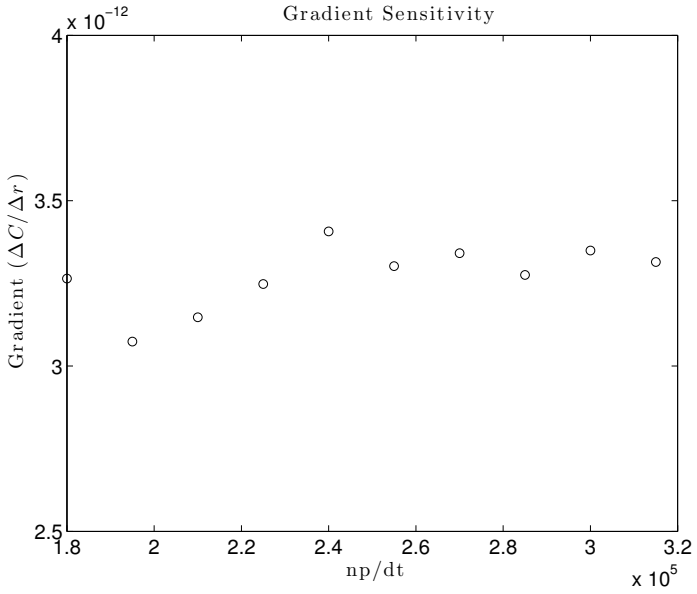

Figure 2.44: Gradient at an area measured after 1 minute of release with a range of particle amounts.

2.5.1.2 Number of Bins Across the Egg, *bin_spread*

The domain dimensions (bin size and number of bins) were optimized to capture the gradient in the pure diffusion case while minimizing the simulation time. Through iteration between the

number of particles and the width of the bins, a final number of bins to span the diameter of the egg was determined to be 8 *bin_spread*. The results are presented in Fig. 2.45.

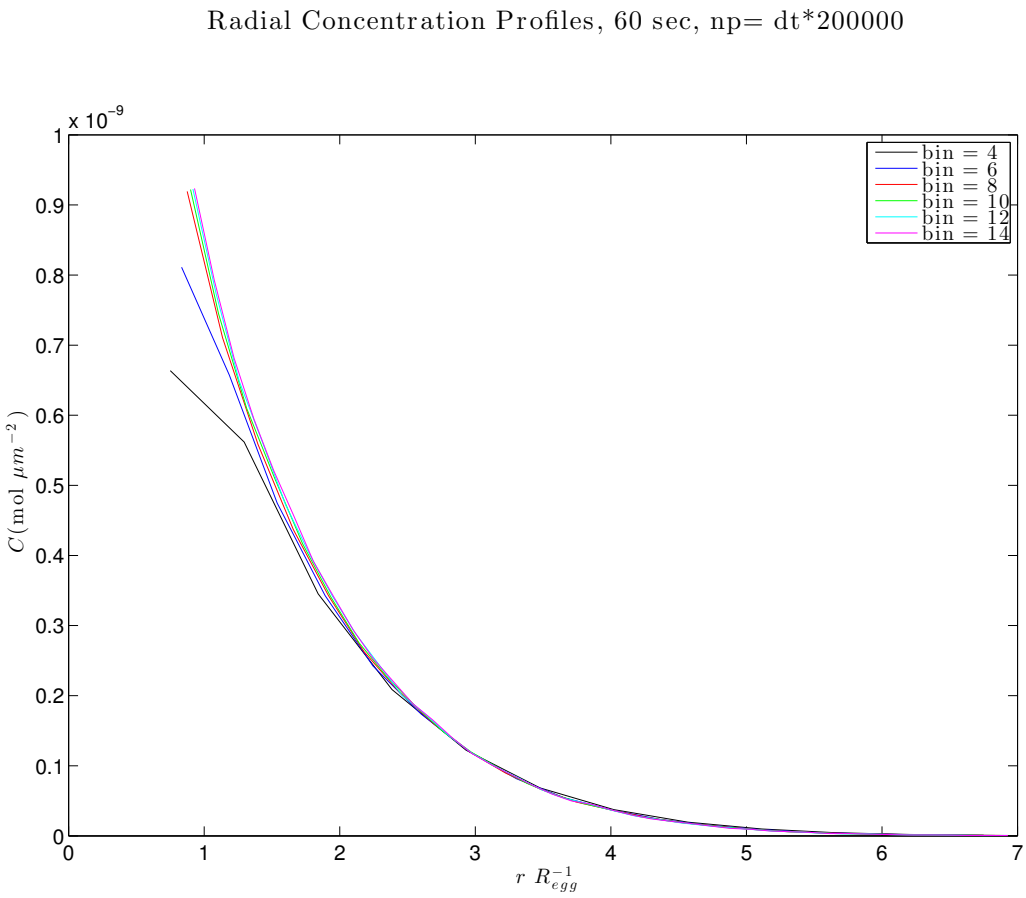

Figure 2.45: Radial concentration profiles taken after 1 minute of flux in a quiescent flow. The profile remains constant once the number of bins that span the egg exceeds 6.

Figure 2.47 portray the problems with too few particles and inaccurate binning parameters. Figure 2.46 shows examples of a sufficient number of particles.

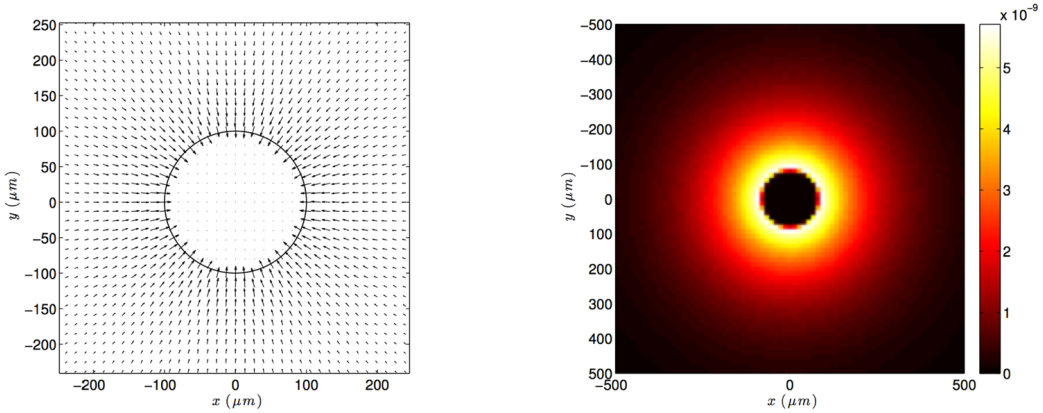

Figure 2.46: On the left, an example of a smooth gradient due to an appropriate amount of particles. On the right, a concentration image (in units of mol μm^{-3}) to show the smoothness that results from an a sufficient number of particles. Even with a coarse grid, the bins are not easy to detect.

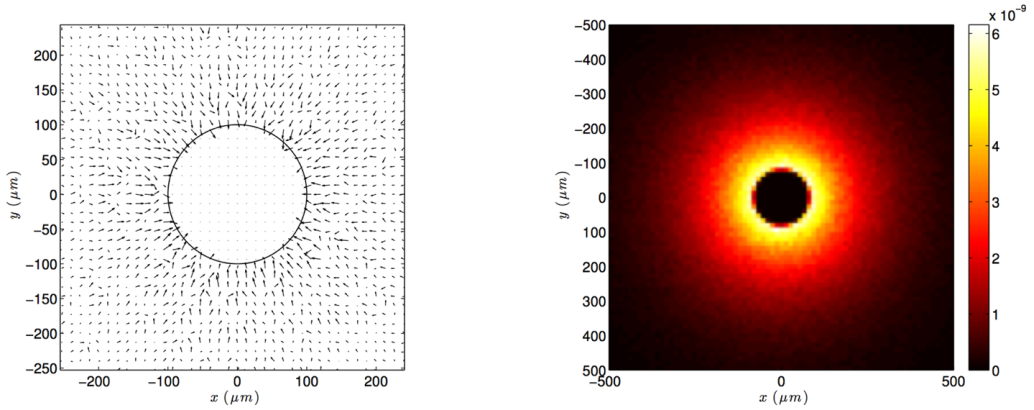

Figure 2.47: On the left, an example of a gradient field with an insufficient number of particles. The gradient, expected to be smooth, is clearly not. The gradients due to local noise is more significant than the overall, pure diffusion gradients that are expected. On the right, A concentration image (in units of mol μm^{-3}) representing a simulation with too few particles. The image is not smooth.

2.5.1.3 Time-Step, dt

Even in the pure diffusion case, the time-step does have an impact on the resulting concentrations. This is due to the manner in which the particles are prevented from returning back into the egg. If the step is too large, this results in a higher probability of the particles being bounced out onto the same radial distance from the egg. This created an unrealistic ring of higher concentration away from the egg. So, a small enough time-step had to be found for the concentration results to

converge. This was determined to be $dt = 0.1$ second (Fig. 2.48)

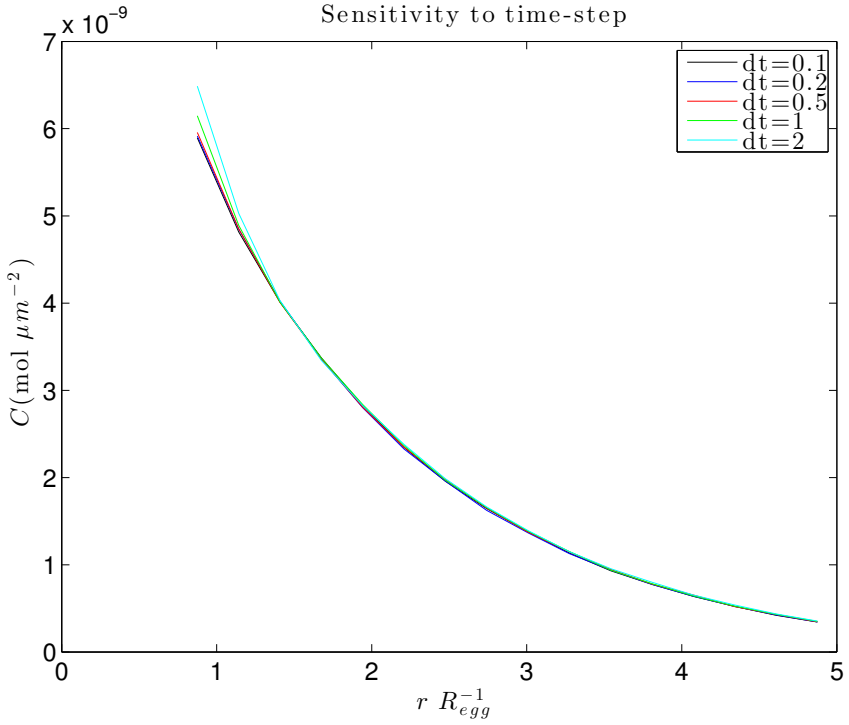

Figure 2.48: Radial concentration profile with increasing time-step, dt. The profile smoothes out and no longer has the sharp, unrealistic gradient when the time-step is $dt = 0.1$ sec.

2.5.2 Fertilization Model

The fertility model is sensitive to the number of sperm used in the simulations. This could be different for each response within each type of flow. Figure 2.49 represents an example of the sensitivity analysis performed on each of the response simulations within each flow condition. This test reveals that the model (The Run Response in a quiescent flow) is insensitive to the number of sperm beyond $Nps = 2E4$.

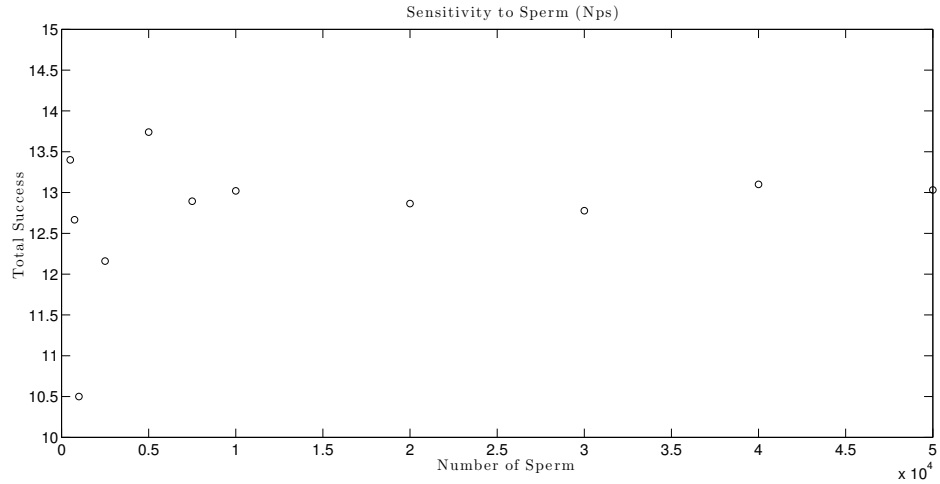

Figure 2.49: Total fertilization success for an increasing number of sperm. The model is insensitive to sperm after about 2E4 sperm.

Chapter 3

Results & Discussion

3.1 How Flow Shapes 2D Chemoattractant Plume

Steady-state chemoattractant plume distributions for the steady shear flow at four different values of shear rate α are shown in Fig. 3.1. The plumes approach a steady-state distribution approximately three minutes after the egg is placed in the flow (the transient response is not shown). The $\alpha = 0$ case (first panel) corresponds to pure diffusion of chemoattractant in quiescent flow, with a resulting symmetric plume that decays radially away from the egg. As shear rate is increased (subsequent panels), the plume is stretched by the flow into an increasingly elongated filament. This stretching sharpens chemoattractant gradients, increases diffusive flux away from the plume, and decreases local plume concentrations relative to the unsheared case. The shear mechanism responsible for dispersing the chemoattractant is essentially the same as the classic phenomenon described by [60], modified locally by the presence of the solid and freely rotating egg. Note that the results shown in Fig. 3.1 are consistent with steady-shear chemoattractant plumes computed with a similar approach by [68].

When shear is unsteady, as it is in turbulent flow, the resulting chemoattractant plumes are more complex (Fig. 3.2). Using the unsteady shear flow model given by Eqs. 2.6 - 2.14, we computed unsteady plume distributions for two values of the unsteady shear amplitude α_0. The plume is allowed to disperse for a period of three minutes after the egg is placed in the unsteady flow such that it reaches a fully developed state across the model domain. The plume, however, continues to change over time in response to changes in the unsteady flowfield. To give a sense of

the temporal variation in the chemoattractant plume structure, we display in Fig. 5 representative snapshots of the spatial distribution at 60-second intervals. For the low-α_0 case ($\alpha_0 = 0.5^{-1}$, Fig. 3.2a), the effect of the unsteady shear is predominately to bend the protruding arms of the stretched chemoattractant plume. For this case, diffusion largely destroys any additional complexity at the ends of the arms (the for this case, using $\alpha_0/2$ as an rms shear rate, is less than 4, and thus the effect of diffusion is relatively strong). For the high-α_0 case ($\alpha_0 = 1.25^{-1}$, Fig. 3.2b), the increases to approximately 10, and stirring by the unsteady shear produces significantly more complexity in the chemoattractant plume. Filaments are stretched and folded, with pronounced striations developing in the scalar field.

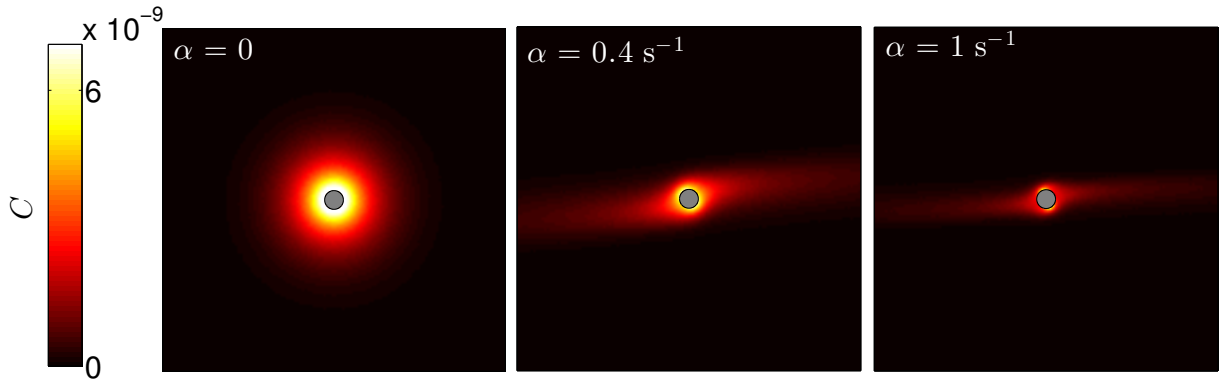

Figure 3.1: Steady-state chemoattractant distributions (in units of mol μm^{-3}) for a range of steady shear flows. The steady state behavior shown above was obtained 3 minutes after the egg was introduced into the flow. The egg is centered in each panel, indicated by the grey circle and the chemoattractant concentration is indicated by the colorbar.

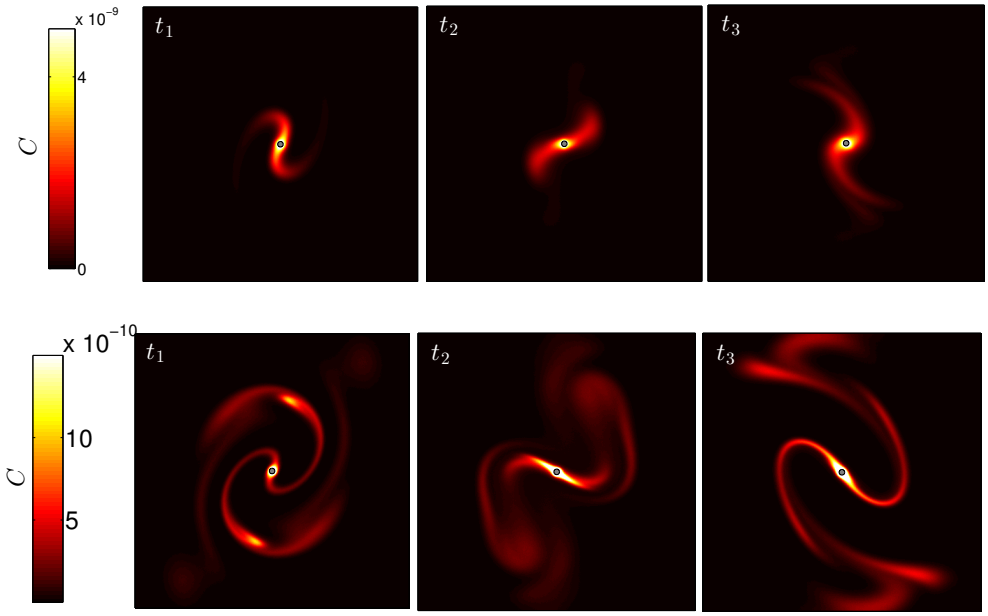

Figure 3.2: Representative snaphots of the quasi steady-state chemoattractant distributions (in units of mol μm^{-3}) for low (1st row) and high (2nd row) unsteady shear flows. We allowed the plumes to develop into a quasi steady state after a 3 minute period. To illustrate the range of behaviors over time, we show three representative slices at one minute intervals. The egg is centered in each panel, indicated by the grey circle.

The chemoattractant plume distributions shown in Figs. 3.1 and 3.2 illustrate the continuous range of concentrations present around the egg. However, some of the concentrations will necessarily be below the minimum threshold concentration required to elicit a behavioral response by sperm. From the perspective of behavioral response, the concentrations below this threshold are functionally unimportant. Figs. 3.3 and 3.4 display the spatial extent of the portions of the plumes that would elicit sperm response for given values of the threshold.

In the steady shear flow cases, Fig. 3.3 shows that in any given panel, the effective plume area decreases as minimum threshold increases. Additionally, as the shear rate α increases, the effective plume area for any given threshold decreases. The increase in the effective egg target size caused by the diffusion and dispersion of the chemoattractant plume has proven to be an evolutionary advantage [26, 38, 39, 42]. We can quantify the effective egg target increase in size provided by the plume for a given threshold. We calculate an effective egg diameter based on the area within any

of the concentration threshold contours (A_{stim}) shown in Fig. 3.3

$$D^* = \sqrt{4A_{stim}/\pi}/R_{egg} \tag{3.1}$$

The normalized effective diameters for each threshold value and each steady shear rate are below in Fig. 3.5. Both shear rate and threshold value decrease the size of the effective diameter as was seen qualitatively in Fig. 3.3.

In the unsteady shear flow cases, Fig. 3.4 shows a similar trend in the decrease in target area for increasing threshold concentration and shear rate. A new phenomenon occurs with the development of non-contiguous islands of above-threshold concentrations for Fig. 3.4b (high-α_0). We anticipate that these would complicated or present challenges to search strategies for sperm seeking eggs.

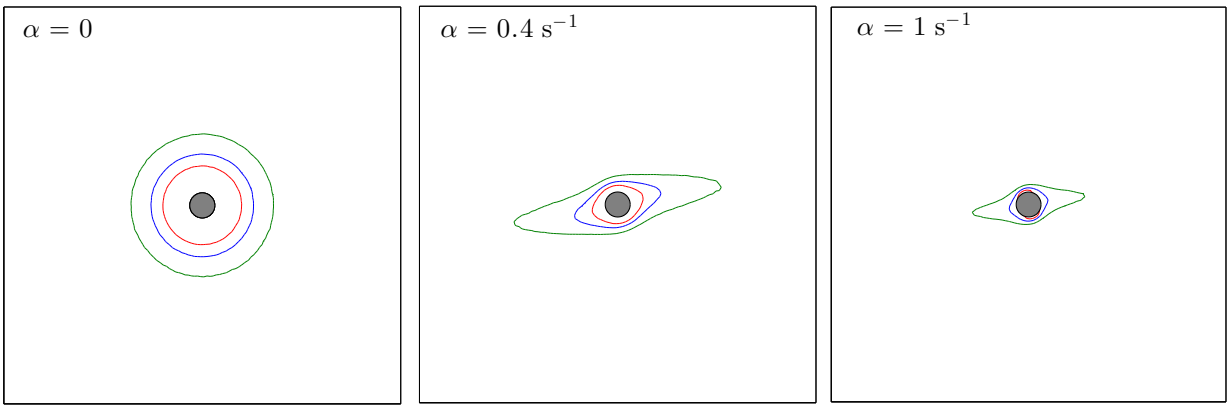

Figure 3.3: Steady shear flow contour levels for three possible threshold concentrations (1×10^{-9} mol μm^{-3} (green); 2×10^{-9} mol μm^{-3} (blue); 3×10^{-9} mol μm^{-3} (red)) for 3 shear rates. These images correspond directly to the concentration images shown in Fig. 3.1. The contours also indicate information about the concentration gradients which will be useful when we look at the response behaviors in Sec. 3.1.1. The gradients are everywhere normal to the contours. The green line depicts the threshold concentration used in the fertilization models. This lies on the higher end of the documented threshold concentration ranges (3×10^{-10} mol μm^{-3} - 4×10^{-9} mol μm^{-3}) [54].

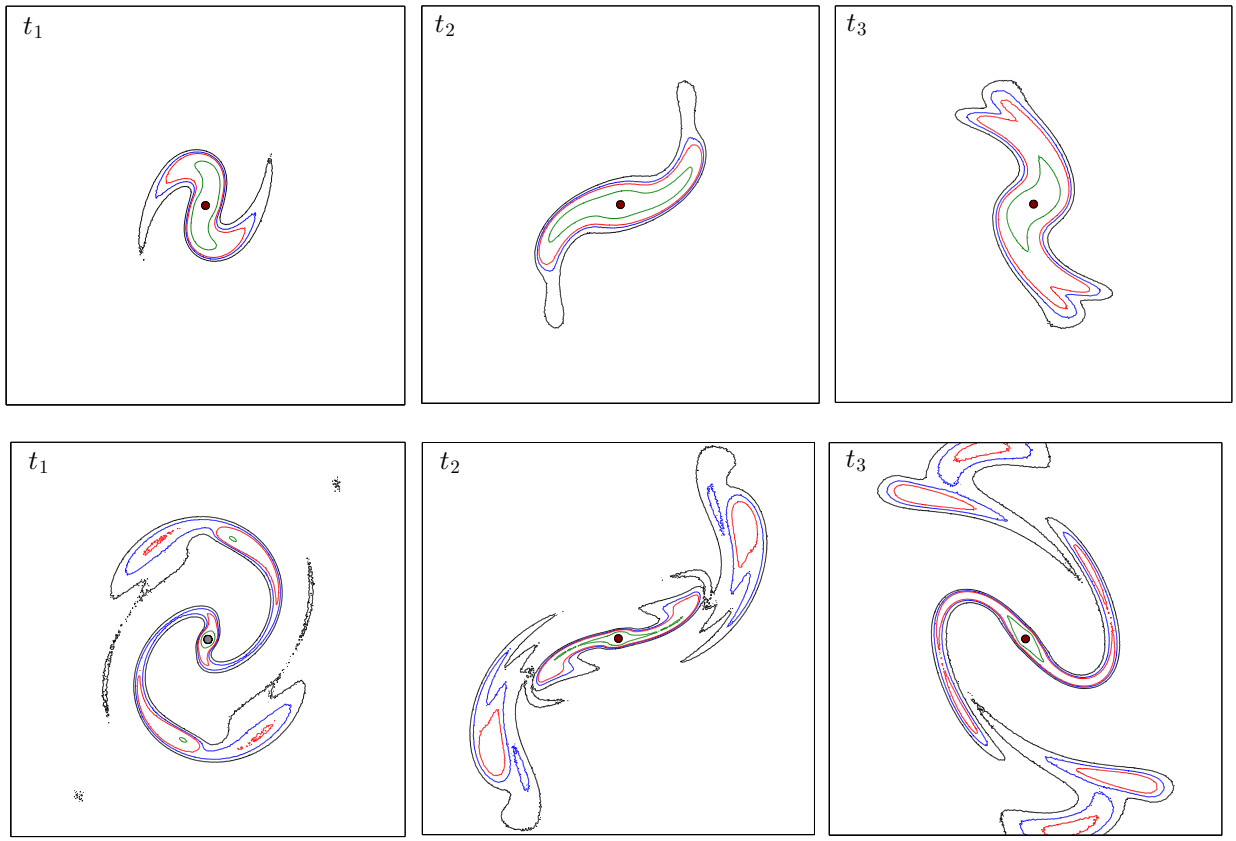

Figure 3.4: Unsteady shear flow contour levels for both the low-α_0 (top row) and high-α_0 (bottom row) cases for one minute time intervals t_1, t_2 and t_3 illustrating the transient chemoattractant threshold concentrations. Four possible threshold values (1×10^{-10} mol μm^{-3} (black); 2×10^{-10} mol μm^{-3} (blue); 3×10^{-9} mol μm^{-3} (red); 1×10^{-9} mol μm^{-3} (black)) are depicted. These images correspond directly to the concentration images shown in Fig. 3.2. Again, the chemoattractant gradient information can be deduced from the level and spacing of the concentration contours. Note that the smallest contour (green) represent a concentration of 1×10^{-9} mol μm^{-3} , the threshold concentration used for the steady shear flows, but that the value used for the complex cases is on the lower end of the range at 1×10^{-9} mol μm^{-3} (black).

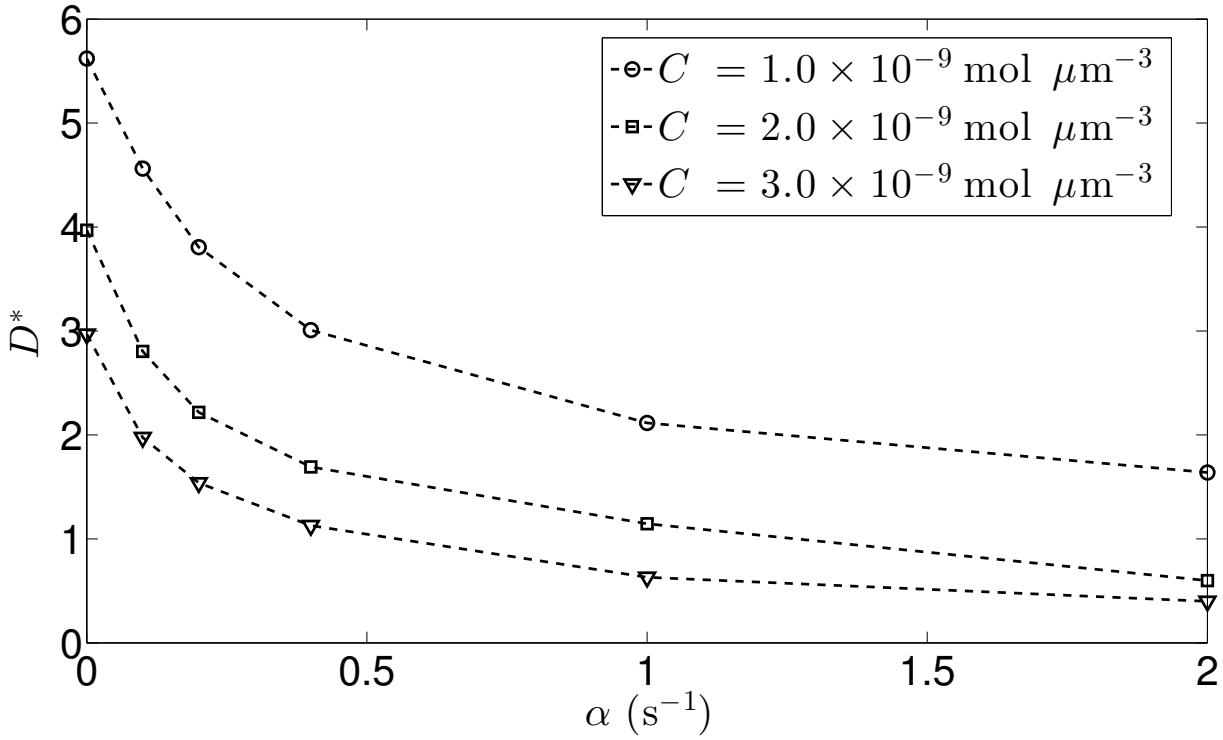

Figure 3.5: The calculated effective diameter (D^*) of the size of the plume under a given threshold concentration for the steady shear flows plotted against the corresponding shear rate values (α).

3.1.1 Sperm Motility

In the quiescent flow and the steady shear flows with $\alpha > 0$, we provide a sense of what the response behaviors look like in the paths shown in Figs 3.6 - 3.8. The paths shown are real paths from the model, but they were consciously selected to show certain mechanisms (i.e., the flow sweeping the sperm passed the egg). Note that if a loitering sperm locates the threshold area, there is a very high change of then reaching the egg.

There are many significant outcomes derived from the sperm paths in the unsteady shear flows and we present some significant messages using paths from the model in Fig. 3.9. Fig. 3.9a illustrates that in the low-α_0 unsteady shear case, once the sperm encounters the threshold concentration, it is likely to find the egg with any of the response types. The path is more complex and circuitous than the simple shear cases: both the flow and the plume are constantly evolving. The sperm are directed by the gradients to stay within the threshold concentration, which is

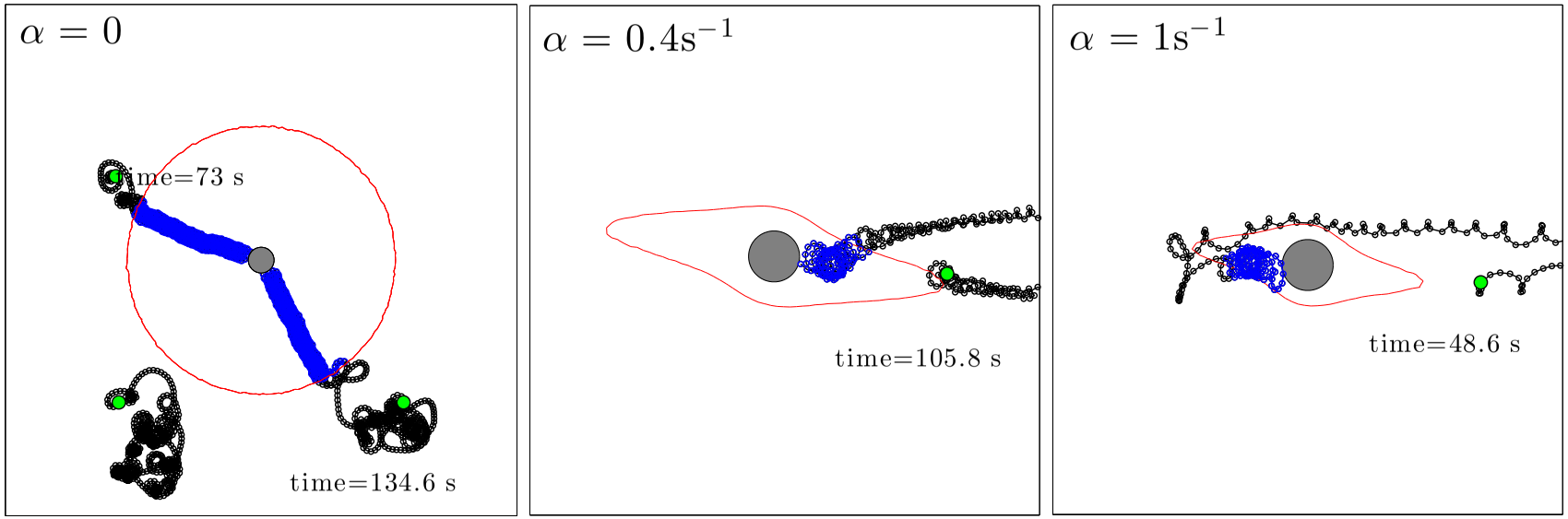

Figure 3.6: Representative sperm paths for both the loitering (black) and response (blue) behavior in 3 steady shear flows.

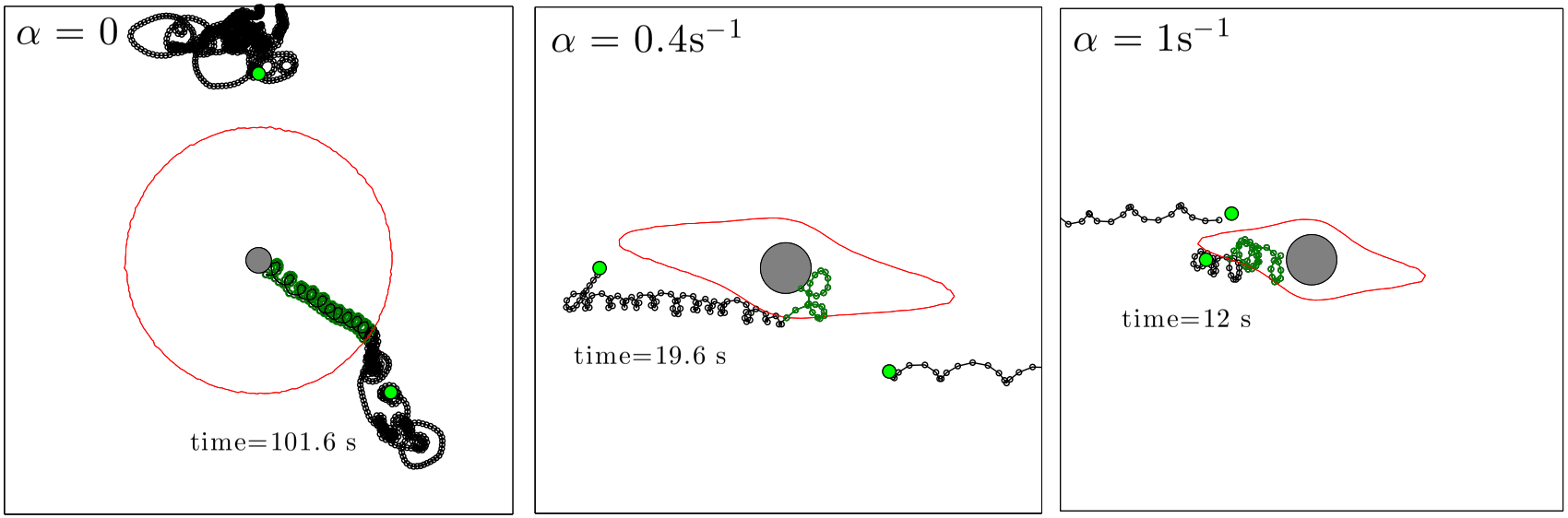

Figure 3.7: Representative sperm paths for both the loitering (black) and response (green) behavior in 3 steady shear flows.

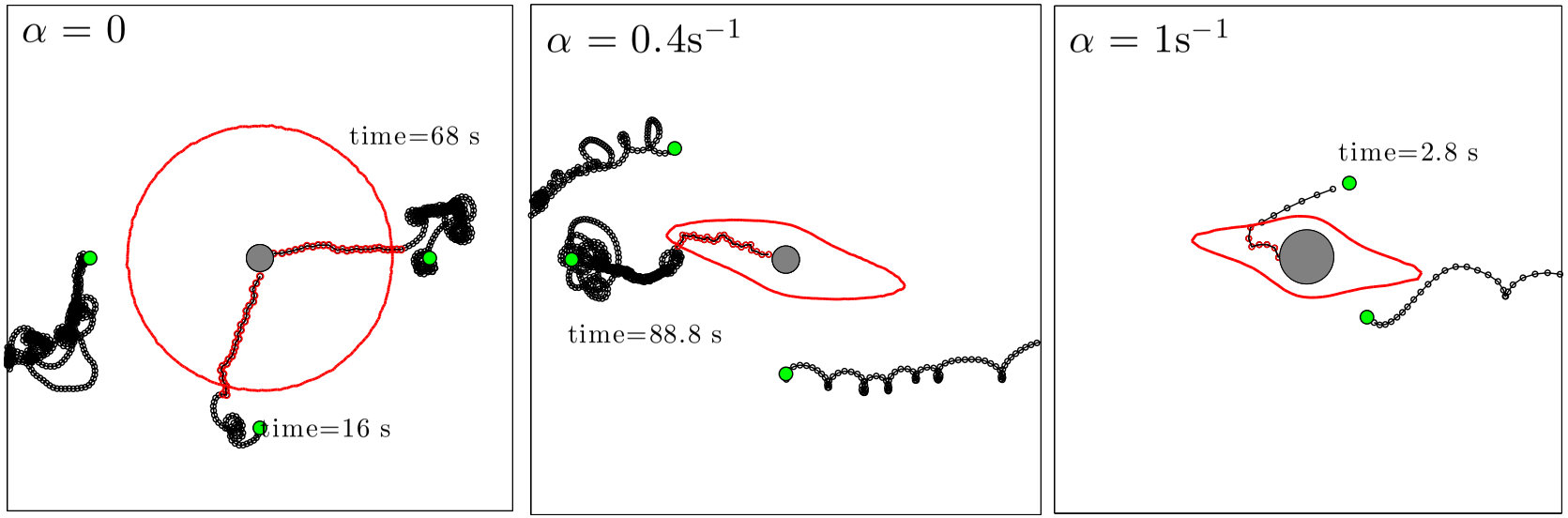

Figure 3.8: Representative sperm paths for both the loitering (black) and response (red) behavior in 3 steady shear flows.

manipulated almost entirely by the flow, as they follow an increasing gradient of chemoattractant. It is not always necessary for the sperm to remain within the threshold contours in order for the egg to be reached. For example, as seen in Fig. 3.9b, the sperm locates the higher concentration at an early time (a), but the flow and the motility of the sperm removes it from the filament. Both these variations in flow and the sperm motility, though, allow the sperm to locate a filament again and eventually follow the gradients to find the egg. Figure 3.9c demonstrates the possibility in the high complex unsteady shear case in which a sperm responds to the high chemoattractant concentration, but this area is surrounded by lower concentration, which makes this area appear as an isolated area of chemoattractant to the sperm. The sperm follows the gradients within this area, but this alone does not lead the sperm to the egg.

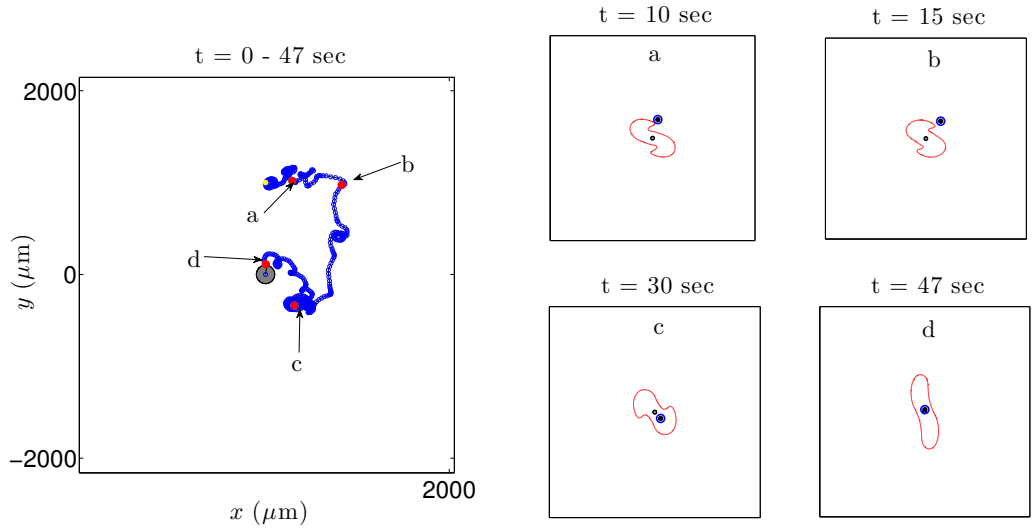
t = 0 - 47 sec
2000
0
−2000
y (μm)
x (μm)
2000
a
b
c
d
t = 10 sec
a
t = 15 sec
b
t = 30 sec
c
t = 47 sec
d

(a)

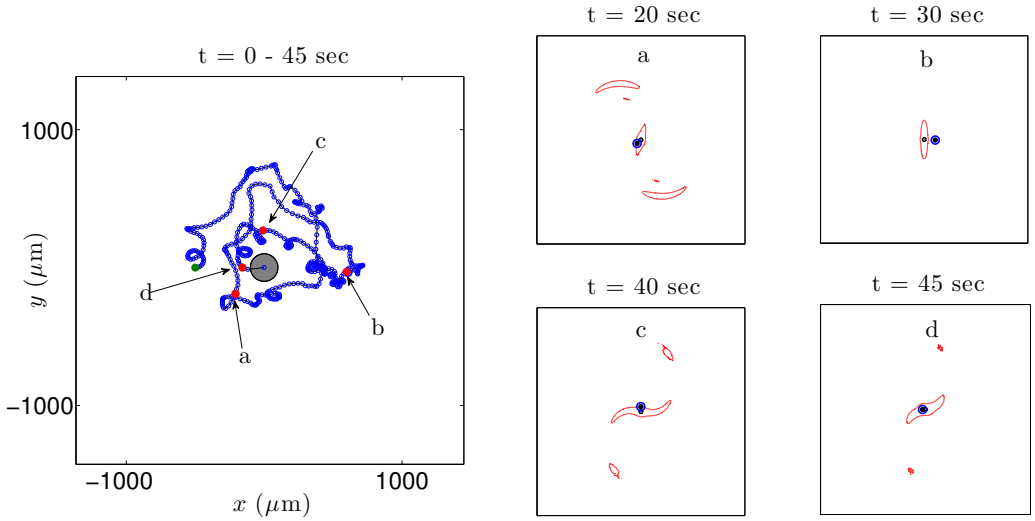
t = 0 - 45 sec
1000
−1000
y (μm)
x (μm)
−1000
1000
a
b
c
d
t = 20 sec
a
t = 30 sec
b
t = 40 sec
c
t = 45 sec
d

(b)

Figure 3.9

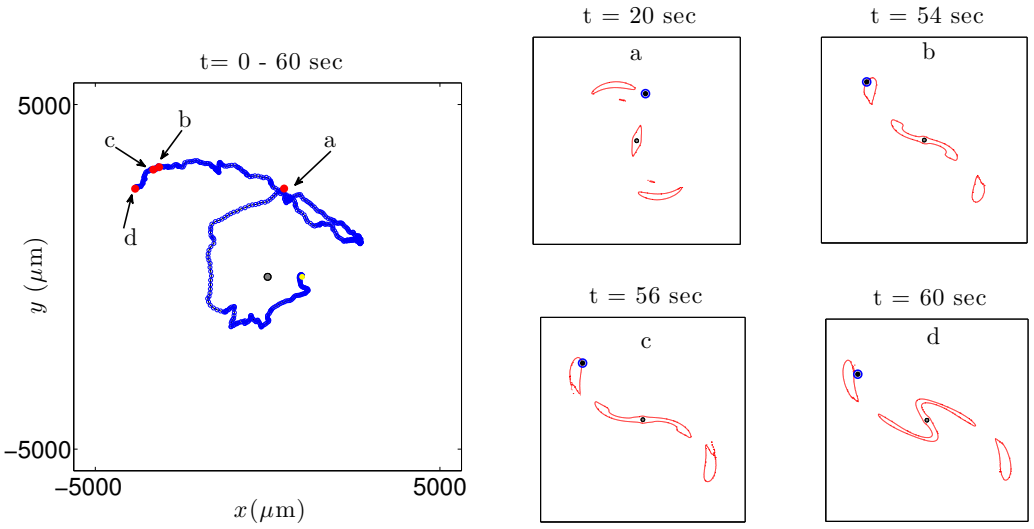

(c)

Figure 3.9: Representative sperm path for a sperm in the low-α_0 unsteady shear case (Fig. 3.9a) and the high-α_0 unsteady shear case (Fig. 3.9b,c). The red lines in subfigures a - d indicate the threshold concentration ($C_{\text{threshold}} = 3 \times 10^{-10}$ mol μm^{-3}). The entire path is shown in the large figure to the left and each of the 4 points in time (indicated by a red dot) are also shown individually along with the subsequent threshold contour in the 4 small subplots to the right. Note that the larger plot is at a smaller scale to show the intricacies of the entire path. The sperm in the low-α_0 unsteady shear case example employed the Run Response at all times when the local concentration was above the threshold. The sperm in the high-α_0 unsteady shear case used the Turn and Run Response (3.9b) and the Run Response (Fig. 3.9c) when stimulated.

3.2 No Flow Case: timescales, effect of distance/behavior

In the no flow case, the only relevant scales are the asymptotical total fertilization rate and the time to the first success. Sperm utilizing any behavioral response achieve a higher success rate than sperm with no response (Fig. 3.11). All behaviors result in the same final fertilization success, but the timescales in the cumulative fertilization rates differ. The effect of the initial location on the fertilization rates is radially-symmetric, but is a function of the initial distance from the egg or the closest threshold location (Fig. 3.12). The same hierarchical order of behaviors with respect to the first success and the first to achieve the converged total fertilization is maintained for all initial conditions in the no flow case: 1. Run; 2. Turn and Run; 3. Drifting Circle; 4. No Response.

The scales associated with the fertilization rates are illustrated in Fig. 3.10 below. For the

3 behaviors with chemotactic abilities, an angle is drawn from the initial location to the threshold location (green line). Once the sperm reach the threshold, the loitering behavior no longer contributes to the fertilization success and the response behavior almost guarantees their success. The subtended angle for the sperm with no response behavior is drawn from the initial location to the boundary of the egg (orange line). The response angle is about 85° and the no response angle is about 20°. These angles correspond the the portion of the threshold area or the egg that the sperm would overlap with due to the diffusivity of their loitering behavior. This percent of the total circumference of the threshold circle and the egg correlates to about 24% and 6% of sperm to reach the egg with a response behavior and no behavior, respectively. We expect higher fertilization rates for both cases since more sperm will overlap this area due to their random loitering behavior. This estimate provides us with a sense of scale for the fertilization rates in the no flow case.

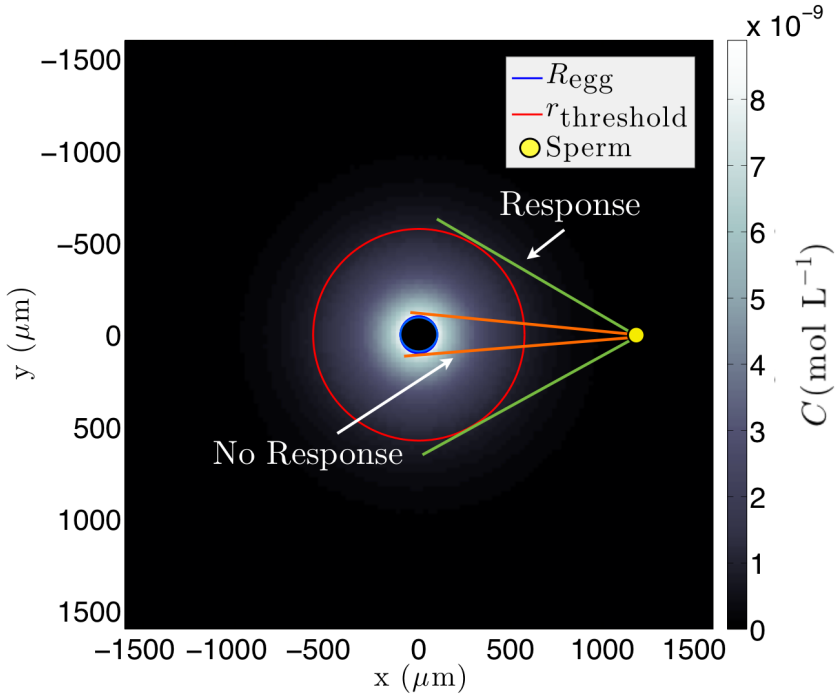

Figure 3.10: Location of relevant parameters and depiction of subtended angles for both the no response (orange lines) and response (green lines) behaviors in the No Flow Case. The red circle shows the threshold concentration and the blue circle indicates the egg. The sperm in this example are placed at ($r_0 = 12R_{\text{egg}}$; $\theta_0 = 0$). Fertilization rates for this case are shown below in Figs. 3.11 and 3.11.

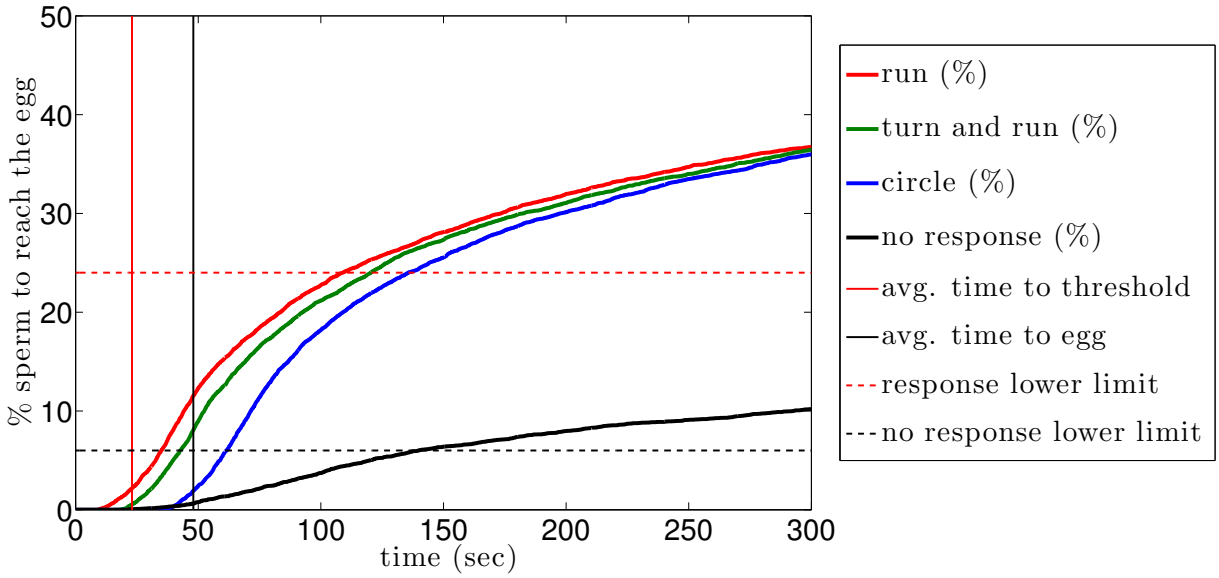

Figure 3.11: Cumulative fertilization rates for each response in the no flow case. The sperm in each case initiated from the same location ($r_0 = 12R_{\text{egg}}$; $\theta_0 = 0$). Rates were collected for the first 300 seconds. Representative sperm paths can be found above in Figs. 3.6 -3.8 (no flow case).

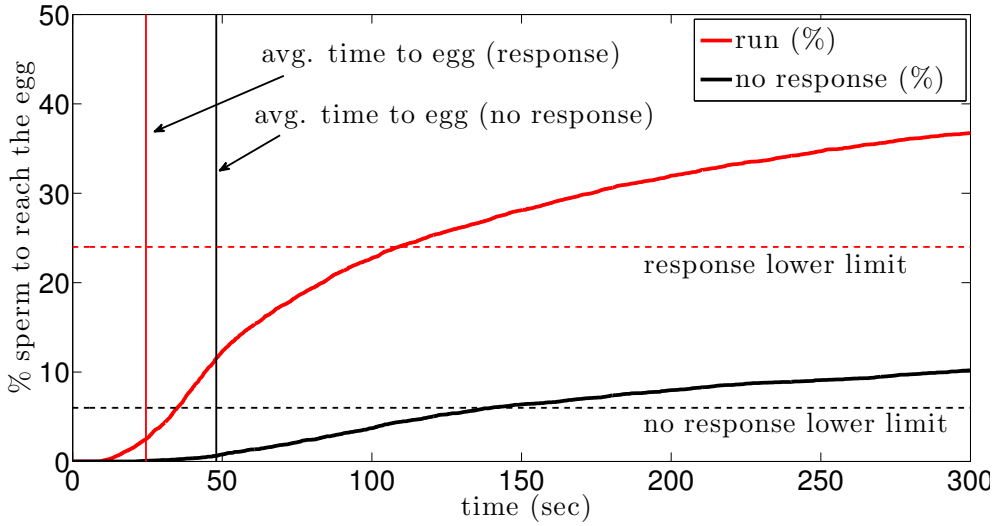

(a) Scales for the Run Response and No Reponse

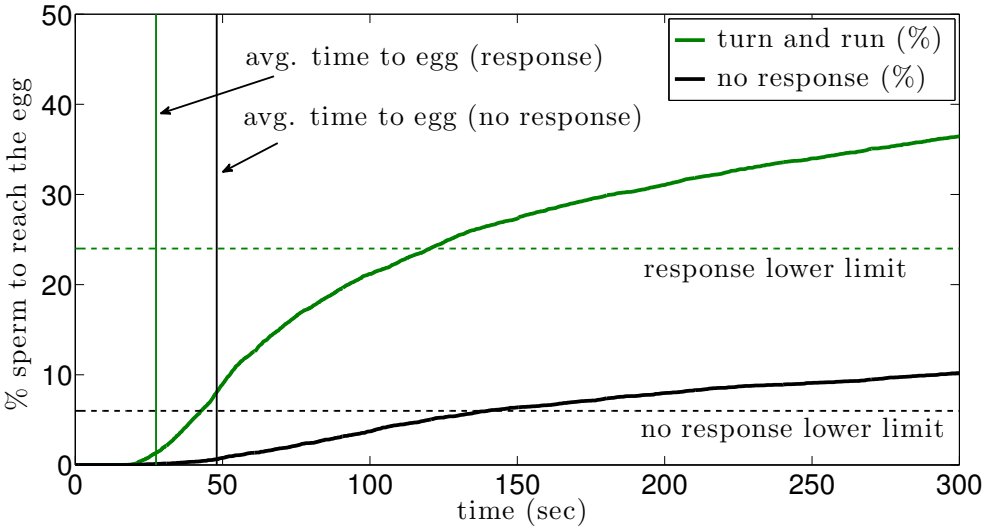

(b) Scales for the Turn and Run Response and No Response

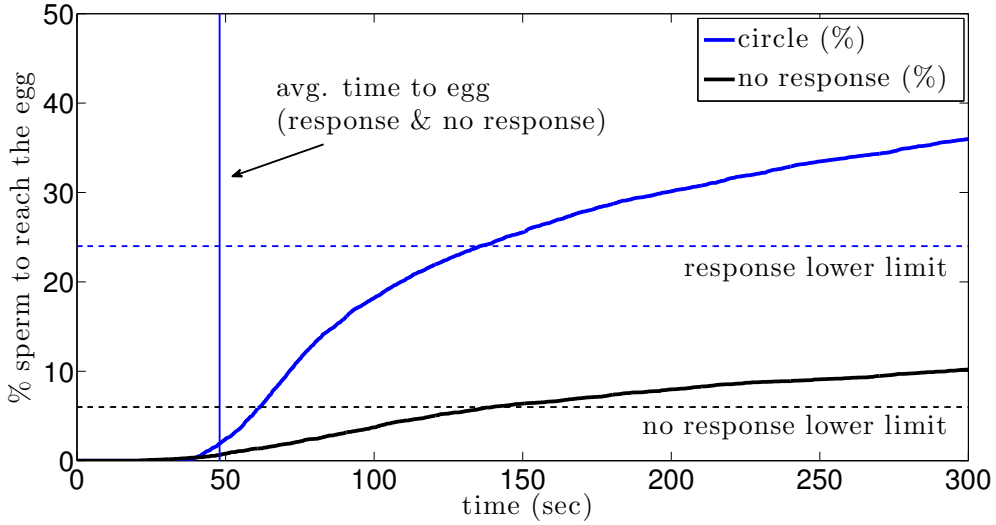

(a) Scales for the Drifting Circle Response and No Response

Figure 3.11: The sperm in each case initiated from the same location ($r_0 = 12R_{\text{egg}}$; $\theta_0 = 0$). Rates were collected for the first 300 seconds. The timescales shown correspond to the average time for sperm with the given response to reach the egg (thin solid colored line) and for sperm with no response (thin solid black line).

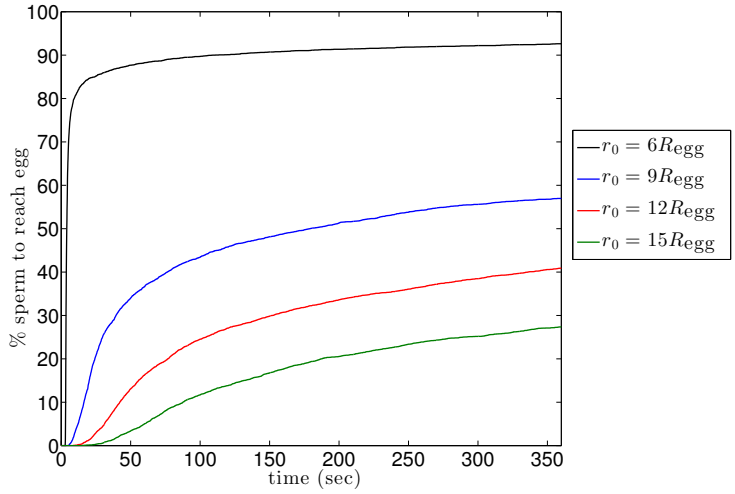

Figure 3.12: Cumulative fertilization rates shown over time for the Run Response for 4 different initial locations to illustrate that cumulative fertilization rates depend on initial distance. Note that the threshold is located at $5.75R_{\text{egg}}$ and all cumulative fertilization rates reach 100% for $r_0 < 5.75R_{\text{egg}}$.

3.3 Effect of Distance

The fertilization model tested the ability of the sperm to reach the egg from 8 different starting locations (Fig. 3.13). Each response was tested from each location in each flow. Figures 3.14 - 3.18 are representative examples of the impact of distance on the success rate. These correspond to the simulations that tested the Turn & Run response within each of the flows from each location.

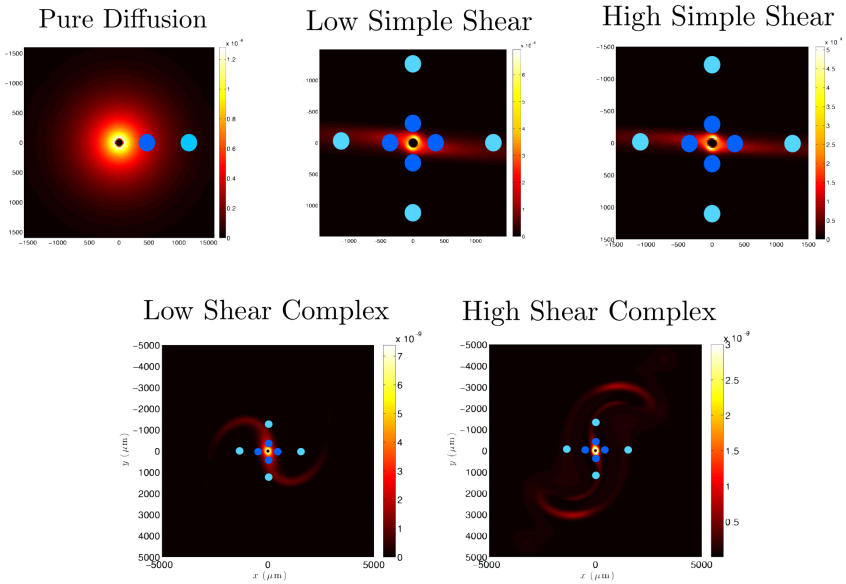

Figure 3.13: Initial locations are shown by blue circles for each flow. The darker dot corresponds to the smaller radial distance, $4R_{\text{egg}}$ and the lighter dot represents the farther radial distance, $12R_{\text{egg}}$.

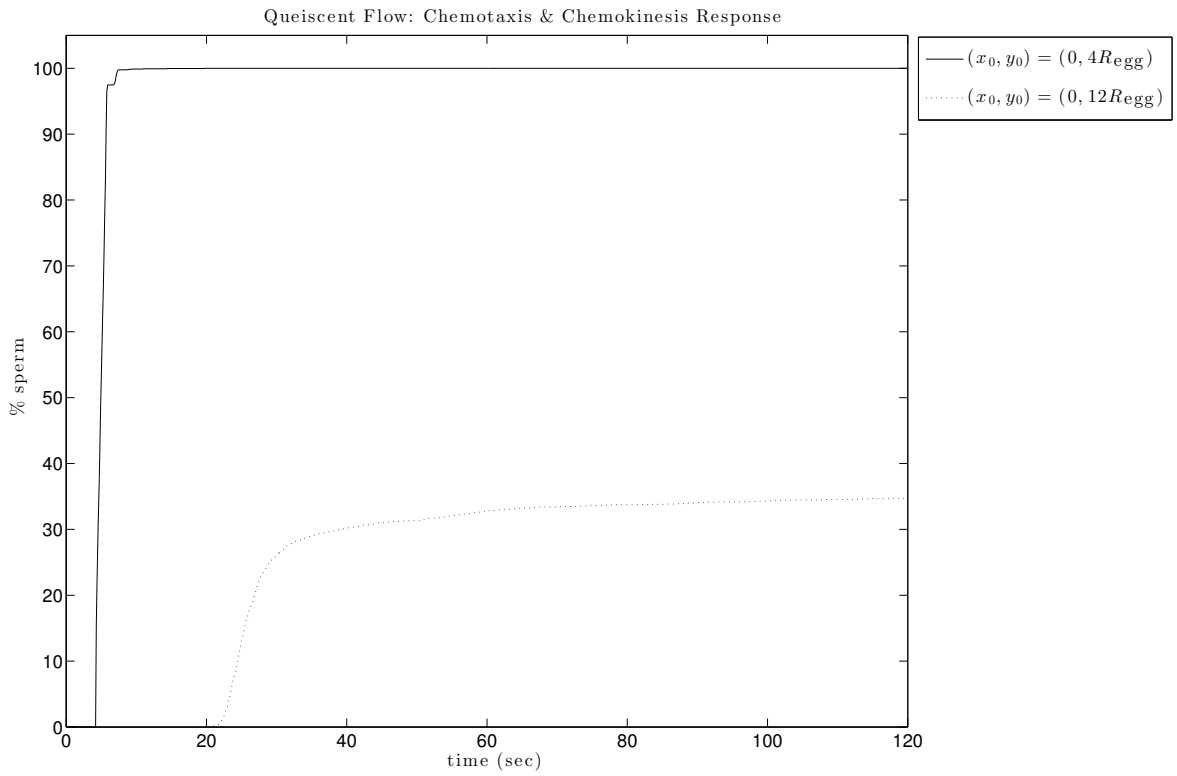

Figure 3.14: Chemotaxis & Chemokinesis response within a quiescent flow.

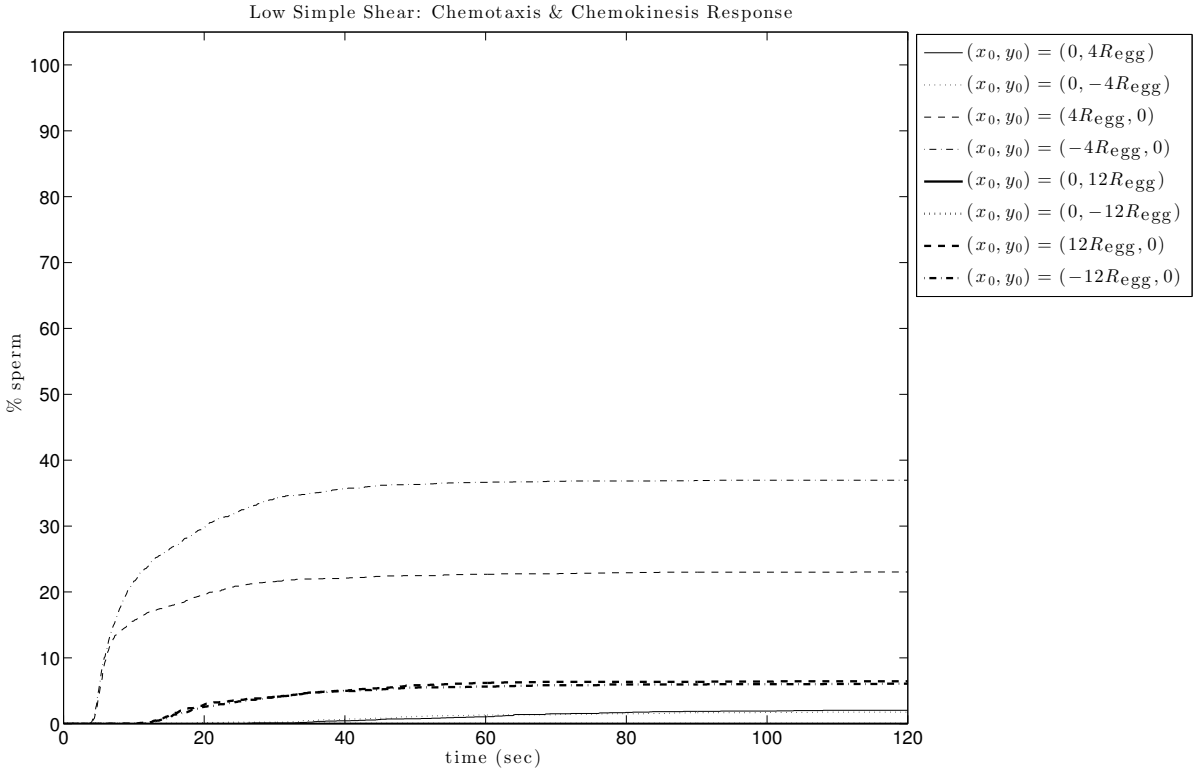

Figure 3.15: Chemotaxis & Chemokinesis response within a low simple shear flow.

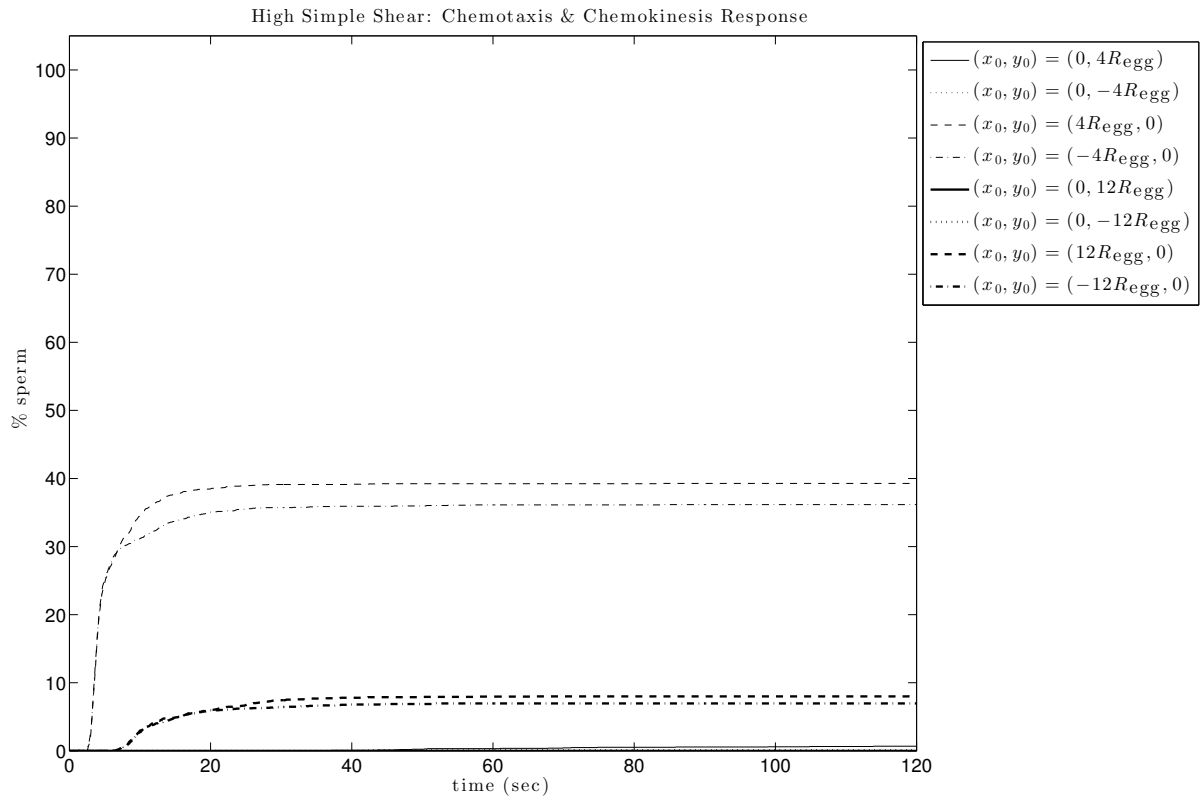

Figure 3.16: Chemotaxis & Chemokinesis response within a high simple shear flow.

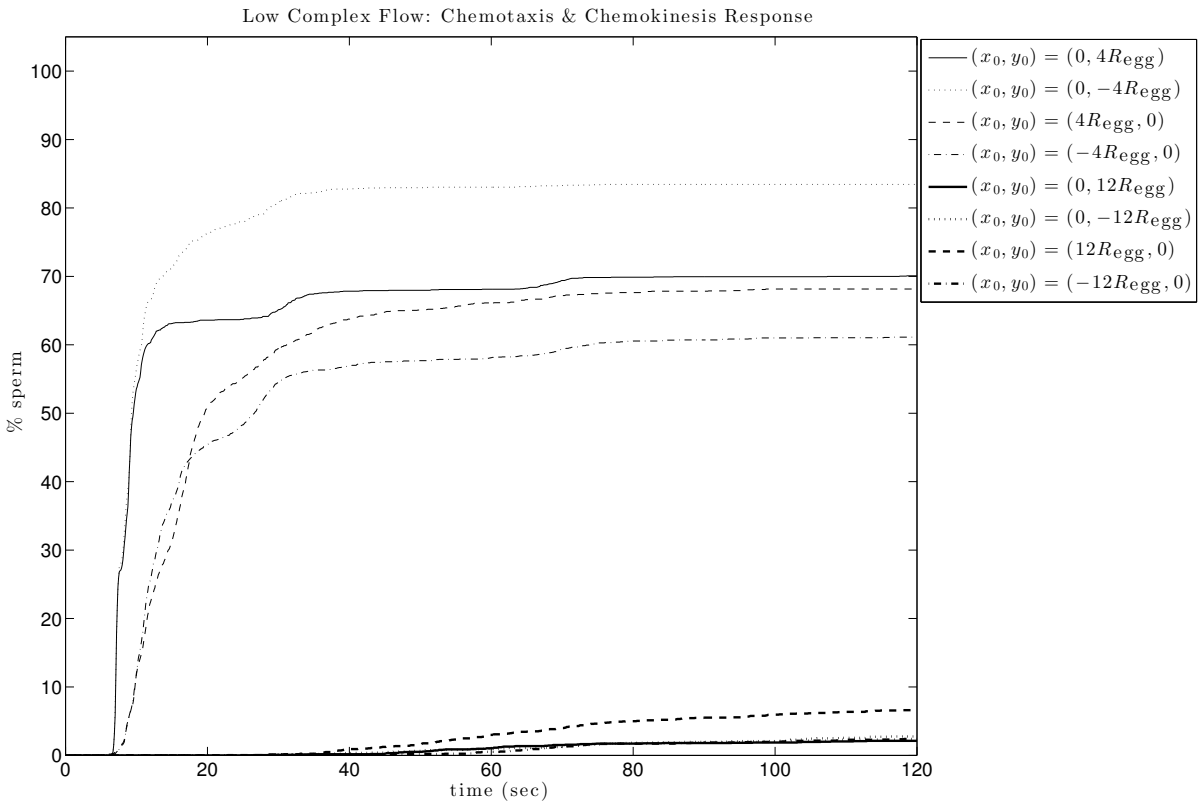

Figure 3.17: Chemotaxis & Chemokinesis response within the low complex flow.

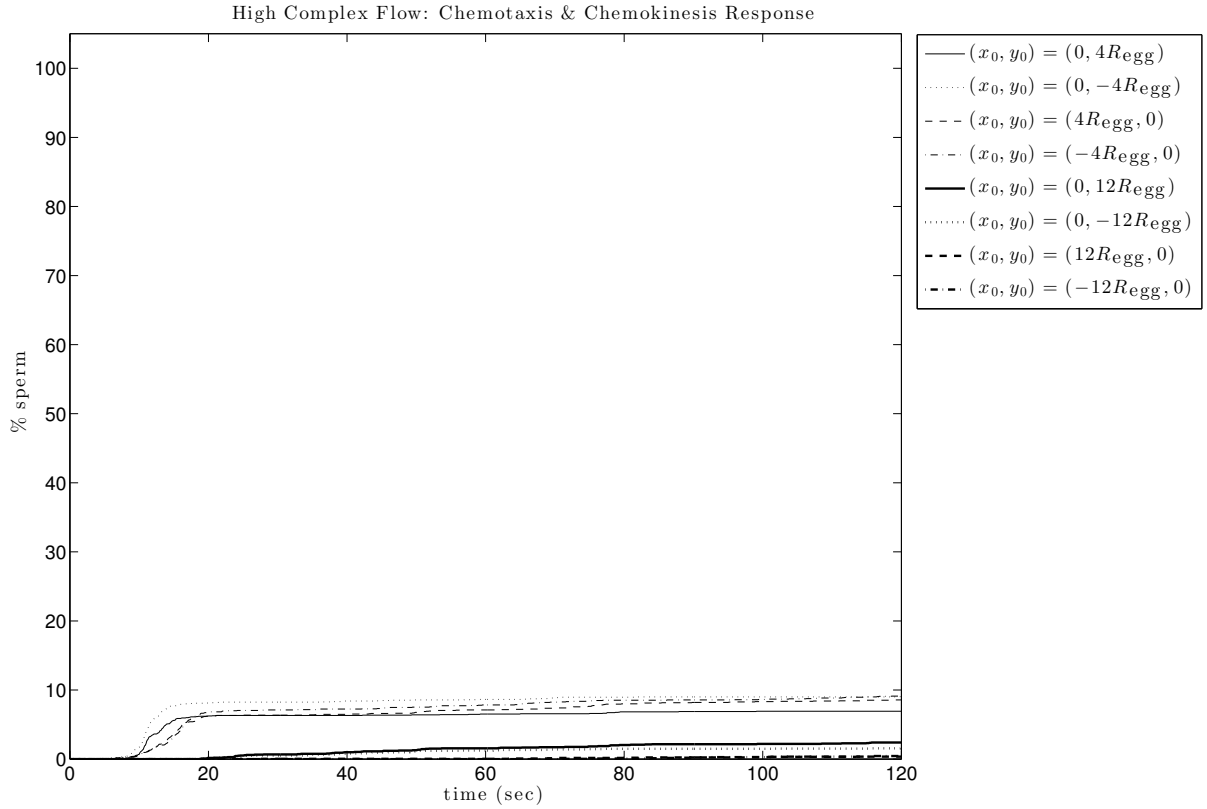

Figure 3.18: Chemotaxis & Chemokinesis response within the high complex flow.

The most obvious result indicates that for the initial locations closer to the egg, the total percentage of sperm able to locate the egg is increased. This is most obvious in the quiescent flow (Fig. 3.14), where 100% of the sperm reached the egg from the closest initial starting location, but only about 35% reached the egg from the further location. The two shear (Figs. 3.15 and 3.16) cases highlight the importance of the location relative to the shear direction. The 4 locations along the x-axis showed significantly higher success rates than those aligned perpendicular to the shear, along the y-axis. The locations closer to the egg, the lighter lines in the plots, again showed an increased success rate that those further away. However, the closer initial points aligned perpendicular to the shear were still less successful than those that were further away, aligned with the flow. The two shear cases also indicate that the window for fertilization in a linear shear flow is very small. The integrated success rate asymptotes very quickly within both the high and the low linear shear

flows, indicating there is not much ability to overcome the flow once a sperm has passed the egg. The two more complex cases agree with the improved success due to closer initial location. The difference between the orientation of the starting location did not have the same significant impact as it did in the linear shear cases, most likely because the shear does not maintain one direction, so there is no difference in the relative alignment with the direction of linear shear. The relative change between the close and far starting locations is very significant for the complex cases, with the closer initial locations seeing about 10 times more success than the far locations.

3.4 Effect of Flow

The impact of the flow on individual responses was also examined. Included is a representative result of the effect of each of the flows on the Turn & Run response from one location $(x_0, y_0) = (-4R_{\text{egg}}, 0)$ (Fig. 3.19). This plot highlights the common observation that the quiescent flow had the highest success rates and the high complex flow usually maintained the lowest success rates. The low complex flow, however, usually had success rates that fell between the quiescent flow and the high complex flow. The difference in shear rates did not have as much of an effect on the fertilization success for the simple linear shear cases. The time required for the rate to asymptote was very short for both linear shear cases as well. The sperm had more opportunities to reach the egg in both complex cases.

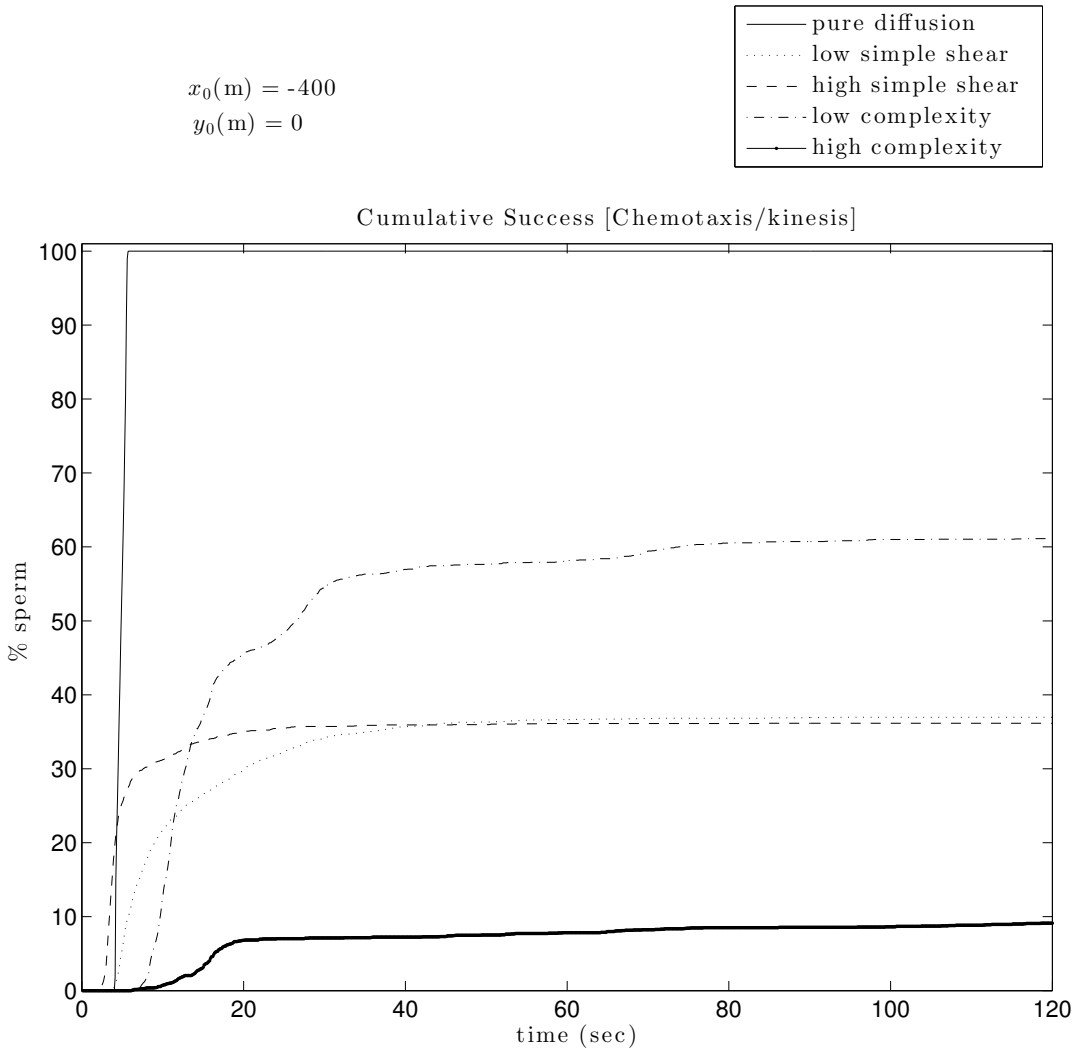

Figure 3.19: Plots depicting the cumulative success rates of each of the 3 responses as well as the no response case for each of the 5 flows. The initial location was $(x_0, y_0) = (-4R_{\text{egg}}, 0)$.

3.5 Efficacy of Responses

Within the quiescent flow, the parameters of each individual response were tested. In each case, the sperm were started at the same location, $(x_0, y_0) = (0, 12R_{\text{egg}})$ (Fig. 3.20). In this section there are two representative figures to show the impact on the parameters within the Chemotaxis & Chemokinesis Response in the quiescent flow. First, the possible ranges for the u_{drift} are tested for their impact on the success rate (Fig. 3.21). This parameter effects the time to the first success

as well as the total success when the integrated rate asymptotes. For the shortest, smallest range, $[1, 2]u_{\text{drift}}$, the time to the initial success was the longest and the overall success was the shortest. The longest, highest range, $[1, 4]u_{\text{drift}}$, showed a bit faster time to the first initial success, but took the longest to asymptote. The range where the low range was the highest in the group, $[2, 3]u_{\text{drift}}$, saw the fastest time to initial success, but a middle value for the overall success. The increase in the drift speed effects the time to initial success and contributes to the total success. Next, the range of the $\dot{\theta}$ values altered during the response behavior are presented (Fig. 3.22). This plot indicates that the response is not highly sensitive to the curvature when the drifting speed is maintained as a separate parameter. The time to the initial success was identical for each range, but the overall success did show some sensitivity to the turning rate and subsequently the curvature. The range that included the highest decrease in the turning rate, $[0.15, 0.75]\dot{\theta}$ exceeded the other ranges in total success. The remaining ranges proved to be more similar, with the wider range attaining a slightly greater total success rate.

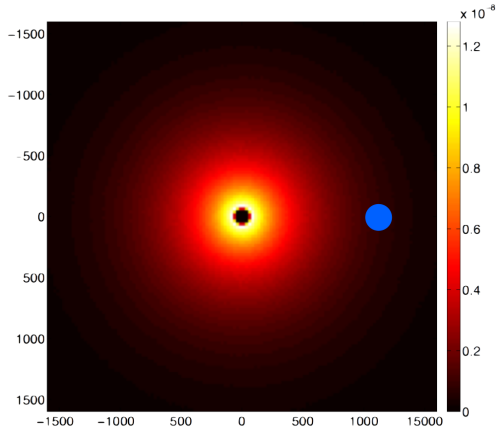

Figure 3.20: Starting location for the sperm for each case examining the effect of varying parameters within individual results.

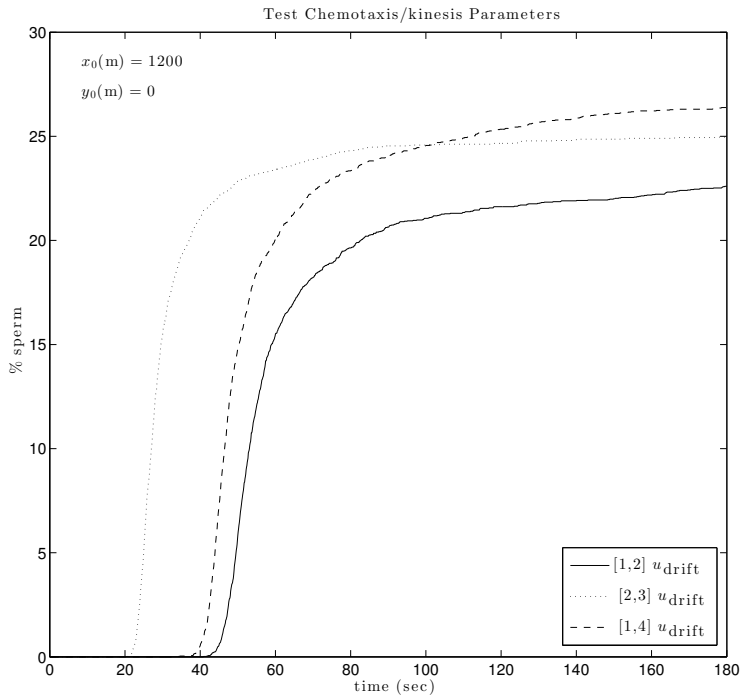

Figure 3.21: Various ranges for the increase in u_{drift} for the Chemotaxis & Chemokinesis Response.

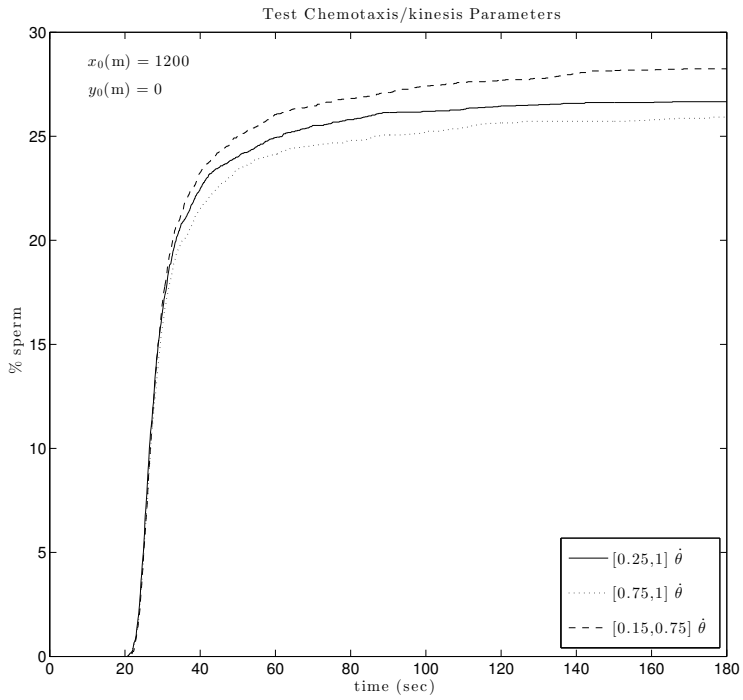

Figure 3.22: Various ranges for the decrease in the $\dot{\theta}$ for the Chemotaxis & Chemokinesis Response.

3.6 Discussion

The results introduce the first attempt to better understand the motility abilities of sperm undergoing broadcast spawning in a flow. This thesis provides an example of how the results will be synthesized and understood in the context of fertilization and fluid mechanics. In general, it is clear that any ability to utilize some type of speed and directional response greatly enhances the ability of a sperm to locate an egg. The quiescent flow resulted in the highest success rates, followed by the low complex flow, both linear shear flows and finally the more complex flow saw the lowest rates for all of the response behaviors. More focus will eventually be put on determining which of the individual responses is the most successful considering different flow conditions. This success will be considered in terms of the ecological efficiency of the behavior and how significant the impact of different flows is on the success rate. If a behavior allows a sperm to successfully reach an egg in any flow, that should be more important than a higher success rate in a quiescent,

less realistic flow, but an inability to locate an egg in a more complex, unsteady shear flow.

The results provide insight into what aspects of this large problem are valuable and productive. Future work could entail modifications to both the loitering and the response behaviors. Different parameters could be altered and additional factors effecting fertilization, such as viability, could be considered. Additionally, the flow could be modeled with less simplicity. A 3D case could also be utilized. This study can contribute a basis for many continued avenues of research within this area.

In the next section is a draft of a paper to be submitted to the Journal of Marine Systems. This paper further explores the implication of this study.

3.7 JMS Paper

The development of chemoattractant plumes released from an egg in various flows and the strategies employed by sperm to locate the egg

Allison F. Bell, John P. Crimaldi

Department of Civil, Environmental and Architectural Engineering, University of Colorado, Boulder, CO, 80309-0428, USA

Abstract

The ability of benthic invertebrate sperm to utilize chemotaxis and chemokinesis to locate an egg during broadcast spawning is examined under a variety of flow conditions. During the fertilization process, males release a cloud of sperm and females release a cloud of eggs into the ambient flow. The two plumes are brought together due to turbulent stirring. Individual eggs release a mass of chemoattractant into the flow upon being spawned. The motile sperm are tasked with swimming to an egg for fertilization to occur. The sperm are able to sense the concentration of chemoattractant released by a conspecific egg and change their swimming behavior. Chemotaxis, the orientation due to a chemoattractant, and chemokinesis, the increase in speed due to a chemoattractant, aid the sperm in finding and reaching the egg in a flow. The mechanics of this process are not well understood. The flow around an egg in a linear shear flow is modeled for both a constant linear shear rate and for an unsteady turbulent flow where the linear shear changes direction and magnitude. Sperm are placed in a mass at an initial location and advect due to their swimming behavior and the flow. The rate at which the sperm reach the egg is quantified. The efficacy of several possible response behaviors are tested within a range of flows and for a variety of initial placement within the flow.

1. Introduction

A variety of benthic invertebrates use broadcast spawning as a reproductive strategy. Sessile adult males and females, separated by a distance on

the order of meters, synchronously release sperm and eggs into the ambient flow. Although sperm are motile, their swimming speed is likely too slow to bridge the initial distance to the eggs, so physical stirring by the large-scale flow is required to aggregate the gametes. Meanwhile, eggs increase their effective target size by releasing plumes of chemoattractant that are stirred and stretched by the local small-scale flow. If flow processes advect sperm sufficiently close to eggs, motile sperm employ chemotaxis to navigate through gradients in the chemoattractant plumes.

From release to fertilization, spawned gametes traverse a physiochemical environment with features that span spatial scales from meters to microns. The impact of these physical and chemical processes at various scales on the resulting efficacy of the fertilization strategy is difficult to study and not well understood. Various large-scale flow phenomena have been proposed to produce gamete aggregation, but the evidence for this is still indirect. At the small-scale end of the spectrum, details of the nature of chemoattractant plumes in realistic flow conditions are all but unknown, as are details of how sperm navigate within complex chemical landscapes. For a review of the current state of knowledge on the impact of flow on fertilization success across a range of scales, see Crimaldi and Zimmer (2014). In the present study, we focus on the small-scale aspects of the problem. We use analytical and numerical models of fluid flow, chemoattractant plume dispersion, and sperm motility and chemotaxis to investigate how unsteady and spatially varying flow processes shape chemoattractant plumes and impact fertilization success at the gamete scale. The study is necessarily idealized by design, given that many of the specific details about various constitutive aspects of the problem are not easily observed or documented using current experimental and laboratory techniques.

1.1. Background

Sperm exhibit a chemotactic response to chemicals released by conspecific eggs for a range of benthic invertebrates including urchin (Kaupp et al., 2003; Böhmer et al., 2005), star fish (Böhmer et al., 2005), sea squirt (Jantzen et al., 2001), siphonophores (Cosson et al., 1984), coral (Morita et al., 2006) and abalone (Riffell et al., 2002). Sperm response behavior is observed when the chemoattractant concentration is above a given threshold (Riffell et al., 2004; Zimmer and Riffell, 2011), and in the presence of a chemoattractant gradient (Riffell et al., 2002, 2004; Ward et al., 1985).

We base the present study on known chemoattractant characteristics associated with gametes of red abalone (*Haliotis rufescens*) because gametes of this organism have been extensively studied. For red abalone, the chemoattractant released by eggs has been identified as the free amino acid L-tryptophan (Riffell et al., 2002), which is released at a constant flux the range of $0.18 - 0.3$ mol egg^{-1} min^{-1} (Krug et al., 2009; Himes et al., 2011) for 45 minutes after being spawned (Krug et al., 2009; Himes et al., 2011). Typical of amino acids, L-tryptophan is weakly diffusive in water, with a reported diffusivity of 6×10^{-9} m^2 s^{-1} (Mark and Nilsson, 2002; Polson, 1937; Zimmer and Riffell, 2011). The threshold concentration of L-tryptophan that elicits chemotactic response in red abalone sperm is reported to be between 3×10^{-10} mol L^{-1} and 4×10^{-9} mol L^{-1} (Riffell et al., 2004; Zimmer and Riffell, 2011).

Much less is known about the behavioral response characteristics of sperm to an associated chemoattractant. Therefore, in this work, we synthesize sperm behavioral response information from a range of benthic invertebrate species. Sperm of most species have similar swimming patterns, resulting from the helical motion of a flagellum (Friedrich and Julicher, 2009), although the resulting swimming speeds are highly variable even within one species (Kupriyanova and Havenhand, 2002).

The paths of swimming sperm have been observed in the field (Miller and Mundy, 2005; Babcock et al., 1994; Quinn and Ackerman, 2011), and more typically under a microscope (Morita et al., 2006; Wood et al., 2005; Böhmer et al., 2005; Cosson et al., 1984; Guerrero et al., 2010a; Riffell et al., 2002, 2004; Riffell and Zimmer, 2007; Himes et al., 2011; Zimmer and Riffell, 2011; Inamdar et al., 2007; Evans et al., 2012; Yoshida et al., 1993) leading to a basic understanding of swimming patterns and parameters. Two distinct sperm behaviors have been observed: one (called loitering) corresponding to sperm exposed to a chemoattractant concentration below the response threshold, and the other (called response behavior) corresponding to exposure above the threshold. Most documented loitering behaviors consist of helical paths (in 3D) (Friedrich and Julicher, 2007, 2009; Riffell and Zimmer, 2007) or drifting circles (in 2D) (Alvarez et al., 2012; Friedrich and Julicher, 2008; Böhmer et al., 2005; Kaupp et al., 2008). Within the loitering behavior, no bias with respect to an egg has been observed (Vogel et al., 1982; Riffell and Zimmer, 2007; Riffell et al., 2002, 2004; Morita et al., 2006). The path is considered random outside any stimulus.

There is greater variation in the documented response behaviors. It is

known that receptors covering the flagellum register a spatial change in chemoattractant concentration and initiate a chain of chemical reactions within the sperm that control its behavior (Alvarez et al., 2012; Kaupp et al., 2003; Guerrero et al., 2010b,a; Wood et al., 2005; Böhmer et al., 2005; Yoshida and Yoshida, 2011; Morita et al., 2009; Alvarez et al., 2012). The observed changes due to stimuli are varied, but two major components are consistent. The response is manifested in a change in direction (chemotaxis) and/or a change in swimming speed (chemokinesis). Some studies have shown a shift in orientation towards the egg without any change in speed (Kupriyanova and Havenhand, 2002; Friedrich and Julicher, 2008; Kaupp et al., 2008), while others note both a change in speed and direction. The addition of chemokinesis alters the swimming path in a few ways: a decrease in the curvature resulting in an increased drifting speed (Ward et al., 1985; Zimmer and Riffell, 2011; Riffell et al., 2004), a path described as a trochoid or prolate trochoid (Böhmer et al., 2005; Guerrero et al., 2010b; Kaupp et al., 2006, 2008), severe suppression of turns such that any turns are no longer recognized (Guerrero et al., 2010a; Riffell et al., 2004) and a doubling of the swimming speed performed in straight run (Riffell et al., 2004; Riffell and Zimmer, 2007; Zimmer and Riffell, 2011).

Mathematical modeling of the mechanics of broadcast spawning has contributed to a better understanding of the mechanics. To replicate sperm motility, previous studies have modeled the swimming paths as a diffusive process (Keller and Segel, 1971; Babcock et al., 1994; Alt, 1980). When chemotaxis is considered, sperm paths have been modeled as a biased random-walk (Alt, 1980; Jabbarzadeh and Abrams, 2005) and as a diffusive process wherein the diffusivity of the linear path is relative to the strength of the chemoattractant (Friedrich and Julicher, 2008, 2009). Yoshida et al. (1993) developed the widely used linear equation chemotaxis index (Yoshida et al., 2002; Guerrero et al., 2010a), which measures the trajectory of the sperm relative to the egg, in order to quantify chemotaxis. Sperm velocity and orientation relative to the egg have been calculated to indicate the linearity of the path and the increase in swimming speed as well (Riffell et al., 2004; Himes et al., 2011; Zimmer and Riffell, 2011). Models have also been used to estimate fertilization rates using a variety of techniques: an advection-diffusion process (Kiselev and Ryzhik, 2012), probability of collision Vogel et al. (1982) and a function of both egg diameter and sperm concentration (Vogel et al., 1982).

In addition to the biological aspects of the problem, flow dynamics at the

gamete scale have been identified and used to study fertilization mechanics. The typical environment where most benthic invertebrates spawn is turbulent with relatively low velocities. The magnitude of the Kolmogorov scale, ν, in these environments is on the order of millimeters. Sperm and egg are on the order of micrometers, below the Kolmogorov scale. Therefore, gametes experience a physical world dominated by a single dissipative vortex at any given time. This imposes a linear shear (Karp-Boss et al., 1996; Jumars et al., 2009; Riffell and Zimmer, 2007; Zimmer and Riffell, 2011) with relatively low shear rates.

Zimmer and Riffell (2011) modeled the development of the chemoattractant plume in steady shear using a numerical simulation and tested the impact of shear rates on fertilization rates using a Taylor-couette flow. Shear enhances fertilization rates for the red abalone beyond those found for no flow in shear rates less than $\alpha = 1\ s^{-1}$, and fertilization decreased in shear flows with higher rates (Riffell and Zimmer, 2007; Zimmer and Riffell, 2011). Increases in energy dissipation rates produced decreased success as do increases in (Denny et al., 2002), bed roughness (Quinn and Ackerman, 2011), flow velocity (Levitan et al., 1992) and turbulence (Denny and Shibata, 1989; Denny et al., 1992; Levitan and Young, 1995). Additionally, the helicity of the sperm path (Farley, 2002), the preference of a sperm for certain eggs within a single species (Evans et al., 2012) and viability of both the egg and sperm (Giorgi and DeMartini, 1977) can decrease actual and predicted fertilization rates. In the absence of flow, the effective target size of the egg increase fertilization rates and decrease the negative impact of sperm limitation and sperm dilution (Levitan and Irvine, 2001; Jantzen et al., 2001; Levitan, 2000; Styan, 1998; Levitan, 1996, 2006; Farley and Levitan, 2001; Levitan, 1993; Farley, 2002).

1.2. Present study

In the current study we use a series of numerical simulations to model interactions of small-scale physical-biological processes in broadcast spawning. We model a flow field consisting of shear that has unsteady direction and magnitude. This flow field is representative of flow experienced by gamete-scale (sub-Kolmogorov) particles within larger-scale turbulence. The flow is modified by the presence of a freely rotating and advecting egg. We then use the model to determine the unsteady spatial distribution of chemoattractant released by the egg. The chemoattractant distribution is governed by stirring from the local flow and by molecular diffusion. Finally, we use

the model to determine sperm trajectories for several behavioral strategies as the sperm navigate through the chemoattractant plume. Ultimately, we gain insight into the role of turbulent flow on shaping gamete-scale chemoattractant plumes, and on the role of several behavioral strategies used by sperm to enhance their likelihood of locating an egg.

For simplicity, the model is developed in two dimensional space. The goal of these simulations is to investigate the process-level role of structured stirring on attractant plume formation and chemotaxis efficacy, and to build a framework for understanding more complex flows. It is common to investigate the mechanistic features of complex 3D stirring processes with simpler 2D models (e.g., Cetegen and Mohamad, 1993; Rehm et al., 1993; Flohr and Vassilicos, 1997; Meunier and Villermaux, 2003; Basu et al., 2007; Martinand and Vassilicos, 2007; Crimaldi et al., 2006, 2008); these models elucidate instantaneous processes seen locally in more complex 3D flows.

2. Methods

2.1. Numerical modeling of plume development at the scale of an egg

2.1.1. Simple Shear Flow

The distribution of chemoattractant mass is modeled for two flows: shear flows with steady shear and flows with unsteady shear. The 2D velocity vector $\vec{u}$ with shear rate α in the presence of a freely-rotating egg (Mikulencak and Morris, 2004) has x and y components

$$\frac{\vec{u_x}}{\alpha R_{\text{egg}}} = \frac{1}{2}y^*\left(1 - r^{*-4}\right) + \frac{1}{2}y^*\left(1 - r^{*-2}\right) - 2x^{*2}y^*\left(r^{*-4} - r^{*-6}\right) - \frac{-\frac{1}{2}y^*}{r^{*2}} \quad (1)$$

$$\frac{\vec{u_y}}{\alpha R_{\text{egg}}} = \frac{1}{2}x^*\left(1 - r^{*-4}\right) + \frac{1}{2}x^*\left(1 - r^{*-2}\right) - 2x^*y^{*2}\left(r^{*-4} - r^{*-6}\right) - \frac{-\frac{1}{2}x^*}{r^{*2}} \quad (2)$$

where $x^* = \frac{x}{R_{\text{egg}}}, y^* = \frac{y}{R_{\text{egg}}}, r^* = \frac{r}{R_{\text{egg}}}$ and r is radial distance from the center of the egg. The streamlines associated with this flow are shown in Fig. 1 for $\alpha = 1\ \text{s}^{-1}$.

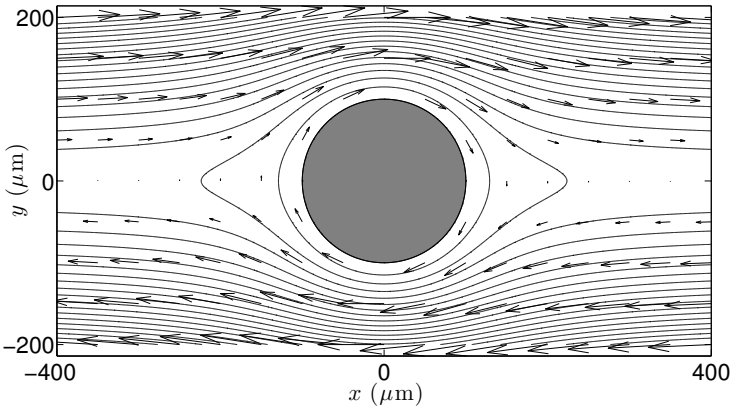

Figure 1: Streamlines (black lines) and velocity vectors (black arrows) for the steady shear flow with shear rate $\alpha = 1$ s^{-1} in the presence of an egg. The egg is depicted by the grey circle. The streamlines indicate the flow near the surface of the egg is circular and that velocity increases away from the egg.

Constant shear rates $\alpha = 0, 0.1, 0.2, 0.4, 1, 2$ s^{-1} are used in Eqs. 1 and 2 to define the six steady shear flows to be used in the model. Note that $\alpha = 0$ corresponds to a quiescent case. We specifically keep the shear rate below the level where sperm motility becomes highly impacted by the rate of shear. Zimmer and Riffell (2011) show that for higher shears, the sperm's ability to turn decreases and reduces their ability to find an egg. Using α^{-1} and $R_{\text{egg}}2/D$ as a characteristic timescales for advection and diffusion, respectively, we can define a Péclet number as $\text{Pe} = \frac{\alpha R_{\text{egg}}2}{D}$ *Add more text about Pe*.

2.1.2. Unsteady Shear Flow

We also consider a more complex flow that is intended to mimic the behavior of an egg in an unsteady, turbulent flow. At any instant, the egg is assumed to be in the middle of a single vortical flow structure, with locally linear shear. We use Eqs. 1 and 2 to define the linear shear flow, but the direction and magnitude of the shear changes with time.

The direction of the shear, defined as angle ϕ from the horizontal, is

updated at each time-step dt according to

$$\phi_{\text{new}} = \phi_{\text{old}} + \dot{\phi} \cdot dt \tag{3}$$

where $\dot{\phi}$ is a normally distributed random variable with zero mean and standard deviation $\sigma_{\dot{\phi}}$ (see Table .1 for value). The magnitude of the shear is varied as

$$\alpha(t) = \alpha_0 \sin(t/\mathrm{T}) \tag{4}$$

where the amplitude α_0 has is different for two cases: low ($\alpha_0 = 0.5\ \mathrm{s}^{-1}$) and high ($\alpha_0 = 1.25\ \mathrm{s}^{-1}$).

The radius of the vortex is held constant for simplicity. The decay rate used to replicate the decay in velocity from the center of the vortex corresponds to the shear stress decay associated with an Oseen vortex (**??**)

$$h(r) = \frac{1}{(r/r_{\text{core}})^2}\left[1 - \exp\left[-\left(\frac{r}{r_{\text{core}}}\right)^2\right]\right] \tag{5}$$

where r_{core} is the scale for the rotational core of the eddy (Table .1)

2.1.3. Chemoattractant Flux Model

We use a quasi-2D model with a domain consisting of a thin sheet passing through the center of the egg. The chemoattractant release comes from a circumferential band consisting of the intersection of the band with the sheet. We use a flux rate of 2.38×10^{-23} mol $\mu\mathrm{m}^{-2}$ s^{-1} calculated from the total release rate of 0.18 fmol egg^{-1} for a 200 micron red abalone egg given by Zimmer and Riffell (2011). The mass of chemoattractant is released 25 μm inside the surface of the egg to account for the existence of a jelly coat. We assume the same diffusivity within the jelly coat.

We model the release, transport and dispersion of tryptophan using a Lagrangian particle tracking method (Kinzelbach, 1988) with 1E6 particles per simulation. These particles then diffuse outward via a random-walk method and advect passively in the flow by Eqs. 1 and 2 for the steady shear flows and Eqs. 1 - 5 for the unsteady shear cases. The 2D particle positions x_n at time-step n in flow $\vec{u}$ is computed via

$$\vec{x}_n = \vec{x}_{n-1} + \vec{u}(\vec{x}_{n-1})dt + \boldsymbol{Z}\sqrt{2Ddt} \tag{6}$$

where D is the molecular diffusivity of tryptophan (Table .1) and $\boldsymbol{Z}$ is a

random vector with a normally distributed magnitude with mean zero and variance of one. Each particle has a constant molar mass. Particles are binned over small regions and concentrations are calculated by counting the number of particles per area and multiplying by the molar mass per particle. The model is run until the concentration fields reach a steady-state for the steady shear flows and until the plumes are fully developed in the unsteady shear flow (3 minutes).

2.2. Model for Loitering Behavior

Motile sperm are also modeled via a Lagrangian approach. In order to gather statistics about sperm paths and fertilization rates, we use 5E5 sperm represented by particles in each simulation. The sperm advect passively in the flow and move according to a prescribed swimming behavior. The sperm exhibit a loitering behavior if the local concentration is below a threshold ($C_{\text{threshold}}$) and they initiate a response behavior if the local concentration is above the threshold. The most commonly observed loitering behavior and many response behavior observations consist of a drifting circle pattern (Alvarez et al., 2012; Friedrich and Julicher, 2008; Böhmer et al., 2005; Kaupp et al., 2008). This is accomplished in the model by the superposition of a circular velocity and a drifting velocity. In all cases, the velocity of the swimming sperm is

$$\vec{v} = \vec{v_{\text{circ}}} + \vec{v_{\text{drift}}} + \vec{v_{\text{run}}} \tag{7}$$

where $\vec{v_{\text{circ}}}$ consists of swimming speed v_{c} and turning rate $\dot{\theta}$, $\vec{v_{\text{drift}}}$ consists of drifting speed v_{d} and drifting direction θ_d, and $\vec{v_{\text{run}}}$ consists of swimming speed v_{r} and direction θ_r. The sperm positions are updated by the superposition of swimming velocity $\vec{x}_{s_n}$ and passive velocity due to the flow $\vec{u}$ at time-step n is then

$$\vec{x}_{s_n} = \vec{x}_{s_{n-1}} + \vec{u}(\vec{x}_{n-1})dt + \vec{v}(\vec{x}_{s_{n-1}})dt \tag{8}$$

Observations of loitering sperm, where the local concentration is less than a threshold concentration, note a drifting circle pattern with no directional bias towards the egg (Vogel et al., 1982; Riffell and Zimmer, 2007; Riffell et al., 2002, 2004; Morita et al., 2006). The loitering velocity in the model is Eq. 7 where v_{c} is held constant and the turning rate $\dot{\theta}$ varies over time such that it is normally distributed with mean $\mu_{\dot{\theta}}$ and standard deviation $\sigma_{\dot{\theta}}$. This initial swimming direction for each sperm is chosen randomly from

$[0, 2\pi]$. The speed v_d varies over time such that it has a triangle distribution centered on v_d, tapering linearly to zero at $v_\mathrm{d} \pm 2\Delta v_\mathrm{d}$. Note that the triangle distribution is used to avoid the possibility of nonphysical behavior associated with the infinite tail of a normal distribution. The direction θ_d, is initially chosen randomly from $[0, 2\pi]$ and varies over time such that it has a triangle distribution centered on θ_d, tapering linearly to zero at $\theta_\mathrm{d} \pm \Delta\theta_\mathrm{d}$. For loitering, $\vec{v_\mathrm{run}} = 0$. The swimming parameters were chosen to agree with the observations of Wood et al. (2005); Böhmer et al. (2005); Kaupp et al. (2003) and exigent models (Friedrich and Julicher, 2008) and to relate to observations of swimming sperm.

2.3. Model for Response Behavior

Three distinct behaviors are established to model the range of observed chemotactic and chemokinetic strategies employed by sperm responding to a stimulus: I) Drifting Circle II) Turn and Run, and III) Run. Sperm with no response to stimuli are also modeled as a base case. Sperm implement a response behavior for all time where the local concentration exceeds a threshold concentration.

I) The Drifting Circle Response models sperm that use chemotaxis, but do not change speed due to stimulation. We chose this case due to observations of chemotaxis without any chemokinetic characteristics (Kupriyanova and Havenhand, 2002; Friedrich and Julicher, 2008; Kaupp et al., 2008) and to study what effect the ability to increase speed has on fertilization success. The velocity component $\vec{v_\mathrm{circ}}$ (Eq. 7) consists of a constant v_c and $\dot{\theta}$. The $\vec{v_\mathrm{drift}}$ component has a constant speed v_d and direction θ_d varies over time such that it has a triangle distribution centered on θ_{Ψ^*}, tapering linearly to zero at $\theta_{\Psi^*} \pm \Delta\theta_\mathrm{d}$

$$\theta_\mathrm{d} = 2\left[\Psi^* - 1\right]\Delta\theta_\mathrm{d} \tag{9}$$

where $\Psi^* = \Psi/\Psi_0$ where Ψ is the local chemoattractant gradient and Ψ_0 where maximum chemoattractant gradient in our model domains ($\Psi_0 =$ 2E3 μm). For the Drifting Circle Response $\vec{v_\mathrm{run}} = 0$.

II) The Turn and Run Response models sperm with the ability to increase swimming speed and effectively decrease the curvature of the swimming path. This strategy is consistent with observations made by Ward et al. (1985); Zimmer and Riffell (2011); Riffell et al. (2004); Böhmer et al. (2005); Guerrero et al. (2010b); Kaupp et al. (2006, 2008). The velocity component $\vec{v_\mathrm{circ}}$ (Eq. 7) has constant magnitude v_c and the turning rate increases linearly with the

local, normalized gradient Ψ^* as

$$\dot{\theta} = \dot{\mu_\theta} \left[1 - a\Psi^*\right] \tag{10}$$

where a is chosen to be 0.5 for our simulations. The $\vec{v_{\text{drift}}}$ magnitude v_{d} also varies linearly with Ψ^* as

$$v_{\text{d}} = 2v_{\text{d}} \left[1 + b\Psi^*\right] \tag{11}$$

where b is chosen to be 1.5 and the constant 2 is so that the velocity at least doubles when the local concentration is above the threshold, even if there is no gradient. The direction θ_{d} is determined as in Eq. 9. For the Turn and Run Response $\vec{v_{\text{run}}} = 0$.

III) The Run Response models sperm that abandon the circling strategy of the loitering behavior and execute a run down gradient. This behavior was chosen due to observations made by Riffell et al. (2004); Riffell and Zimmer (2007); Zimmer and Riffell (2011) and studies the significance of the circling aspect of the swimming paths with respect to finding an egg. The linear swimming velocity $\vec{v_{\text{run}}}$ (Eq. 7) has magnitudev_{r} which depends on the relative strength of the local gradient

$$v_{\text{r}} = v_{\text{c}} \left[1 + \Psi^*\right] \tag{12}$$

and the swimming direction θ_{r} varies linearly with the gradient as in Eq. 9

$$\theta_{\text{r}} = 2 \left[\Psi^* - 1\right] \Delta\theta_{\text{r}} \tag{13}$$

In the Run Response $v_{\text{c}} = v_{\text{d}} = 0$.

2.4. Fertilization Rate Model

We use a Monte Carlo approach to calculate the possibility of a sperm reaching a single egg. A collection of sperm are placed at one location in the proximity of one egg and simultaneously begin to swim. We assume second order reaction kinetics based on previous models (Vogel et al., 1982; Levitan et al., 1991; Crimaldi et al., 2006). For simplicity, we consider fertilization as the contact with the surface of the egg. In reality, this would not guarantee a successful fertilization, but the objective is to understand what effects the sperm's ability to reach an egg. The fertilization results are cumulative fertilization rates over time.

3. Results

Section 2 gave the details for a numerical model of flow, chemoattractant plume development, and sperm loitering and response behavior in regions surrounding an egg. We now present results from this model. We first investigate the spatial and temporal development of chemoattractant plumes around eggs in steady and and unsteady flows (Section 3.1). Next, we present and analyze Lagrangian tracks for both loitering sperm and sperm exhibiting one of three different response behaviors in and around the computed plumes (Section 3.2). Finally, we quantify the percentage of sperm that successfully locate eggs under a range of flow conditions for all three behavioral responses (Section 3.3).

3.1. How Flow Shapes 2D Chemoattractant Plume

Steady-state chemoattractant plume distributions for the steady shear flow (Fig. 1) at four different values of shear rate α are shown in Fig. 2. The plumes approach a steady-state distribution approximately three minutes after the egg is placed in the flow (the transient response is not shown). The $\alpha = 0$ case (first panel) corresponds to pure diffusion of chemoattractant in quiescent flow, with a resulting symmetric plume that decays radially away from the egg. As shear rate is increased (subsequent panels), the plume is stretched by the flow into an increasingly elongated filament. This stretching sharpens chemoattractant gradients, increases diffusive flux away from the plume, and decreases local plume concentrations relative to the unsheared case. The shear mechanism responsible for dispersing the chemoattractant is essentially the same as the classic phenomenon described by (Taylor, 1953), modified locally by the presence of the solid and freely rotating egg. Note that the results shown in Fig. 2 are consistent with steady-shear chemoattractant plumes computed with a similar approach by Zimmer and Riffell (2011).

When shear is unsteady, as it is in turbulent flow, the resulting chemoattractant plumes are more complex (Fig. 3). Using the unsteady shear flow model given by Eqs. 1 - 5, we computed unsteady plume distributions for two values of the unsteady shear amplitude α_0. The plume is allowed to disperse for a period of three minutes after the egg is placed in the unsteady flow such that it reaches a fully developed state across the model domain. The plume, however, continues to change over time in response to changes in the unsteady flowfield. To give a sense of the temporal variation in the chemoattractant plume structure, we display in Fig. 5 representative snapshots of the

spatial distribution at 60-second intervals. For the low-α_0 case ($\alpha_0 = 0.5\text{s}^{-1}$, Fig. 3a), the effect of the unsteady shear is predominately to bend the protruding arms of the stretched chemoattractant plume. For this case, diffusion largely destroys any additional complexity at the ends of the arms (the Pe for this case, using $\alpha_0/2$ as an rms shear rate, is less than 4, and thus the effect of diffusion is relatively strong). For the high-α_0 case ($\alpha_0 = 1.25\text{s}^{-1}$, Fig. 3b), the Pe increases to approximately 10, and stirring by the unsteady shear produces significantly more complexity in the chemoattractant plume. Filaments are stretched and folded, with pronounced striations developing in the scalar field.

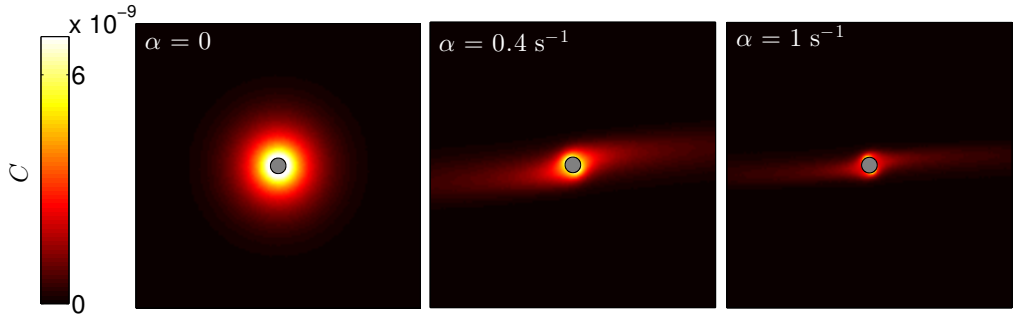

Figure 2: Steady-state chemoattractant distributions for a range of steady shear flows. The steady state behavior shown above was obtained 3 minutes after the egg was introduced into the flow (shown in fig. 1). The egg is centered in each panel, indicated by the grey circle and the chemoattractant concentration is indicated by the colorbar.

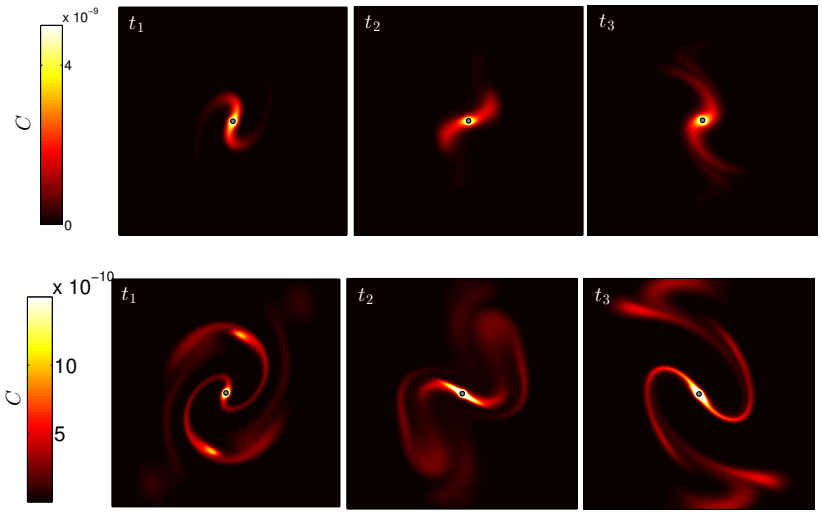

Figure 3: Representative snaphots of the quasi steady-state chemoattractant distributions for low (1st row) and high (2nd row) unsteady shear flows. We allowed the plumes to develop into a quasi steady state after a 3 minute period. To illustrate the range of behaviors over time, we show three representative slices at one minute intervals. The egg is centered in each panel, indicated by the grey circle.

The chemoattractant plume distributions shown in Figs. 2 and 3 illustrate the continuous range of concentrations present around the egg. However, some of the concentrations will necessarily be below the minimum threshold concentration required to elicit a behavioral response by sperm. From the perspective of behavioral response, the concentrations below this threshold are functionally unimportant. Figs. 4 and 5 display the spatial extent of the portions of the plumes that would elicit sperm response for given values of the threshold.

In the steady shear flow cases, Fig. 4 shows that in any given panel, the effective plume area decreases as minimum threshold increases. Additionally, as the shear rate α increases, the effective plume area for any given threshold decreases. The increase in the effective egg target size caused by the diffusion and dispersion of the chemoattractant plume has proven to be an evolutionary advantage (Levitan, 1993, 2000, 2006; Jantzen et al., 2001). We can quantify the effective egg target increase in size provided by the plume for a given threshold. We calculate an effective egg diameter based on the

area within any of the concentration threshold contours (A_{stim}) shown in Fig. 4

$$D^* = \sqrt{4A_{stim}/\pi}/R_{egg} \tag{14}$$

The normalized effective diameters for each threshold value and each steady shear rate are below in Fig. 6. Both shear rate and threshold value decrease the size of the effective diameter as was seen qualitatively in Fig. 4.

In the unsteady shear flow cases, Fig. 5 shows a similar trend in the decrease in target area for increasing threshold concentration and shear rate. A new phenomenon occurs with the development of non-contiguous islands of above-threshold concentrations for Fig. 5b (high-α_0). We anticipate that these would complicated or present challenges to search strategies for sperm seeking eggs.

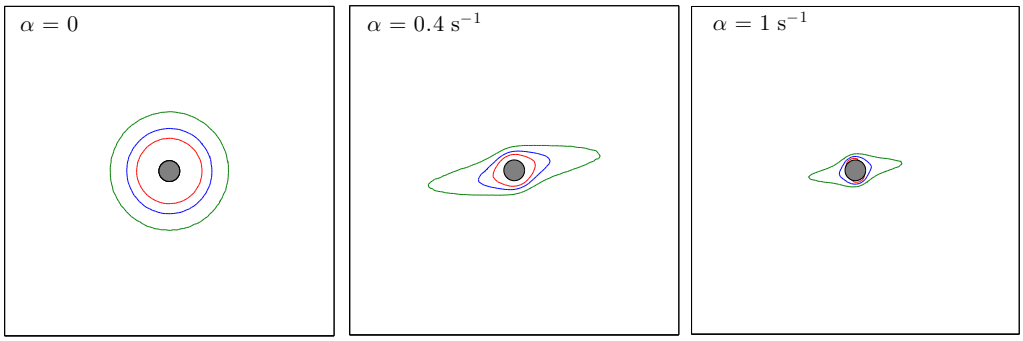

Figure 4: Steady shear flow contour levels for three possible threshold concentrations (1×10^{-9} mol μm^{-3} (green); 2×10^{-9} mol μm^{-3} (blue); 3×10^{-9} mol μm^{-3} (red)) for 3 shear rates. These images correspond directly to the concentration images shown in Fig. 2. The contours also indicate information about the concentration gradients which will be useful when we look at the response behaviors in Sec. 3.2. The gradients are everywhere normal to the contours. The green line depicts the threshold concentration used in the fertilization models. This lies on the higher end of the documented threshold concentration ranges (3×10^{-10} mol μm^{-3} - 4×10^{-9} mol μm^{-3}) (Riffell et al., 2004; Zimmer and Riffell, 2011).

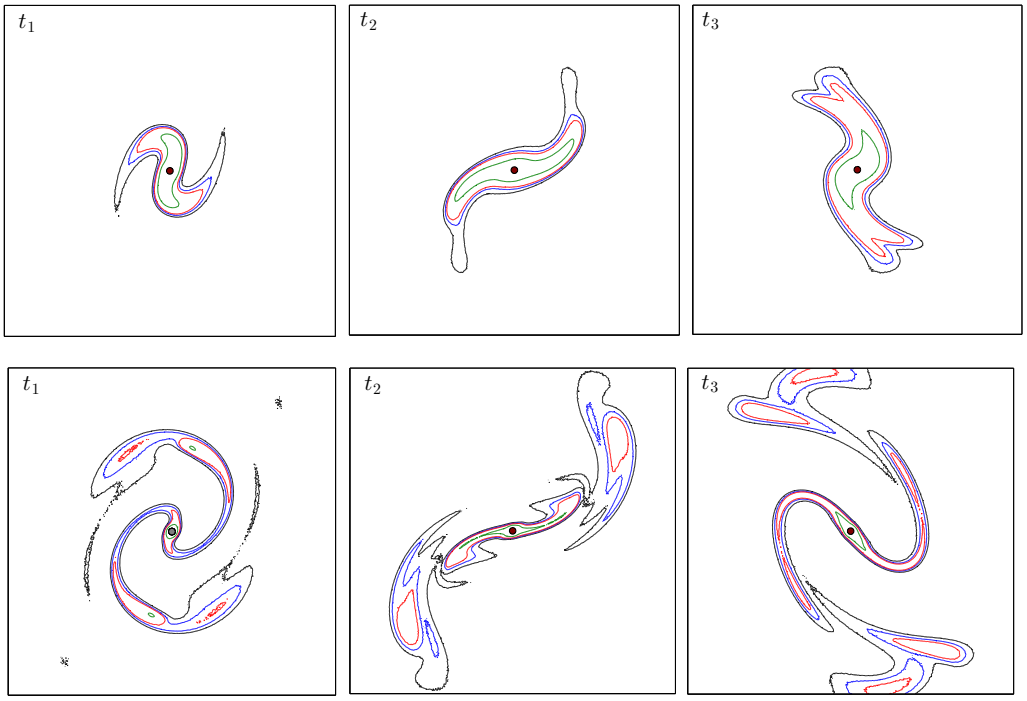

Figure 5: Unsteady shear flow contour levels for both the low-α_0 (top row) and high-α_0 (bottom row) cases for one minute time intervals t_1, t_2 and t_3 illustrating the transient chemoattractant threshold concentrations. Four possible threshold values (1×10^{-10} mol μm^{-3} (black); 2×10^{-10} mol μm^{-3} (blue); 3×10^{-9} mol μm^{-3} (red); 1×10^{-9} mol μm^{-3} (black)) are depicted. These images correspond directly to the concentration images shown in Fig. 3. Again, the chemoattractant gradient information can be deduced from the level and spacing of the concentration contours. Note that the smallest contour (green) represent a concentration of 1×10^{-9} mol μm^{-3} , the threshold concentration used for the steady shear flows, but that the value used for the complex cases is on the lower end of the range at 1×10^{-9} mol μm^{-3} (black).

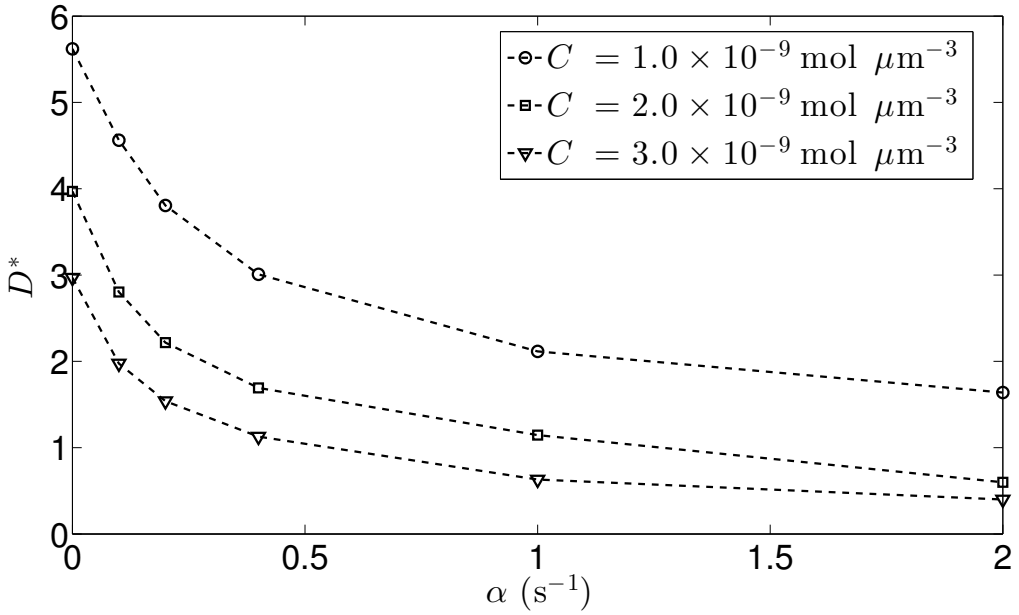

Figure 6: The calculated effective diameter (D^*) of the size of the plume under a given threshold concentration for the steady shear flows plotted against the corresponding shear rate values (α).

3.2. Sperm Motility

In the absence of a chemoattractant stimulus, sperm exhibit a loitering behavior consisting of unbiased drifting circles. We begin by assessing the relative dispersion of sperm due to this loitering behavior. Note that, due to their relatively large size, true diffusion of non-motile sperm in a molecular Brownian-motion sense is negligible. However, a collection of loitering sperm will disperse in space due to differences in drifting directions. This dispersion has long been assumed to be diffusive (meaning that spatial variance grows linearly with time) in models of sperm motility (e.g., Keller and Segel (1971)). More recently, Inamdar et al. (2007) used dead and live sperm to demonstrate experimentally that sperm motility does indeed result in diffusive-like spreading. A collection of sperm diffusing in two dimensions from a single point would have concentrations predicted by the solution to the 2D diffusion equation (Fischer et al., 1979).

$$C(x, y = 0) = \frac{M}{4D_s t\pi} \exp\left[-\frac{x^2}{4D_s t}\right], \tag{15}$$

which indicates that the resulting variance σ^2 of the cloud should grow linearly as $4D_s t$, where D_s is the effective diffusivity produced by the motility.

To investigate the dispersive behavior of sperm in our numerical model, we placed a large collection of loitering sperm at a single location in a quiescent flow and tracked their locations over time. Representative paths of three sperm over 30 seconds are shown in Fig. 7a. The variance growth of the entire cloud is plotted in Fig. 9b as $\sigma^2/4$ vs. t. The linear result indicates that the spreading is diffusive in nature, with an effective diffusivity (obtained as the slope of a fit to the data) of 1.8E-9 $\mathrm{m}^2\ \mathrm{s}^{-1}$. This is within the measured range of effective diffusivities obtained experimentally for urchin sperm by Inamdar et al. (2007).

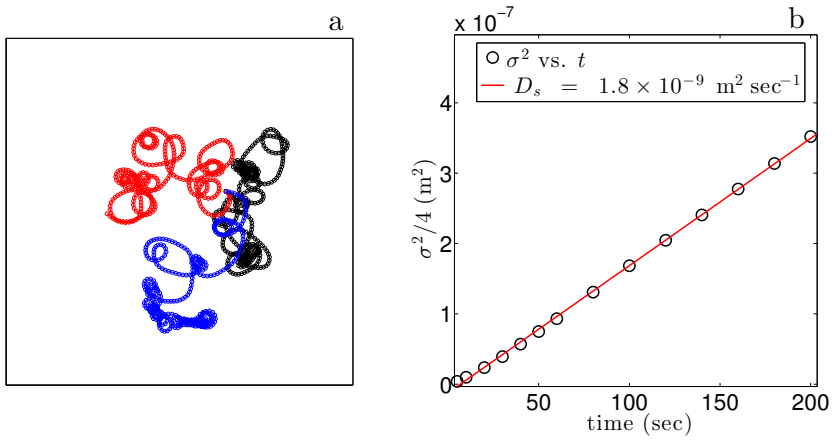

Figure 7: The plot on the left shows $\sigma^2/4$ calculated from the loitering sperm over the first 200 seconds plotted against the time (circles). The loitering parameters match the values used in the simulations (Table .1). The linear regression line to the points (solid line) is used to calculate the diffusivity. The plot on the right shows the diffusive behavior of loitering sperm for three sperm that begin swimming at the same time from the same point. The paths are shown for 30 seconds and each circle indicates the successive location every 0.2 seconds.

In the quiescent flow and the steady shear flows with $\alpha > 0$, we provide a sense of what the response behaviors look like in the paths shown in Figs

8 - 10. We will quantify how quickly and how likely they are to reach the egg in the next section (Sec. 3.3). The paths shown are real paths from the model, but they were consciously selected to show certain mechanisms (i.e., the flow sweeping the sperm passed the egg). Note that if a loitering sperm locates the threshold area, there is a very high change of then reaching the egg.

There are many significant outcomes derived from the sperm paths in the unsteady shear flows and we present some significant messages using paths from the model in Fig. 11. Fig. 11a illustrates that in the low-α_0 unsteady shear case, once the sperm encounters the threshold concentration, it is likely to find the egg with any of the response types. The path is more complex and circuitous than the simple shear cases: both the flow and the plume are constantly evolving. The sperm are directed by the gradients to stay within the threshold concentration, which is manipulated almost entirely by the flow, as they follow an increasing gradient of chemoattractant. It is not always necessary for the sperm to remain within the threshold contours in order for the egg to be reached. For example, as seen in Fig. 11b, the sperm locates the higher concentration at an early time (a), but the flow and the motility of the sperm removes it from the filament. Both these variations in flow and the sperm motility, though, allow the sperm to locate a filament again and eventually follow the gradients to find the egg. Figure 11c demonstrates the possibility in the high complex unsteady shear case in which a sperm responds to the high chemoattractant concentration, but this area is surrounded by lower concentration, which makes this area appear as an isolated area of chemoattractant to the sperm. The sperm follows the gradients within this area, but this alone does not lead the sperm to the egg.

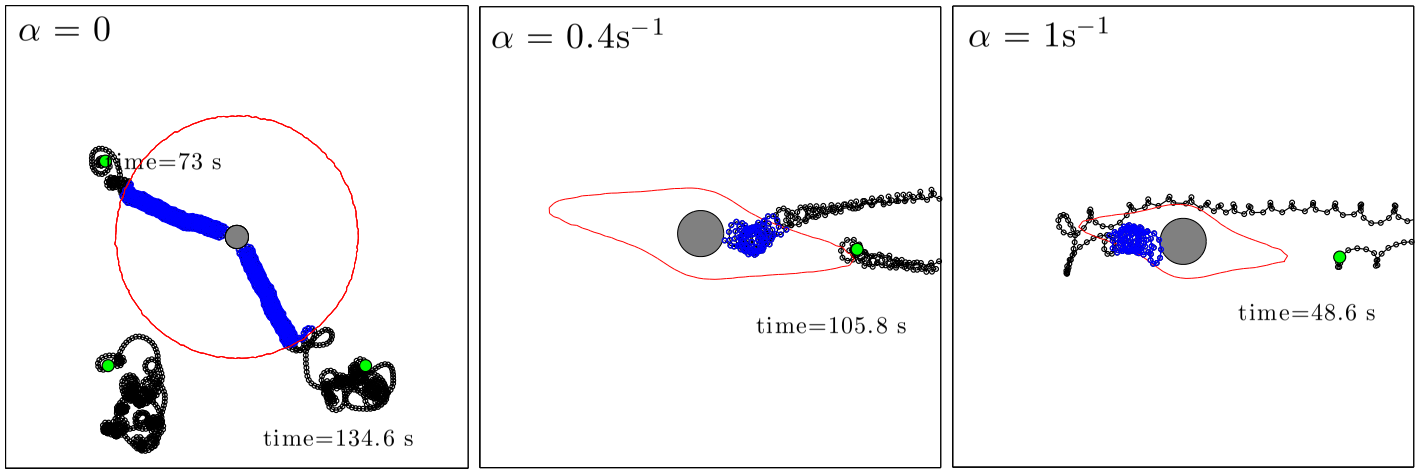

Figure 8: Representative sperm paths for both the loitering (black) and resposne (red) behavior in 3 steady shear flows.

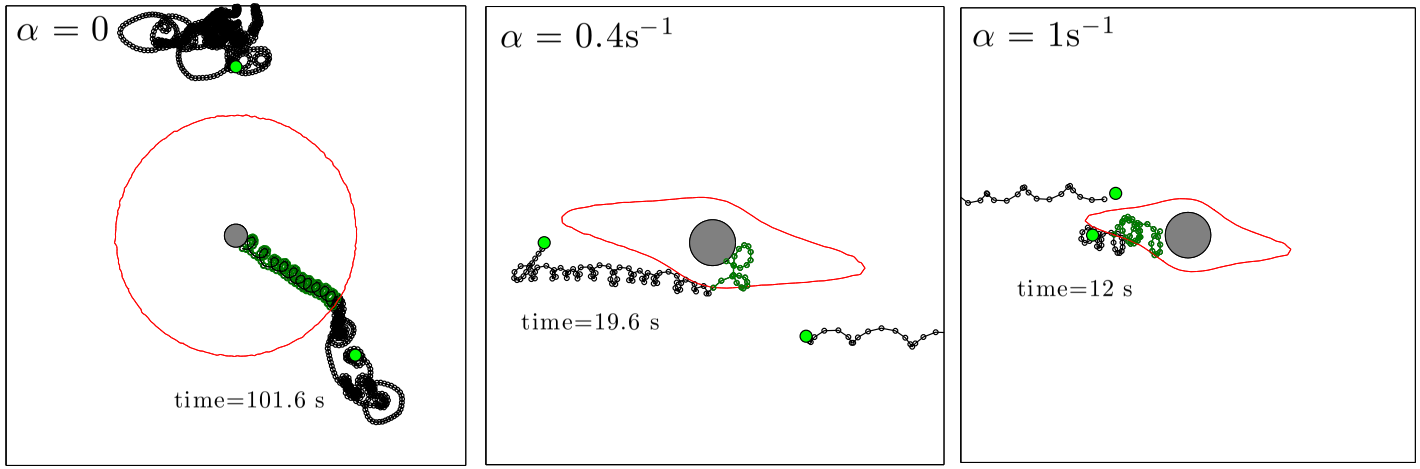

Figure 9: Representative sperm paths for both the loitering (black) and resposne (red) behavior in 3 steady shear flows.

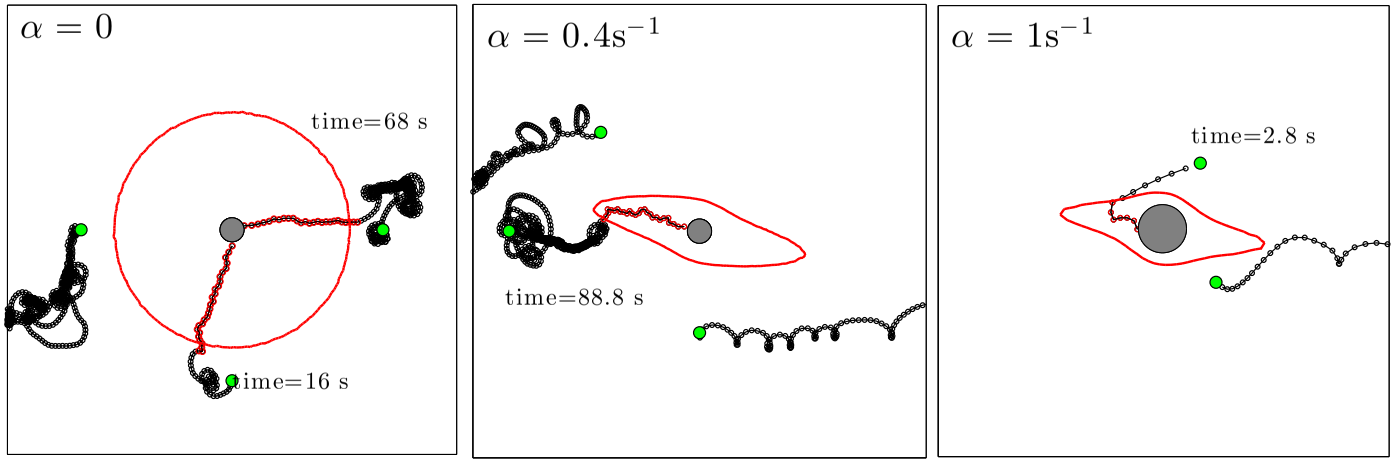

Figure 10: Representative sperm paths for both the loitering (black) and resposne (red) behavior in 3 steady shear flows.

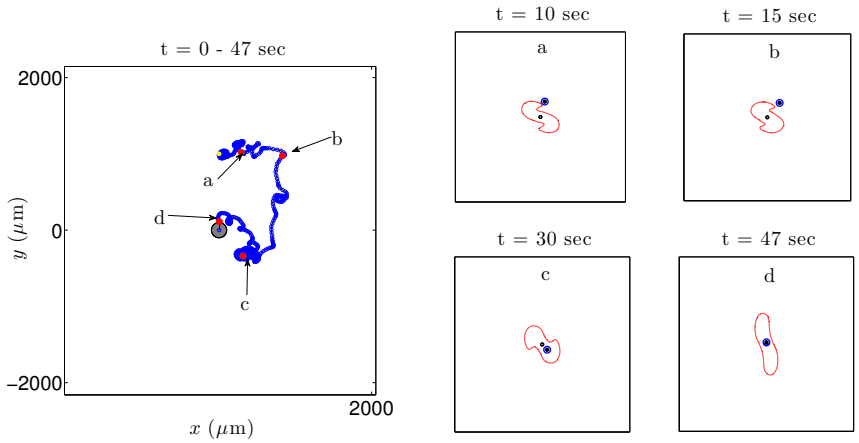
t = 0 - 47 sec
2000
0
−2000
2000
y (μm)
x (μm)
a
b
c
d
t = 10 sec
t = 15 sec
t = 30 sec
t = 47 sec

(a)

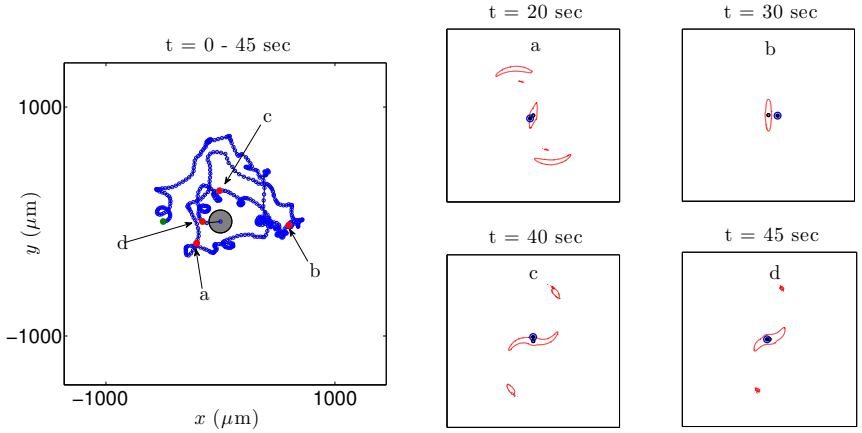
t = 0 - 45 sec
1000
−1000
−1000
1000
y (μm)
x (μm)
a
b
c
d
t = 20 sec
t = 30 sec
t = 40 sec
t = 45 sec

(b)

Figure 11

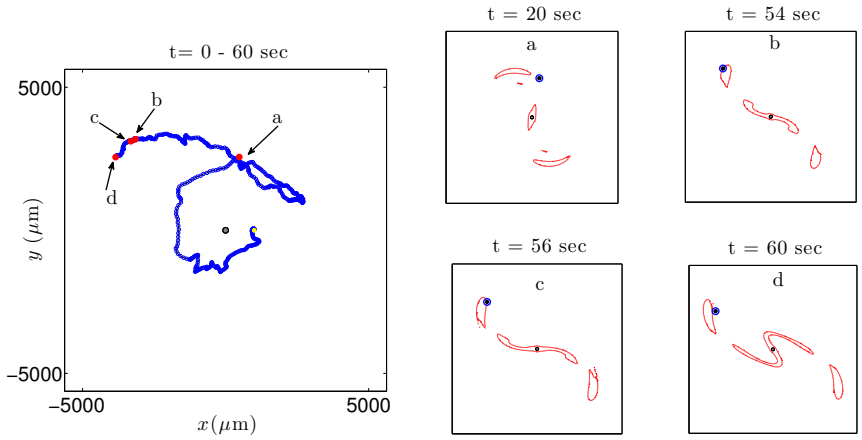

(c)

Figure 11: Representative sperm path for a sperm in the low-α_0 unsteady shear case (Fig. 11a) and the high-α_0 unsteady shear case (Fig. 11b,c). The red lines in subfigures a - d indicate the threshold concentration ($C_{\text{threshold}} = 3 \times 10^{-10}$ mol μm^{-3}). The entire path is shown in the large figure to the left and each of the 4 points in time (indicated by a red dot) are also shown individually along with the subsequent threshold contour in the 4 small subplots to the right. Note that the larger plot is at a smaller scale to show the intricacies of the entire path. The sperm in the low-α_0 unsteady shear case example employed the Run Response at all times when the local concentration was above the threshold. The sperm in the high-α_0 unsteady shear case used the Turn and Run Response (11b) and the Run Response (Fig. 11c) when stimulated.

3.3. Fertilization Rates

3.3.1. Simple Shear

In the steady shear case where $\alpha = 0$, the relevant scales are the asymptotical total fertilization rate and the time to the first success. Sperm utilizing any behavioral response achieve a higher success rate than sperm with no response. Once the sperm has found the area of chemoattractant above the threshold, the likelihood of reaching the egg is near 100%. All behaviors result in the same final fertilization success, but the timescales in the cumulative fertilization rates differ. The effect of the initial location on the fertilization rates is radially-symmetric and is a function of the initial dis-

tance from the egg or the closest threshold location. The same hierarchical order of behaviors with respect to the first success and the first to achieve the converged total fertilization is maintained for all initial conditions in the no flow case: 1. Run; 2. Turn and Run; 3. Drifting Circle; 4. No Response.

For the steady shear cases where $\alpha > 0$,t he same hierarchical ordering of fertilization success that was consistent for the quiescent case is maintained. Any of the three different behaviors continue to result in higher fertilization rates than that from no behavior. The fertilization rates are no longer radially-symmetric (typical case shown in Fig. 13. The sperm placed parallel to the flow (initial locations depicted in Fig. 12)), centered at the egg (θ_0 = a or e) have the highest success rates because the flow at this location is the lowest so the sperm have enough time to diffuse from their starting point and overlap with the threshold concentrations, where they can use chemotaxis, before they are swept far from the egg. Some of the sperm also enter the flow that bring them towards the egg, increasing their chance to reach the egg even further. Note, again, this would not hold the same if we have simulated multiple eggs. The fertilization rates then decrease for the sperm placed upstream and even more for those initially placed downstream. While the sperm placed upstream are in a flow that will bring them towards the egg, the sperm still must swim far enough to encounter the threshold area or the egg before they are carried too far from the egg. This task is even harder for the sperm placed downstream as they have to diffuse far enough out and overcome the flow to find the egg. The lowest rates result from the sperm placed perpendicular to the flow. The flow at this location is the highest and by the time the loitering sperm spread far enough to be in contact with the higher threshold area, they had already been swept away.

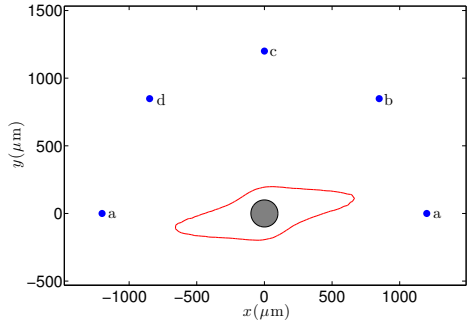

Figure 12: All initial locations used to calclualte the results below (Fig. 13). This shows only the locations for the Simple Shear Case where $\alpha = 0.4\ \mathrm{s}^{-1}$.

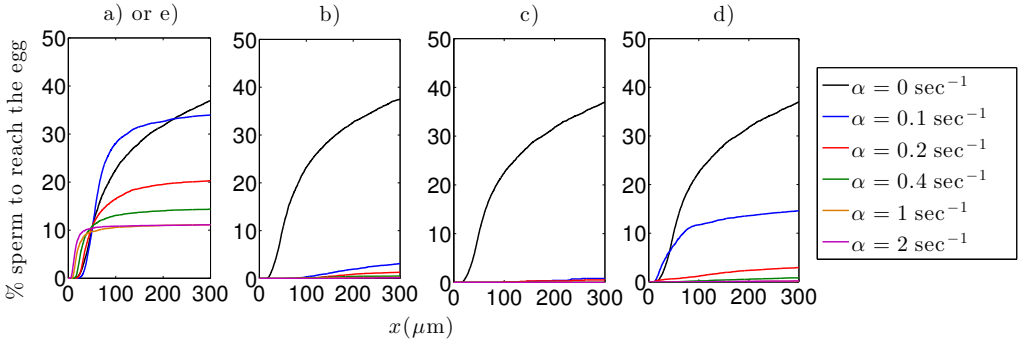

Figure 13: Cumulative fertilization rates quantified of the Turn and Run Response for 300 seconds. The sperm all initiated from the same distance ($r_0 = 12R_{\mathrm{egg}}$), but the radial direction is varied. See Fig. 12 which depicts each starting location. Results from each Simple Shear case are shown together with each shear rate represented by a different color.

The fertilization rates are also dependent on behavior as well as the radial placement of the initial condition and the shear rate. Figure 14 depicts a representative case (initial starting location shown in Fig. 12) of the effect of both shear and behavior on the fertilization rates. While the rates of any behavior are still consistently higher than rates of no behavior, this difference becomes less significant as shear increases. Once the shear rate reaches $\alpha = 1\ \mathrm{s}^{-1}$, the Run Response is only superior to the Turn and Run Response at early and late times, and their difference is very minimal. Shear

serves to enhance success at early times, but impedes success at late times, and as the shear increases, this effect becomes more severe. The flow helps to bring the sperm closer to the egg faster than their pure swimming can do in the no flow case. At later times, it should be noted that success rates decline because the sperm are swept passed the egg and then have little chance of returning. This is because we have only considered one egg and would not be the case for multiple eggs. Recall that the target area of the chemoattractant also decreases with increasing shear, contributing to the effect on the fertilization rates (Fig. 4 above for target areas in each steady shear flow and Fig. 6 for the quantified effective diameters).

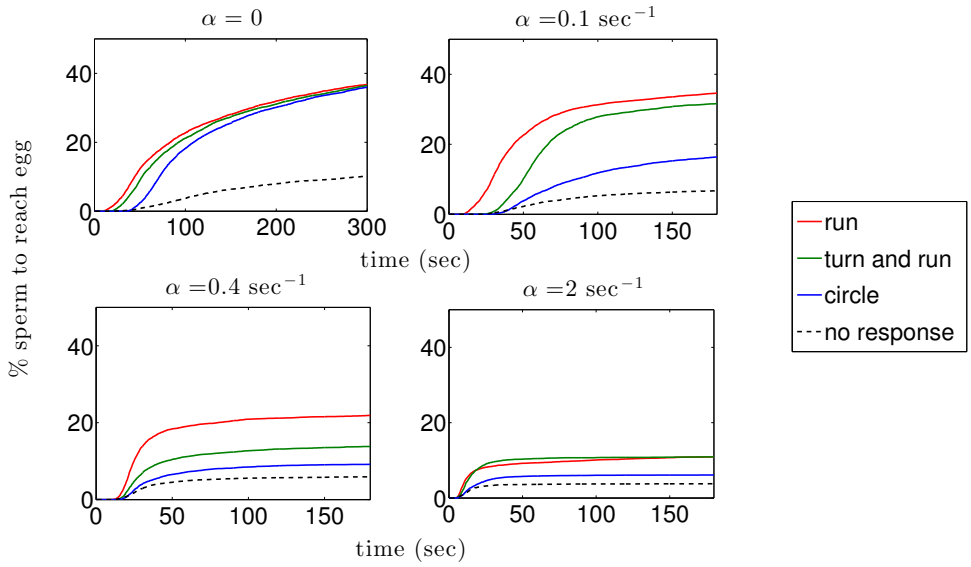

Figure 14: Cumulative fertilization rates for each response within each shear flow case and a single egg, as quantified for 200 seconds. (Starting conditions are constant: $r_0 = 12R_{\text{egg}}$; $\theta_0 = 0$). Representative paths of sperm swimming in steady sheared flows are shown above in Fig. 8.

3.3.2. Unsteady Shear Flows

The same hierarchical order is still maintained for both the high and low-α unsteady shear cases, regardless of initial starting location or shear. Additionally, it still holds true that any response is more successful than no response. There is much more variation in the results, though. There is no symmetry for the effect of initial location on the results. The shape of the

cumulative fertilization rates (Figs. 15 - 16) varies for each response and each initial location, unlike the more monotonic, constant patterns that emerge in the steady shear cases. The fertilization rates are generally much lower in the high-α unsteady shear case compared to all of the steady shear flows and the low-α unsteady shear cases due to the higher shear rates and constantly evolving plume. However, high-α unsteady shear case does outperform the steady shear cases for higher shears where the starting location was once not ideal, such as directly above the egg (perpendicular to flow in the steady shear cases) or radially from from the egg (compare to Figs. 14 and 13).

Besides the constant hierarchical order and outperformance of behavior over no behavior, the both the high and low-α unsteady shear cases saw much more diversity within the cumulative fertilization rates. For example, in the high-α unsteady shear flow, starting the sperm at ($r_0 = 12R_{\text{egg}}$ $\theta_0 = \pi/2$) resulted in success rates over 5 times better than the 3 other starting locations of the same radius (Fig. 15). Similarly, for a starting radius of $r_0 = 6R_{\text{egg}}$ there are cases in which the Run Response achieves almost 100 % fertilization, and others where the rates top off around 50 %. Sometimes the Turn and Run Response barely outperforms the Drifting Circle Response, and others the rates are 5 times higher. In both cases, the Drifting Circle Response proved to be the least effective behavior, sometimes barely outperforming the no response case, indicating that a change in speed is imperative to fertilization success in an unsteady flow.

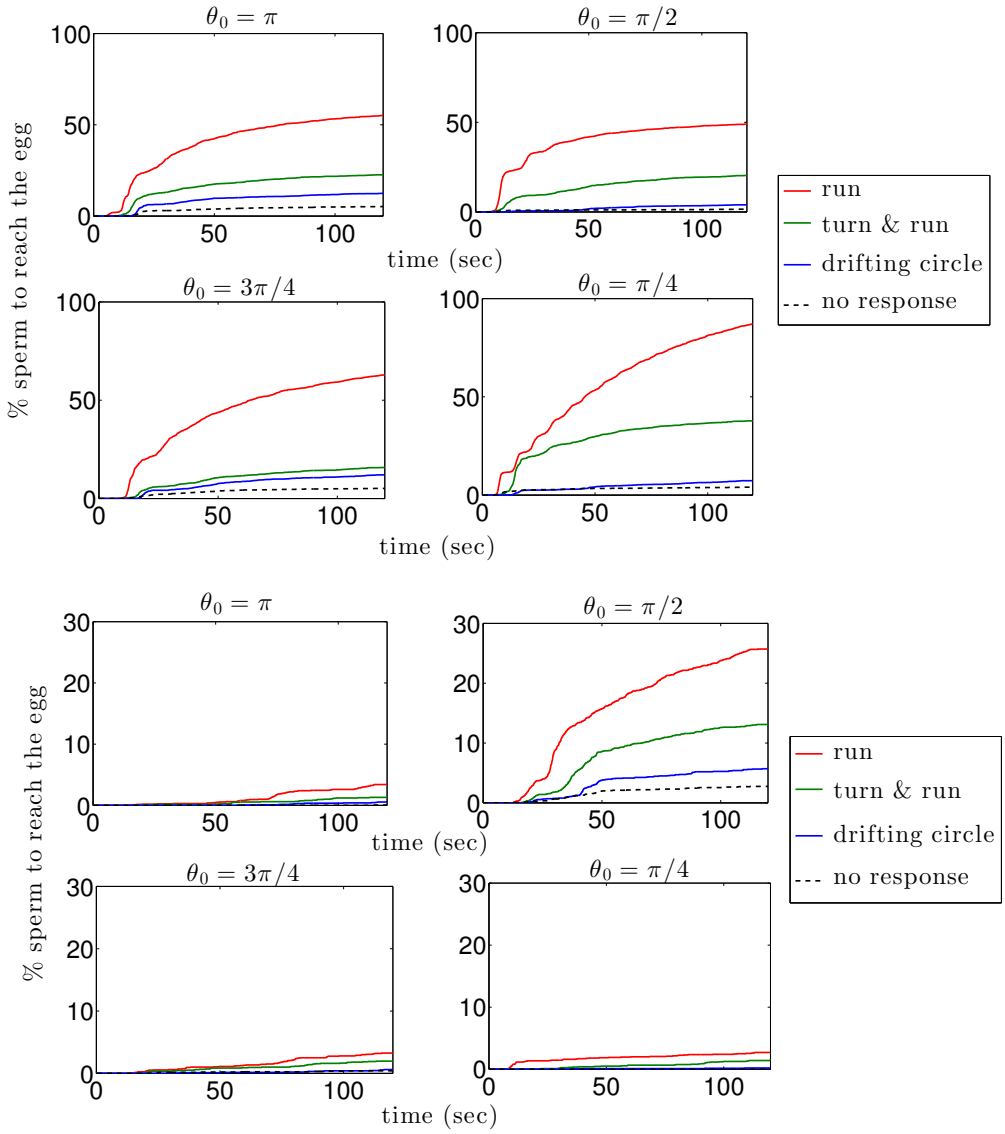

Figure 15: High-α unsteady shear case integrated fertilization rates for each response (for the first 120 seconds). Representative paths for this flow can be seen in Fig. 11. The initial starting radial distance from the egg for the top set of 4 plots are $r_0 = 6R_{\text{egg}}$ and $r_0 = 12R_{\text{egg}}$ in the bottom set of 4 figures with θ_0 defined in the title of each plot. Note that the bottom set of plots has a vertical scale that ranges from 0 to 30 %.

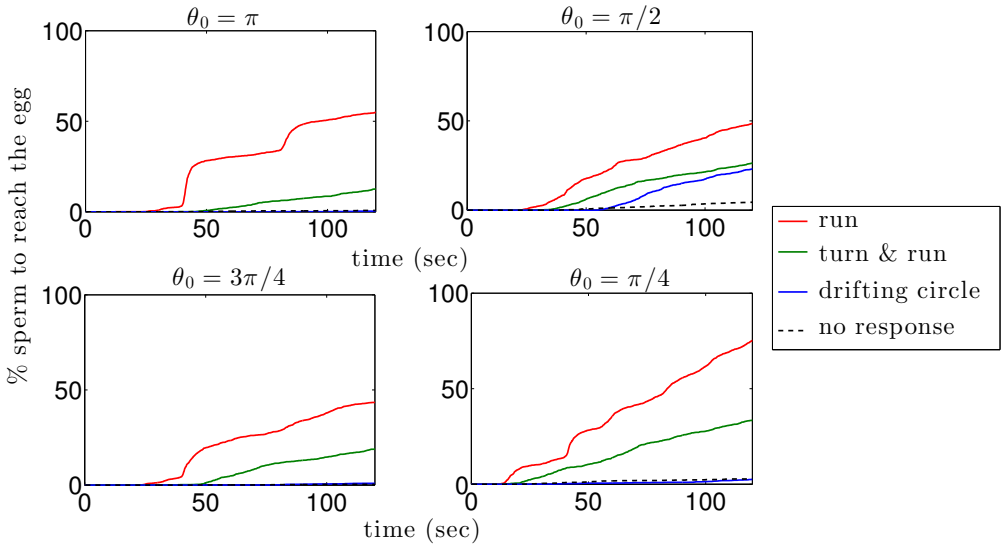

Figure 16: Low-α unsteady shear case integrated fertilization rates for each response (for the first 120 seconds). Representative paths for this flow can be seen in Fig. 11. The initial starting radial distance from the egg is $r_0 = 12R_{\text{egg}}$ with θ_0 defined in the title of each plot. The fertilization rates all approach 100% for $r_0 = 6R_{\text{egg}}$ (not pictured).

4. Discussion

This study helped to establish a conceptual framework for a holistic model that incorporates flow around an egg, dispersion of chemoattractant from that egg and behavioral response of sperm navigating through that plume to find the egg. We presented a model to provide a computational approach to accomplish these tasks. There are clearly limitations in the model, as there are limitations in the sensory of the ecology of sperm itself. The results, while they do not take every detail into account and are based on some idealizations, they provide important insights and a stepping stone to move forward in understanding the most fundamental biological process.

We quantified the effect of shear and concentration level on the effective target size of an egg and determined that an increases in either shear or concentration will reduce the perceived size of the egg. We are also able to get a picture of what a chemoattractant plume looks like to an individual

sperm in unsteady shear and what additional obstacles that presents (such as islands of higher concentrations).

The results in the model indicate that any chemotactic and chemokinetic response provides an advantage over no response in almost every tested condition. A general hierarchy in the strategies used was established and held constant over a range of conditions. The Run Response proved to be the most successful behavior in any flow condition, but it is also the biggest change from the loitering behavior. The energy required to maintain a straight path and suppress curvature is greater than that to keep the natural circling pattern. The Turn and Run Response, while usually less likely to locate an egg, had generally similar fertilization rates and is perhaps a more natural strategy. The Drifting Circle Response is consistently less successful and does not perform well in flows with higher shear rates, suggesting that chemokinesis is indeed necessary for successful fertilization. With all factors considered, proximity to the egg and location within the flow are still the most significant element, highlighting the importance of stirring and mixing at a large scale as well as the diffusivity of a mass of sperm. We now have a better picture of the problem and the factors to consider when moving forward in the understanding of this biological process.

Table .1: Parameter values used in models throughout the study

Parameter	Value	Section	Equation Number
Plume Parameters			
Flow Characteristics			
σ_ϕ	$\pi/10$	2.1.2	3
$\mathrm{T}_{\mathrm{period}}$	60 sec	2.1.2	4
r_{core}	$15R_{\mathrm{egg}}$	2.1.2	5
Egg Characteristics			
$D_{\mathrm{tryptophan}}$	660 μm^2 sec^{-1}	2.1.3	6
R_{egg}	100 μm	r2.1.3	
F	0.18 fmol egg^{-1}	2.1.3	
Sperm Parameters			
v_{c}	150 μm sec^{-1}	2.2	7
v_{d}	20 μm sec^{-1}	2.2	7
$\mu_{\dot{\theta}}$	π rad sec^{-1}	2.2	7
$\sigma_{v_{\mathrm{d}}}$	0.7	2.2	7
$\sigma_{\theta_{\mathrm{d}}}$	$3/\pi$	2.2	7
$\sigma_{\dot{\theta}}$	$1/\pi$	2.2	7
Ψ^*	2E3 μm	2.2	

Appendix A. References

Alt, W., 1980. Biased random walk models for chemotaxis and related diffusion approximations. Journal of Mathematical Biology 9, 147–177.

Alvarez, L., Dai, L., Friedrich, B. M., Kashikar, N. D., Gregor, I., Pascal, R., Kaupp, U. B., February 2012. The rate of change in Ca^{2+} concenctration controls sperm chemotaxis. The Journal of Cell Biology 196 (5), 653–663.

Babcock, R. C., Mundy, C. N., Whitehead, D., February 1994. Sperm diffusion models and in situ confirmation of long-distance fertilization in the free-spawning asteriod acanthaster planci. Biological Bulletin 186, 17–28.

Böhmer, M., Van, Q., Weyand, I., Hagen, V., Beyermann, M., Matsumoto, M., Hoshi, M., Hildebrand, E., Kaupp, U. B., Aug 2005. Ca^{2+} spikes in the flagellum control chemotactic behavior of sperm. EMBO J 24 (15), 2741–52.

Cosson, M. P., Carre, D., Cosson, J., 1984. Sperm chemotaxis in siphonophores: calsium-dependent asymmetrical movement of spermatozoa induced by the attractant. Journal of Cell Science 68, 163–181.

Crimaldi, J. P., Hartford, J. R., Weiss, J. B., July 2006. Reaction enhancement of point sources due to vortex stirring. Physical Review E 74.

Crimaldi, J. P., Zimmer, R. K., 2014. The physics of broadcast spawning in benthic invertebrates. Annual Review of Marine Science 6 (1), null, pMID: 23957600.
URL http://www.annualreviews.org/doi/abs/10.1146/annurev-marine-010213-135119

Denny, M., Dairki, J., Distefano, S., October 1992. Biological consequences of topography on wave-swept rocky shores: I. enhancement of external fertilization. Biological Bulletin 183, 220–232.

Denny, M. W., Nelson, E. K., Mead, K. S., December 2002. Revised estimates of the effects of turbulence on fertilization in the purple sea urchin, strongylocentrotus purpuratus. Biological Bulletin 203, 275–277.

Denny, M. W., Shibata, M. F., December 1989. Consequences of surf-zone turbulence for settlement and external fertilization. American Society of Natrualists 134 (6), 859–889.

Evans, J. P., Garcia-Gonzalez, F., Almbro, M., Robinson, O., Fitzpatrick, J. L., March 2012. Assessing the potential for egg chemoattractants to mediate sexual selection in a broadcast spawning marine invertebrate. Proceedings of the Royal Soceity B 279, 2855–2861.

Farley, G. S., August 2002. Helical nature of sperm swimming affects the fit of fertilization-kinetics model to empirical data. Biological Bulletin 203, 51–57.

Farley, G. S., Levitan, D. R., June 2001. The role of jelly coat in sperm-egg encounters, fertilization success and selection on egg size in broadcast spwaners. American Society of Natrualists 157 (6), 626–636.

Fischer, H., List, E., Koh, R., Imberger, J., Brooks, N., 1979. Mixing in Inland and Coastal Waters. Academic Press, Inc.

Friedrich, B. M., Julicher, F., August 2007. Chemotaxis of sperm cells. Proceedings of the National Academy of Sciences of the United States of America 104 (33), 13256–13261.

Friedrich, B. M., Julicher, F., December 2008. The stochastic dance of circling sperm cells: sperm chemotaxis in the plane. New Journal of Physics 10.

Friedrich, B. M., Julicher, F., August 2009. Steering chiral swimmers along noisy helical paths. The American Phyisical Society 103.

Giorgi, A. E., DeMartini, J. D., October 1977. A study of the reproductive biology of the red abalone, haliotis rufescens swainson, near mendocino, california. California FIsh and Game 63 (3), 80–94.

Guerrero, A., Nishigaki, T., Carneiro, J., Tatsu, Y., Wood, C. D., Darszon, A., May 2010a. Tuning sperm chemotaxis by calcium burst timing. Delevopmental Biology 344, 52–56.

Guerrero, A., Wood, C. D., Nishigaki, T., Carneiro, J., Darszon, A., Oct 2010b. Tuning sperm chemotaxis. Biochem Soc Trans 38 (5), 1270–4.

Himes, J. E., Riffell, J. A., Zimmer, C. A., Zimmer, R. K., February 2011. Sperm chemotaxis as revealed with live and synthetic eggs. Biological Bulletin 220, 1–5.

Inamdar, M. V., Kim, T., Chung, Y.-K., Was, A. M., Xiang, X., Wang, C. W., Takayama, C., Lastoskie, C. M., Thomas, F. I. M., Sastry, A. M., July 2007. Assessment of sperm chemokinesis with exposure to jelly coats of sea urchin eggs and resact: a microfluidic experiement and numerical study. The Journal of Experimental Biology 210, 3805–3820.

Jabbarzadeh, E., Abrams, C. F., January 2005. Chemotaxis and random motility in unsteady chemoattractant fields: a computational study. Journal of Theoretical Biology 235, 221–232.

Jantzen, T. M., de Nys, R., Havenhand, J. N., April 2001. Fertilization success and the effects of sperm chemoattractants on effective egg size in marine invertebrates. Marine Biology 138, 1153–1161.

Jumars, P. A., Trowbridge, J. H., Boss, E., Karp_Boss, L., February 2009. turbulence-plankton interactions: a new cartoon. Marine Ecology 30, 133–150.

Karp-Boss, L., Boss, E., Jumars, P. A., 1996. Nutrient fluxes to planktonic osomotrophs in the presence of fluid motion. Oceanography and Marine Biology 34, 71–107.

Kaupp, U. B., Hildebrand, E., Weyland, I., 2006. Sperm chemotaxis in marine invertebrates-molecules and mechanisms. Journal of Cellular Physiology 208, 487–494.

Kaupp, U. B., Kashikar, N. D., Weyand, I., 2008. Mechanisms of sperm chemotaxis. Annual Review Physiology 70, 93–117.

Kaupp, U. B., Solzin, J., Hildebran, E., Brown, J. E., Helbig, A., Hagen, V., Beyermann, M., Pampaloni, F., Weyland, I., February 2003. The signal flow and motor response controling chemotaxis of sea urchin sperm. Nature Cell Biology 5, 109–117.

Keller, E. F., Segel, L. A., February 1971. Model for chemotaxis. The Journal of Theoretical Biology 30, 225–234.

Kinzelbach, W., 1988. The random walk method in pollutant transport simulation. Groundwater Flow and Quality Modeling, 227–245.

Kiselev, A., Ryzhik, L., 2012. Biomixing by chemotaxis and enhancement of biological reactions. Communications in Partial Differential Equations 37 (2), 298–318.

Krug, P. J., Riffell, J. A., Zimmer, R. K., Apr 2009. Endogenous signaling pathways and chemical communication between sperm and egg. J Exp Biol 212 (Pt 8), 1092–100.

Kupriyanova, E., Havenhand, J. N., January 2002. Variation in sperm swimming behaviour and its effect on fertilization success in the serpulid polychaete galeolaria caespitosa. Invertebrate Reproduction and Development 41 (1-3), 21–26.

Levitan, D., 1993. The importance of sperm limitation to the evolution of egg size in marine invertebrates. The American Naturalist 141, 517–536.

Levitan, D. R., July 1996. Predicting optimal and unique egg sizes in free-spawning marine invertebrates. The American Naturalist 148 (1), 174–188.

Levitan, D. R., August 2000. Optimal egg size in marine invertebrates: theory and phylogenetic analysis of the critical relationship between egg size and development time in echinoids. The American Naturalist 156 (2), 175–192.

Levitan, D. R., March 2006. The relationship between egg size and fertilization success in broadcast-spawning marine invertebrates. Integrative and Comparative Biology 46 (3), 298–311.

Levitan, D. R., Irvine, S. D., 2001. Fertilization selection on egg and jelly-coat size in the sand dollar dendraster excentricus. Evolution 55 (12), 2479–2483.

Levitan, D. R., Sewell, M. A., Chia, F.-S., December 1991. Kinetics of fertilization in the sea urchin strongylocentrotus franciscanus: interaction of gamete dilution, age and contact time. Biological Bulletin 181, 371–378.

Levitan, D. R., Sewell, M. A., Chia, F.-S., February 1992. How distribution and abundance influence fertilization success in the sea urchin strongylocentotus franciscanus. Ecological Society of America 73 (1), 248–254.

Levitan, D. R., Young, C. M., February 1995. Reproductive success in large populations: empirical measures and theoretical predictions of fertilization in the sea biscuit clypeaster rosaceus. Journal of Experimental Marine Biology and Ecology 190, 221–241.

Mark, P., Nilsson, L., 2002. A molecular dynamics study of tryptophan in water. Journal of Physical Chemistry 106, 9440–9445.

Mikulencak, D. R., Morris, J. F., August 2004. Stationary shear flow around fixed and free bodies at finite reynolds number. Journal of Fluid Mechanics 520, 215–242.

Miller, K. J., Mundy, C. N., March 2005. In situ fertilisation success in the scleractinian coral goniastrea favulus. Coral Reefs 24 (2), 313–317.

Morita, M., Kitamura, M., Nakajima, A., Sri Susilo, E., Takemura, A., Okuno, M., Apr 2009. Regulation of sperm flagellar motility activation and chemotaxis caused by egg-derived substance(s) in sea cucumber. Cell Motil Cytoskeleton 66 (4), 202–14.

Morita, M., Nishikawa, A., Nakajima, A., Iguchi, A., Sakai, K., Takemura, A., Okuno, M., August 2006. Eggs regulate sperm flagellar motility initiation, chemotaxis and inhibition in the coral acropora digitifera, a. gemnifera and a. tenuis. The Journal of Experimental Biology 209, 4574–4579.

Polson, A., October 1937. On the diffusion constants of the amino-acids. Biochemical Journal 31 (10), 1903–1912.

Quinn, N. P., Ackerman, J. D., October 2011. The effect of near-bed turbulence on sperm dilution and fertilization success of broadcast-spawning bivalves. Limnology and Oceanography: Fluids and Environments 1, 176–193.

Riffell, J. A., Krug, P. J., Zimmer, R. K., January 2004. The ecological and evolutionary consequences of sperm chemoattraction. Proceedings of the National Academy of Sciences of the United States of America 101 (13), 4501–4506.

Riffell, J. A., Krugg, P. J., Zimmer, R. K., February 2002. Fertilization in the sea: the chemical identity of an abalone sperm attractant. The Journal of Experimental Biology 205, 1439–1450.

Riffell, J. A., Zimmer, R. K., Oct 2007. Sex and flow: the consequences of fluid shear for sperm-egg interactions. J Exp Biol 210 (Pt 20), 3644–60.

Styan, C. A., August 1998. Polyspermy, egg size, and the fertilization kinetics of free-spawning marine invertebrates. The American Naturalist 152 (2), 290–297.

Taylor, G., 1953. Dispersion of soluble matter in solvent flowing slowly through a tube. Royal Society of London Proceedings Series A 219, 186–203.

Vogel, H., Czihak, G., Chang, P., Wolf, W., 1982. Fertilization kinetics of the sea urchin eggs. Mathematical Biosciences 58, 189–216.

Ward, G. E., Brokaw, C. J., Garbers, D. L., Vacquier, V. D., December 1985. Chemotaxis of arbacia punctulata spermatozoa to resact, a peptide from the egg jelly layer. The Journal of Cell Biology 101, 2324–2329.

Wood, C. D., Nishigaki, T., Furuta, T., Baba, S. A., Darszon, A., June 2005. Real-time analysis of the role of Ca^{2+} in flagellar movement and motility in single sea urchin sperm. The Journal of Cell Biology 169 (5), 725–731.

Yoshida, M., Inaba, K., Morisawa, M., January 1993. Sperm chemotaxis during the process of fertilization in the ascidians ciona savignyi and ciona intestinalis. Developmental Biology 157, 497–506.

Yoshida, M., Murata, M., Inaba, K., Morisawa, M., November 2002. A chemoattractant for ascidian spermatozoa is a sulfated steriod. Proceedings of the National Academy of Sciences of the United States of America 99 (23), 14831–14836.

Yoshida, M., Yoshida, K., Aug 2011. Sperm chemotaxis and regulation of flagellar movement by Ca^{2+}. Mol Hum Reprod 17 (8), 457–65.

Zimmer, R. K., Riffell, J. A., Aug 2011. Sperm chemotaxis, fluid shear, and the evolution of sexual reproduction. Proc Natl Acad Sci U S A 108 (32), 13200–5.

Bibliography

[1] Luis Alvarez, Luru Dai, Benjamin M Friedrich, Nachiket D. Kashikar, Ingo Gregor, Rene Pascal, and U. Benjamin Kaupp. The rate of change in ca2+ concenctration controls sperm chemotaxis. The Journal of Cell Biology, 196(5):653–663, February 2012.

[2] Anat Bahat and Michael Eisenbach. Sperm thermotaxis. Molecular and Cellular Endocrinology, 252:115–119, 2006.

[3] Martin Böhmer, Qui Van, Ingo Weyand, Volker Hagen, Michael Beyermann, Midori Matsumoto, Motonori Hoshi, Eilo Hildebrand, and Ulrich Benjamin Kaupp. Ca2+ spikes in the flagellum control chemotactic behavior of sperm. EMBO J, 24(15):2741–52, Aug 2005.

[4] Stephen M. Cox. Chaotic mixing of a competitive-consecutive reaction. Physica D, 199:369–386, 2004.

[5] John Crank. The Mathematics of Diffusion. Oxford University Press, 2 edition, 1975.

[6] Hugh C. Crenshaw. A new look at locomotion in microorganisms: rotating and translating. American Zoologist, 36:608–618, 1996.

[7] John P. Crimaldi. The role of structured stirring and mixing on gamete dispersal and aggregation in broadcast spawning. The Journal of Experimental Biology, 215:1031–1039, October 2011.

[8] John P. Crimaldi, Jillian R. Cadwell, and Jeffrey B. Weiss. Reaction enhancement of isolated scalars by vortex stirring. Physics of Fluids, 20, July 2008.

[9] John P. Crimaldi, Jillian R. Hartford, and Jeffrey B. Weiss. Reaction enhancement of point sources due to vortex stirring. Physical Review E, 74, July 2006.

[10] Mark W. Denny, Elizabeth K. Nelson, and Kristina S. Mead. Revised estimates of the effects of turbulence on fertilization in the purple sea urchin, strongylocentrotus purpuratus. Biological Bulletin, 203:275–277, December 2002.

[11] Michael Eisenbach. Sperm chemotaxis. Reviews of Reproduction, 4:56–66, 1999.

[12] Jonathan P. Evans, Francisco Garcia-Gonzalez, Maria Almbro, Oscar Robinson, and John L. Fitzpatrick. Assessing the potential for egg chemoattractants to mediate sexual selection in a broadcast spawning marine invertebrate. Proceedings of the Royal Soceity B, 279:2855–2861, March 2012.

[13] Gregory S. Farley. Helical nature of sperm swimming affects the fit of fertilization-kinetics model to empirical data. Biological Bulletin, 203:51–57, August 2002.

[14] Gregory S. Farley and Don R. Levitan. The role of jelly coat in sperm-egg encounters, fertilization success and selection on egg size in broadcast spwaners. American Society of Natrualists, 157(6):626–636, June 2001.

[15] B. M. Friedrich and F. Julicher. The stochastic dance of circling sperm cells: sperm chemotaxis in the plane. New Journal of Physics, 10, December 2008.

[16] Benjamin M Friedrich and Frank Julicher. Chemotaxis of sperm cells. Proceedings of the National Academy of Sciences of the United States of America, 104(33):13256–13261, August 2007.

[17] Benjamin M Friedrich and Frank Julicher. Steering chiral swimmers along noisy helical paths. The American Phyisical Society, 103, August 2009.

[18] Albert E. Giorgi and John D. DeMartini. A study of the reproductive biology of the red abalone, haliotis rufescens swainson, near mendocino, california. California FIsh and Game, 63(3):80–94, October 1977.

[19] Adan Guerrero, Takuya Nishigaki, Jorge Carneiro, Yoshiro Tatsu, Christopher D. Wood, and Alberto Darszon. Tuning sperm chemotaxis by calcium burst timing. Delevopmental Biology, 344:52–56, May 2010.

[20] Adán Guerrero, Christopher D Wood, Takuya Nishigaki, Jorge Carneiro, and Alberto Darszon. Tuning sperm chemotaxis. Biochem Soc Trans, 38(5):1270–4, Oct 2010.

[21] Donat P. Hader, Andreas Rosum, Jochen Schafer, and Ruth Hemmersbach. Gravitaxis in the flagellate euglena gracilis is controlled by active gravireceptor. Journal of Plant Physiology, 146:474–480, February 1995.

[22] Julie E. Himes, Jeffrey A. Riffell, Cheryl Ann Zimmer, and Richard K. Zimmer. Sperm chemotaxis as revealed with live and synthetic eggs. Biological Bulletin, 220:1–5, February 2011.

[23] J. C. R. Hunt and J. C. Vassilicos. Kolmogorov's contributions to the physical and geometrical understanding of small-scale turbulence and recent developments. Proceedings of the Royal Soceity A, 434:183–210, 1991.

[24] Munish V. Inamdar, Taeyong Kim, Yao-Kuang Chung, Alex M. Was, Xinran Xiang, Chia Wei Wang, Chuichi Takayama, Christian M. Lastoskie, Florence I. M. Thomas, and Ann Marie Sastry. Assessment of sperm chemokinesis with exposure to jelly coats of sea urchin eggs and resact: a microfluidic experiement and numerical study. The Journal of Experimental Biology, 210:3805–3820, July 2007.

[25] Ehsan Jabbarzadeh and Cameron F. Abrams. Chemotaxis and random motility in unsteady chemoattractant fields: a computational study. Journal of Theoretical Biology, 235:221–232, January 2005.

[26] T. M. Jantzen, R. de Nys, and J. N. Havenhand. Fertilization success and the effects of sperm chemoattractants on effective egg size in marine invertebrates. Marine Biology, 138:1153–1161, April 2001.

[27] U. B. Kaupp, E. Hildebrand, and I. Weyland. Sperm chemotaxis in marine invertebrates-molecules and mechanisms. Journal of Cellular Physiology, 208:487–494, 2006.

[28] U Benjamin Kaupp, Nachiket D Kashikar, and Ingo Weyand. Mechanisms of sperm chemotaxis. Annual Review Physiology, 70:93–117, 2008.

[29] U. Benjamin Kaupp, Johannes Solzin, Eilo Hildebran, Joel E. Brown, Annika Helbig, Volker Hagen, Michael Beyermann, Francesco Pampaloni, and Inglo Weyland. The signal flow and motor response controling chemotaxis of sea urchin sperm. Nature Cell Biology, 5:109–117, February 2003.

[30] Evelyn F. Keller and Lee A. Segel. Model for chemotaxis. The Journal of Theoretical Biology, 30:225–234, February 1971.

[31] Jackson C. Kirkman_Brown, Keith A. Sutton, and Harvey M. Florman. How to attract a sperm. Nature Cell Biology, 5:93–96, February 2003.

[32] Alexander Kiselev and Lenya Ryzhik. Biomixing by chemotaxis and enhancement of biological reactions. Communications in Partial Differential Equations, 37(2):298–318, 2012.

[33] Charles A. Kossack and Andreas Acrivos. Steady simple shear flow past a circular cylinder at moderate reynolds numbers: a numerical solution. Journal of Fluid Mechanics, 66(2):353–376, October 1973.

[34] Patrick J Krug, Jeffrey A Riffell, and Richard K Zimmer. Endogenous signaling pathways and chemical communication between sperm and egg. J Exp Biol, 212(Pt 8):1092–100, Apr 2009.

[35] Elena Kupriyanova and Jon N. Havenhand. Variation in sperm swimming behaviour and its effect on fertilization success in the serpulid polychaete galeolaria caespitosa. Invertebrate Reproduction and Development, 41(1-3):21–26, January 2002.

[36] J. R. N. Lazier and K. H. Mann. Turbulence and the diffusive layers around small organisms. Deep-Sea Research, 36(11):1721–1733, June 1989.

[37] Don R. Levitan. Predicting optimal and unique egg sizes in free-spawning marine invertebrates. The American Naturalist, 148(1):174–188, July 1996.

[38] Don R. Levitan. Optimal egg size in marine invertebrates: theory and phylogenetic analysis of the critical relationship between egg size and development time in echinoids. The American Naturalist, 156(2):175–192, August 2000.

[39] Don R. Levitan. The relationship between egg size and fertilization success in broadcast-spawning marine invertebrates. Integrative and Comparative Biology, 46(3):298–311, March 2006.

[40] Don R. Levitan and Stacey D. Irvine. Fertilization selection on egg and jelly-coat size in the sand dollar dendraster excentricus. Evolution, 55(12):2479–2483, 2001.

[41] Don R. Levitan, Mary A. Sewell, and Fu-Shiang Chia. Kinetics of fertilization in the sea urchin strongylocentrotus franciscanus: interaction of gamete dilution, age and contact time. Biological Bulletin, 181:371–378, December 1991.

[42] DR. Levitan. The importance of sperm limitation to the evolution of egg size in marine invertebrates. The American Naturalist, 141:517–536, 1993.

[43] Pekka Mark and Lennart Nilsson. A molecular dynamics study of tryptophan in water. Journal of Physical Chemistry, 106:9440–9445, 2002.

[44] Kristina S. Mead and Mark W. Denny. The effects of hydrodynamic shear stress on fertilization and early development of the purple sea urchin strongylocentrotus purpuratus. Biological Bulletin, 188:46–56, February/March 1995.

[45] Duane R. Mikulencak and Jeffrey F. Morris. Stationary shear flow around fixed and free bodies at finite reynolds number. Journal of Fluid Mechanics, 520:215–242, August 2004.

[46] K. J. Miller and C. N. Mundy. In situ fertilisation success in the scleractinian coral goniastrea favulus. Coral Reefs, 24(2):313–317, March 2005.

[47] Masaya Morita, Akira Nishikawa, Ayako Nakajima, Akira Iguchi, Kazuhiko Sakai, Akihiro Takemura, and Makoto Okuno. Eggs regulate sperm flagellar motility initiation, chemotaxis and inhibition in the coral acropora digitifera, a. gemnifera and a. tenuis. The Journal of Experimental Biology, 209:4574–4579, August 2006.

[48] Masaya Morita, Ryota Svwa, Akira Iguchi, Masako Nakamura, Kazuaki Shimada, Kazuhiko Sakai, and Atsushi Suzuki. Ocean acidification recudes sperm flagellar motility in broadcast spawning reef invertebrates. Zygote, pages 103–107, November 2009.

[49] Javier Munoz-Garcia, Zoltan Neufeld, and Colin Torney. Nutrient exposure of chemotactic organisms in small-scale turbulent flows. New Journal of Physics, 12, October 2010.

[50] J. M. Ottino. The kinematics of mixing: stretching, chaos, and transport. Cambridge University Press, 1989.

[51] Alfred Polson. On the diffusion constants of the amino-acids. Biochemical Journal, 31(10):1903–1912, October 1937.

[52] Noel P. Quinn and Josef D. Ackerman. The effect of near-bed turbulence on sperm dilution and fertilization success of broadcast-spawning bivalves. Limnology and Oceanography: Fluids and Environments, 1:176–193, October 2011.

[53] Ingmar H. Reidel, Karsten Kruse, and Jonathon Howard. A self-organized vortex of hydrodynaimcally entrained sperm cells. Science, 309:300–303, July 2005.

[54] Jeffrey A. Riffell, Patrick J. Krug, and Richard K. Zimmer. The ecological and evolutionary consequences of sperm chemoattraction. Proceedings of the National Academy of Sciences of the United States of America, 101(13):4501–4506, January 2004.

[55] Jeffrey A. Riffell, Patrick J. Krugg, and Richard K. Zimmer. Fertilization in the sea: the chemical identity of an abalone sperm attractant. The Journal of Experimental Biology, 205:1439–1450, February 2002.

[56] Jeffrey A Riffell and Richard K Zimmer. Sex and flow: the consequences of fluid shear for sperm-egg interactions. J Exp Biol, 210(Pt 20):3644–60, Oct 2007.

[57] Roman Stocker, Justin E. Seymour, Azadeh Samadani, Dana E. Hunt, and Martin F. Polz. Rapid chemotactic response enables marine bacteria to exploit ephemeral microscale nutrient patches. Proceedings of the National Academy of Sciences of the United States of America, 105(11):4209–4214, January 2008.

[58] Craig A. Styan. Polyspermy, egg size, and the fertilization kinetics of free-spawning marine invertebrates. The American Naturalist, 152(2):290–297, August 1998.

[59] Ting-Wei Su, Liang Xue, and Aydogan Ozcan. High-throughput lensfree 3d tracking of human sperms reveals rare statistics of helical trajectories. Proceedings of the National Academy of Sciences of the United States of America, 109(40):16018–16022, October 2012.

[60] G.I. Taylor. Dispersion of soluble matter in solvent flowing slowly through a tube. Royal Society of London Proceedings Series A, 219:186–203, 1953.

[61] Victor D. Vacquier. Evolution of gamete recognition proteins. Science, 281:1995–1998, September 1998.

[62] Victor D. Vacquier, Kristin R. Carner, and C. David Stout. Species-specific sequences of abalone lysin, the sperm protien that creates a hole in the egg envelope. Proceedings of the National Academy of Sciences of the United States of America, 87:5792–5796, August 1990.

[63] Helmut Vogel, Gerhard Czihak, Patrick Chang, and Wieland Wolf. Fertilization kinetics of the sea urchin eggs. Mathematical Biosciences, 58:189–216, 1982.

[64] Cynthia R. Ward and Gregory S. Kopf. Molecular events mediating sperm activation. Developmental Biology, 158:9–34, March 1993.

[65] Gary E. Ward, Charles J Brokaw, David L. Garbers, and Victor D. Vacquier. Chemotaxis of arbacia punctulata spermatozoa to resact, a peptide from the egg jelly layer. The Journal of Cell Biology, 101:2324–2329, December 1985.

[66] Christopher D. Wood, Takuya Nishigaki, Toshiaki Furuta, Shoji A. Baba, and Alberto Darszon. Real-time analysis of the role of ca^{2+} in flagellar movement and motility in single sea urchin sperm. The Journal of Cell Biology, 169(5):725–731, June 2005.

[67] Richard K. Zimmer and Cheryl Ann Butman. Chemical signaling processes in the marine environment. Biological Bulletin, 198:167–187, April 2000.

[68] Richard K Zimmer and Jeffrey A Riffell. Sperm chemotaxis, fluid shear, and the evolution of sexual reproduction. Proc Natl Acad Sci U S A, 108(32):13200–5, Aug 2011.

Appendix A

Ring Behavior

A.1 Ring Behavior

As a baseline model, the sperm were allowed to complete drifting circles without any variations on any of the parameter that define the behavior. The sperm were released from the same point, with a random initial direction and random drift direction. As the amount of sperm released increased enough, a beating phenomenon became apparent. Regardless of the direction of both initial direction and drift, the sperm swam in the same phase with one another. This caused a pattern: the ring would develop from thin line and evolve to become the thickness of $2\dot{\theta}_{radii}$. As half of the sperm were moving away from the egg as far as one cycle would permit, the other half were moving towards the egg at the same velocity with the same maximum difference.

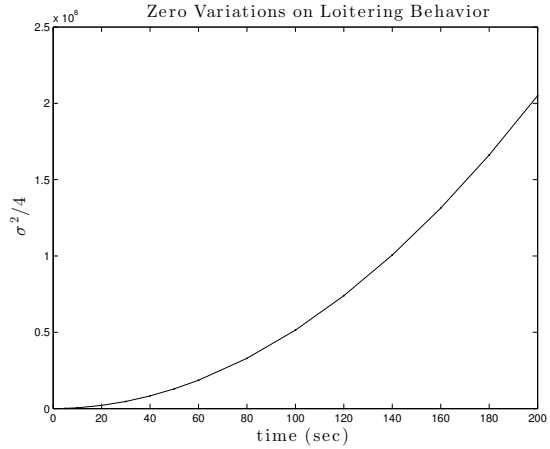

Figure A.1: A plot of the variance vs. time to show that this loitering behavior is super diffusive. The variance grows quadratically with time instead of linearly, as desired.

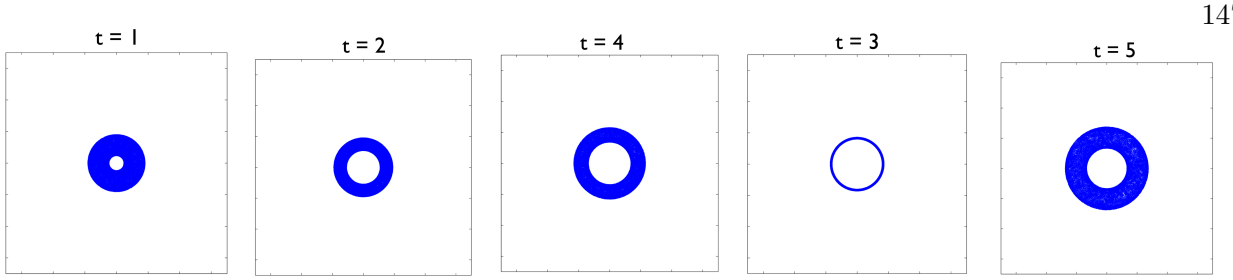

Figure A.2: Time evolution of the ring behavior.

To avoid this unrealistic result, this simplistic patter was abandoned in favor of a more complex, realistic behavior. This behavior requires turning rates with variations within a reasonable range and much higher variation on the drift speed and direction. This lead to the use of a uniform distribution in determining the turn rate at each time step and higher standard deviation parameters on the triangle distributions used to calculate new drift speed and direction at every time-step. In addition, this highlighted the diffusive behavior that is more expected from a large number of sperm swimming randomly. This diffusive behavior was quantified in section 2.3.3.

An additionally notable behavior results from a constant initial swimming direction. When this restriction is implemented, the ring width is maintained, but circles are created with this intact ring. The sperm are all in the same phase, creating the same size circles at the same rate.